

**MODELING FULL-SCALE FIRE TEST BEHAVIOUR OF
POLYURETHANE FOAMS
USING CONE CALORIMETER DATA**

A Thesis Submitted to the College of
Graduate Studies and Research
In Partial Fulfillment of the Requirements
for the Degree of Master of Science
in the Department of Mechanical Engineering
University of Saskatchewan
Saskatoon

By

John Uzodinma Ezinwa

PERMISSION TO USE

In presenting this thesis in partial fulfilment of the requirements for a postgraduate degree from the University of Saskatchewan, I agree that the Libraries of this University may make it freely available for inspection. I further agree that permission for copying of this thesis in any manner, in whole or in part, for scholarly purposes may be granted by the professor or professors who supervised my thesis work or, in their absence, by the Head of the Department or the Dean of the College in which my thesis work was done. It is understood that any copying or publication or use of this thesis or parts thereof for financial gain shall not be allowed without my written permission. It is also understood that due recognition shall be given to me and to the University of Saskatchewan in any scholarly use which may be made of any material in my thesis.

Requests for permission to copy or make other use of material in this thesis in whole or part should be addressed to:

Head of the Department of Mechanical Engineering

University of Saskatchewan

Saskatoon, Saskatchewan S7N 5A9

ABSTRACT

Flexible polyurethane foam (PUF) is a very versatile material ever created. The material is used for various applications and consumer end-use products such as upholstered furniture and mattresses. The increased use of these polymeric materials causes fire safety concerns. This has led to the development of various regulations and flammability test standards aimed at addressing the hazards associated with polyurethane foam fires. Several fire protection engineering correlations and thermal models have also been developed for the simulation of fire growth behaviour of polyurethane foams. Thus, the overall objective of this research project is to investigate the laboratory test behaviour of this material and then use finer modeling techniques to predict the heat release rate of the specimens, based on information obtained from cone calorimeter tests.

Full-scale fire tests of 10 cm thick polyurethane foams of different sizes were conducted using center and edge-ignition locations. Flame spread and heat release rates were compared. For specimens of the same size, center-ignition tests produced flame areas and peak heat release rates which were respectively 10 and 20% larger compared to edge-ignition tests. Average flame spread rates for horizontal and vertical spread were determined, and results showed excellent agreement with literature. Cone calorimeter tests of the specimens were performed using steel edge frame and open durarock board. Results indicate that different test arrangements and heat sources have significant effects on the fire behaviour of the specimens.

Predictions using the integral convolution model and other fire protection engineering correlations were compared with the full-scale tests results. Results show that the model was more efficient in predicting the heat release rates for edge-ignition tests than the center-ignition tests. The model also was more successful in predicting the heat release rates during the early part of the growth phase than during the later stages of the fire. The predicted and measured peak heat release rates and total heat release were within 10-15% of one another. Flame spread and t-squared fire models also gave satisfactory predictions of the full-scale fire behaviour of the specimens.

ACKNOWLEDGEMENTS

The author wishes to thank the Lord God for the divine enablement to bring this research project to completion. The author would also like to sincerely acknowledge the following people and organizations for their support and assistance with this research project:

- Professor D.A. Torvi for his supervision of this research and for his continued support and direction. His technical guidance and encouragement have been the driving force throughout this research project.
- Professor D.J. Bergstrom and Professor J.D. Bugg for their direction as part of the author's supervisory committee.
- The Department of Mechanical Engineering and the College of Graduate Studies and Research at the University of Saskatchewan, and the Natural Sciences and Engineering Research Council of Canada (NSERC) for their financial support.
- Professor E.J. Weckman, David Adeosun, Gord Hitchman and Janel Rigg of the Department of Mechanical and Mechatronics Engineering, University of Waterloo are gratefully acknowledged for their assistance and technical support during the small and full-scale tests.
- Departmental assistants Dave Deutscher and Chris James provided assistance on various aspects of this study.
- Mr. Thomas Meyer of the Department of Electrical and Computer Engineering, University of Saskatchewan, for his assistance with aspects of the computer code development.
- My sincere gratitude goes to my family for their immense love throughout my entire life. God bless you all.

TABLE OF CONTENTS

PERMISSION TO USE	i
ABSTRACT	ii
ACKNOWLEDGEMENTS	iii
TABLE OF CONTENTS	iv
LIST OF TABLES	x
LIST OF FIGURES	xi
NOMENCLATURE	xix
CHAPTER ONE: INTRODUCTION	1
1.1 Polyurethane Foam	2
1.2 Combustion of Polyurethane Foams	4
1.2.1 Smouldering Combustion	8
1.2.2 Flaming Combustion	8
1.3 Flame Spread	9
1.4 Compartment Fires and Polyurethane Foams	10
1.5 Pool Fires	12
1.6 Oxygen Consumption Calorimetry	13
1.7 Large-Scale Fire Tests	14
1.7.1 Furniture Calorimeter	14
1.7.2 Room Fire Tests	15

1.7.3 The Intermediate-Scale Calorimeter	16
1.8 Small-Scale Tests	16
1.8.1 Cone Calorimeter	17
1.9 Standard Fire Tests For Mattresses	19
1.9.1 Open Flame Tests	20
1.10 Previous Research	21
1.10.1 Combustion Behaviour of Upholstered Furniture (CBUF) Project	21
1.10.2 Consumer Product Safety Commission (CPSC) Project	24
1.10.3 Previous Research at the University of Saskatchewan	25
1.11 Research Objectives And Scope	30
1.12 Thesis Outline	31
CHAPTER TWO: MODELS FOR POLYURETHANE FOAM FIRES	32
2.1 Heat Transfer Model	32
2.2 Flame Spread Models	37
2.2.1 CBUF Flame Spread Model	38
2.2.2 Burning Area Model For Combustible Lining Materials	40
2.2.3 Single Burning Item (SBI) Model	42
2.3 Heat Release Rate Models	44
2.3.1 Combustion Science Heat Release Rate Model	44
2.3.2 CBUF Thermal Fire Spread Model For Mattresses	45

2.3.3 Time-Squared Heat Release Rate Model	49
2.3.4 NIST-CBHF Heat Release Rate Correlation	51
2.4 Burning Rate and Duration	52
2.5 Flame Pulsation	56
2.6 Fire Scaling	57
2.7 Summary of Chapter	57
CHAPTER THREE: FULL-SCALE TESTS OF POLYURETHANE FOAMS	59
3.1 Introduction	59
3.2 Materials	59
3.3 Experimental Procedure	61
3.3.1 Specimen Preparation	61
3.3.2 Furniture Calorimeter Calibration	62
3.3.3 Photography	63
3.3.4 Test Procedure	63
3.4 Determination of Flame Spread	65
3.4.1 Infra-red Camera	69
3.4.2 Video Camera	75
3.4.3 Still Camera	77
3.5 Flame Spread Rates	78
3.5.1 Center-Ignition Tests	78

3.5.2 Edge-Ignition Tests	85
3.5.3 Comparison of Center and Edge-Ignition Test	90
3.5.4 Vertical Flame Spread Rates	93
3.6 Heat Release Rates	96
3.6.1 Center-Ignition Tests	97
3.6.2 Edge-Ignition Tests	100
3.6.3 Comparison of Center and Edge-Ignition Tests	102
3.7 Mass Loss Rates	105
3.8 Summary of Chapter	107

CHAPTER FOUR: SMALL-SCALE TESTS OF POLYURETHANE

FOAMS	108
4.1 Introduction	108
4.2 Specimen Preparation	108
4.3 Calibration	112
4.4 Experimental Procedure	113
4.5 Vertical Flame Spread Tests	115
4.6 Cone Calorimeter Results	117
4.7 Summary of Chapter	128

CHAPTER FIVE: NUMERICAL RESULTS	130
5.1 Validation of The Integral Model	130
5.2 Input Data	139
5.3 Convolution Model Results	142
5.3.1 Sensitivity Analysis	144
5.4 Flame Spread Model Results	148
5.5 Time-Squared Heat Release Rate Model	151
5.6 NIST-CBHF Heat Release Rate Correlation	152
5.7 Summary of Chapter	154
CHAPTER SIX: COMPARISON OF PREDICTED AND MEASURED RESULTS	156
6.1 Comparison of Predicted And Measured Results	157
6.2 Discussion of Results	162
6.3 Possible Modifications of The Convolution Model	172
6.4 Summary of Chapter	177
CHAPTER SEVEN: CONCLUSIONS AND RECOMMENDATIONS	179
7.1 Conclusions	179
7.2 Recommendations	181

REFERENCES	184
-------------------	-----

APPENDICES:

Appendix A: C++ Source code	193
Appendix B: C++ header file	201

LIST OF TABLES

TABLE 2-1	Different values of fire growth coefficient	50
TABLE 2-2	Heat transfer mode dependence on pool diameter	55
TABLE 3-1	Furniture calorimeter test specimens and test dates/environmental conditions	60
TABLE 3-2	Summary of peak flame areas and spread rates of polyurethane foam specimens	90
TABLE 3-3	Summary of HRR test results of polyurethane foam specimens	97
TABLE 4-1	Summary of physical properties of specimens tested with the steel edge frame	114
TABLE 4-2	Summary of physical properties of specimens tested using non-conventional techniques (durarock board and butane- ignition)	115
TABLE 4-3	Summary of performance characteristics of specimens tested in steel edge frame	117
TABLE 4-4	Performance characteristics of specimens tested on durarock board	118
TABLE 4-5	Comparison of average HRR density at various times after ignition	118
TABLE 4-6	Vertical flame spread measurements	119
TABLE 5-1	Dataset obtained from Gaussian curve fit for 10 cm foam tested at 35 kW/m ²	141
TABLE 5-2	NIST/CBHF peak HRR predictions	154
TABLE 6-1	Summary of the measured and predicted full-scale combustion characteristics of polyurethane foams	157
TABLE 6-2	Summary of the predicted full-scale results using the integral model	173

LIST OF FIGURES

FIGURE 1-1	Idealized fire HRR profile	11
FIGURE 1-2	Photographs at early stages of room fire (a) and at flashover (b)	12
FIGURE 1-3	University of Waterloo Furniture calorimeter	15
FIGURE 1-4	Cone calorimeter (top) and combustion chamber (bottom)	18
FIGURE 1-5	The CBUF project structure	22
FIGURE 1-6	Comparison of measured and predicted temperatures	26
FIGURE 1-7	Photographs of furniture calorimeter test of 1.2 by 1.2 by 10 cm foam specimen	27
FIGURE 1-8	Comparison of HRR curves measured in furniture calorimeter tests of various pieces of polyurethane foam	28
FIGURE 1-9	HRR density from cone calorimeter tests of 5 cm thick pieces of polyurethane foam	29
FIGURE 1-10	Comparison of HRR measured during test of 0.6 by 1.2 m by 5 cm specimen and predicted using medium t^2 fire and flame spread model	29
FIGURE 2-1	Idealized flame spread mechanism for an edge-ignited specimen	37
FIGURE 2-2	Example of ideal flame area growth showing an exponential profile	41
FIGURE 2-3	Flame area growth showing exponential and steady state profile	44
FIGURE 2-4	Gaussian function representing an idealised HRR density	48

FIGURE 2-5	Set of t-squared growth curves	50
FIGURE 3-1	Grid marking of a 10 by 10 cm cell on a foam specimen	61
FIGURE 3-2	Furniture calorimeter HRR calibration using a propane burner	62
FIGURE 3-3	Infra-red camera and camcorder positions	63
FIGURE 3-4	Flame impingement at the ignition point on edge of foam	64
FIGURE 3-5	Schematic of ideal radial flame spread over a center-ignited specimen	66
FIGURE 3-6	Schematic of ideal radial flame spread on an edge-ignited specimen	66
FIGURE 3-7	Radial flame growth over a center-ignited specimen (top) and elliptic flame growth over an edge-ignited specimen (bottom)	67
FIGURE 3-8	Flame spread across the length of the specimen	68
FIGURE 3-9	Infra-red image of the initial burning area for specimen C3	70
FIGURE 3-10	Infra-red image showing truncated flame front for specimen C3	71
FIGURE 3-11	Vertical flame spread and onset of burn-out for specimen C3	71
FIGURE 3-12	Well developed burn-out section and flame decay for specimen C3	72
FIGURE 3-13	Flame growth towards the edge of the specimen EE3	73
FIGURE 3-14	Flame growth across the length of the specimen EE3	74
FIGURE 3-15	Schematic showing the rectangular and semi-circular burning sections of a foam	74
FIGURE 3-16	Initial burning area for specimen C3	75

FIGURE 3-17	Truncated flame front at the edge of specimen C3	76
FIGURE 3-18	Vertically-downwards flame spread at the sides of specimen C3	76
FIGURE 3-19	Flame tilting and pulsation for specimen E4	77
FIGURE 3-20	Comparison of video, IR and digital photo-determined flame spread rate of specimen C1	79
FIGURE 3-21	Flame areas determined using IR video for specimens C1, C2 and C3	81
FIGURE 3-22	Linear regression rate for specimen C1	83
FIGURE 3-23	Exponential flame area growth curve for specimen C1	84
FIGURE 3-24	Flame areas estimated using camcorder, IR camera and digital photos for specimen E5	86
FIGURE 3-25	Flame areas estimated from IR video of edge-ignition tests	87
FIGURE 3-26	Linear regression rate for specimen E5	89
FIGURE 3-27	Flame area growth for specimen E5	89
FIGURE 3-28	Comparison of flame areas estimated using IR video of center-ignited tests C1 and C2 and edge-ignited test E5	90
FIGURE 3-29	Comparison of flame areas estimated using IR video of center-ignited tests C3 and edge-ignited tests EE3 and EE4	93
FIGURE 3-30	Locations of vertical flame spread measurement for specimen EE3	94
FIGURE 3-31	Average depth of vertical burn at different locations of specimens E5,	

	EE3 and EE4	95
FIGURE 3-32	Instantaneous flame spread rate at each location for specimens E5, EE3 and EE4	95
FIGURE 3-33	HRR-time histories for specimens C1,C2 and C3 during center ignition tests	98
FIGURE 3-34	Burning of portions of the specimens at the four edges of specimen C1	99
FIGURE 3-35	Relationship between HRR and flame area growth for specimen C1	100
FIGURE 3-36	HRR-time histories for edge-ignited specimens E4, E5, EE3 and EE4	101
FIGURE 3-37	Relationship between HRR and flame area growth for specimen EE4	102
FIGURE 3-38	Comparison of HRR for center (C3) and edge-ignited (EE3 & EE4) specimens	104
FIGURE 3-39	Comparison of HRR for center (C1 & C2) and edge-ignited (E4 & E5) specimens	104
FIGURE 3-40	Comparison of mass loss rates during center-ignition tests of specimens C1 and C2	105
FIGURE 3-41	Comparison of mass loss rates during center and edge-ignition tests of specimens E5, EE3 and EE4	106

FIGURE 4-1	Foam specimens positioned atop a metal rack inside a conditioning container	109
FIGURE 4-2	Thin aluminum foils for wrapping the conditioned specimens	110
FIGURE 4-3	Specimen set-up using durarock board mounting	111
FIGURE 4-4	Specimen mounting using steel edge frame	112
FIGURE 4-5	Vertical flame spread rate test of 10 cm specimen using the cone calorimeter	116
FIGURE 4-6	Average HRR densities for 10 cm thick specimens tested in edge Frame, and on durarock board with cone and butane ignition	121
FIGURE 4-7	Average HRR densities for 7.5 cm thick specimens tested in edge frame, and on durarock board with cone and butane ignition	123
FIGURE 4-8	Average HRR densities for 5 cm thick specimens tested in edge frame, and on durarock board with cone and butane ignition	124
FIGURE 4-9	Average HRR densities for 2.5 cm thick specimens tested in edge frame, and durarock board with cone and butane ignition	125
FIGURE 4-10	Comparing different thicknesses of specimens tested in steel edge frame with cone ignition	127
FIGURE 4-11	Comparing different thicknesses of specimens tested on durarock board with cone ignition	128
FIGURE 5-1	A hypothetical HRR density using a single Gaussian function	133
FIGURE 5-2	Idealised flame area compared with flame areas for specimens EE3	

	and EE4 measured during May 2008 full-scale tests	133
FIGURE 5-3	Comparison of numerical results obtained using the exact method and computer program	135
FIGURE 5-4	Comparing the effects of time to peak (c) and width of peak (b) on HRR density	135
FIGURE 5-5	Effects of using different HRR densities on the predicted full-scale HRR	136
FIGURE 5-6	60 s Average HRR density (350 kW/m ²)	137
FIGURE 5-7	Comparison of convolution model results using different time-steps	138
FIGURE 5-8	Comparison of exact solution (flame spread model) and the discrete model using dt = 1 s	138
FIGURE 5-9	Comparison of measured and calculated HRR density for a durarock-mounted, cone-ignited 10 cm specimen	140
FIGURE 5-10	Measured flame area for specimen C1	141
FIGURE 5-11	Calculated HRR result for specimen C1 and C2 using 10 cm (durarock-mounted, cone-ignited) HRR density expression	142
FIGURE 5-12	Calculated HRR result for specimen C3 using 10 cm (durarock-mounted, cone-ignited) HRR density expression	143
FIGURE 5-13	Calculated HRR results for specimens E5 and EE3 using 10 cm (durarock-mounted, cone-ignited) HRR density expression	144

FIGURE 5-14	$\pm 10\%$ difference in the transient HRR density for a 10 cm durarock-mounted, cone-ignited specimen	145
FIGURE 5-15	Effects of changing the HRR density on the predicted full-scale HRR for specimen C1	146
FIGURE 5-16	Measured flame area for specimen C1 and a $\pm 10\%$ change	147
FIGURE 5-17	Effects of flame area on the predicted full-scale HRR for specimen C1	147
FIGURE 5-18	Predicted HRR for specimens C1 and C3 using 60 s average HRR density of 350 kW/m^2	149
FIGURE 5-19	Predicted HRR for edge-ignited specimens E5 and EE3	150
FIGURE 5-20	Effects of average HRR densities on predicted full-scale HRR for specimen C3	151
FIGURE 6-1	Comparison between measured and predicted HRR for specimen C1	159
FIGURE 6-2	Comparison between measured and predicted HRR for specimen C3	160
FIGURE 6-3	Comparison between measured and predicted HRR for specimen E5	161
FIGURE 6-4	Comparison between measure and predicted HRR for specimen EE3	162

FIGURE 6-5	Comparing the measured and predicted result for 61 by 122 by 5 cm specimen tested during July 2006	167
FIGURE 6-6	Effects of using flame area decay in the convolution model	168
FIGURE 6-7	Truncated HRR density for 10 cm specimen	169
FIGURE 6-8	Comparison of measured and predicted HRR using truncated and non-truncated HRR density for specimen E5	171
FIGURE 6-9	Comparison of measured and predicted HRR using truncated HRR and non-truncated HRR density for specimen EE3	171
FIGURE 6-10	Curve fit of HRR density for 5 cm cone specimen tested at 35 kW/m ²	172
FIGURE 6-11	Predicted HRR using two 5 cm HRR densities incorporating 17 s time delay	173
FIGURE 6-12	Comparison of the measured and predicted results for specimen C1 using 5 cm composite HRR density	176
FIGURE 6-13	Comparison of the measured and predicted HRR for specimen C3 using 5 cm composite HRR density	175
FIGURE 6-14	Comparison of the measured and predicted HRR for specimen EE3 using 5 cm composite HRR density	177

NOMENCLATURE

Notation

A	flame area (m^2)
c	specific heat ($\text{J/kg} \cdot \text{K}$)
D	diameter (m)
dt	time step (s)
F	frequency (Hz)
H	height (m)
h	convective heat transfer coefficient ($\text{kW/m}^2 \cdot \text{K}$)
k	thermal conductivity ($\text{W/m} \cdot \text{K}$)
k_m	flame absorption coefficient (m^{-1})
L	length (m)
L_o	thermal conduction length (m)
\dot{m}''	mass loss rate per unit area ($\text{kg/m}^2 \cdot \text{s}$)
\dot{Q}	heat release rate (kW)
\dot{q}''	transient heat release rate density (kW/m^2)
q''	heat flux (kW/m^2)
R	radius (m)

\dot{R}	linear regression rate (m/s)
r_f	flame front (m)
r_m	the optical mean beam length given as $3.5V_f / A_f$ (m)
r_p	exposure range (m)
T	temperature at ignition (K, °C)
$T1, T2$	transition points
V_f	volume of flame column (m ³)
v	velocity of flame propagation (m/s)
W	width of specimen (m)
X	combustion efficiency factor
z	height of the flame cylinder above the burning surface (m)

Greek Symbols

α	fire growth coefficient (kW/s ²), linear regression rate (m/s), surface absorptivity (m ² /s)
δ	thickness of the specimen (m)
ε	emissivity
ε_f	flame emissivity
Θ	angle of tilt
λ	flame growth constant (s ⁻¹)

ρ	density (kg/m ³)
σ	Stefan Boltzmann constant ($5.67 \cdot 10^{-8}$ W/m ² · K ⁴)
τ	dummy variable of integration
Φ	view factor
$\Delta H_{c,eff}$	effective heat of combustion (kJ/kg)

Subscripts

<i>aveg</i>	average
<i>c</i>	combustion, convective
<i>e</i>	irradiating
<i>eff</i>	effective
<i>f</i>	flame
<i>FS</i>	full scale
<i>ig</i>	ignition
<i>m</i>	mean
<i>max</i>	maximum
<i>o</i>	initial,incubation
<i>p</i>	exposure
<i>s</i>	surface
<i>t</i>	total
∞	ambient, maximum

Abbreviations

ASTM	American Society For Testing and Materials
CBHF	California Bureau of Home Furnishings
CBUF	Combustion Behaviour of Upholstered Furniture
CFR	Code of Federal Regulation
CPSC	Consumer Products Safety Commission
HRR	Heat Release Rate
ISO	International Organization For Standardization
MLR	Mass Loss Rate
NIST	National Institute of Standards and Technology
PHRR	Peak Heat Release Rate
THR	Total Heat Release

CHAPTER ONE: INTRODUCTION

The fire behaviour of modern flexible polyurethane foams has received considerable attention among the fire community, regulators and research organizations and manufacturers. This is because of the fire hazards associated with polyurethane foam flammability. The most important flammability property of interest to fire protection engineers is the heat release rate (HRR). As a result, the subject of this study will focus on the heat release rate of polyurethane foams under tightly controlled environmental test conditions.

Several advances have been made to model the heat release rate and flame spread behaviour of polyurethane foams for performance-based design fires using various fire protection engineering correlations. However, modeling the fire behaviour of polyurethane foams is complicated as the products decompose to molten materials and often, burn as a layered material in the thickness direction. As part of a larger research project on the fire modeling of polyurethane foams at the University of Saskatchewan, the overall objective of this research is to investigate finer modeling techniques (convolution integral formulation) developed by the European Combustion Behaviour of Upholstered Furniture (CBUF) investigators. This model calculates the heat release rate of polyurethane foams in full-scale using the product of time dependent flame area determined from full-scale tests and the transient heat release rate density from a cone calorimeter test of a representative specimen. Modifications to this model will be performed to estimate the heat release rate from the foams as layered specimens. Analyses of furniture calorimeter and cone calorimeter test data of foam specimens constitute a significant section of this work.

This chapter will describe the fire hazards of polyurethane foams and the heat transfer models which describe the thermo-physical behaviour of polyurethane in fires. Test standards and regulatory approaches which have been developed to help investigate the fire behaviour of foams and to reduce fire fatalities will be presented. Previous experimental studies and modeling work relating to mattresses which are important to this project will also be discussed.

1.1 Polyurethane Foam

Products that are manufactured from flexible polyurethane foams have found a wide range of applications in modern technologies and in homes. This is because of properties such as low cost, light weight, resiliency, durability and high level of comfort [1-5]. However, as these materials are made of organic materials, which can burn very rapidly when ignited, the increased use of polyurethane foams has continued to pose challenges to the fire community. The large amount of heat energy released as they burn can result in large fires if adequate control measures are not in place [6, 7].

Aside from the generation of a large amount of heat energy when polyurethane foams burn, other concerns are their ease of ignition and their ability to propagate flame to other items in the vicinity of their burn. In most cases, the propagation of flames to other items is the result of their potential to melt and flow to involve other combustible items [8, 9]. More so, the combustion of these organic items generate a tremendous amount of smoke and other dangerous gases which increases the fire hazards associated with polyurethane foam fires [10, 11].

Several statistics of the financial and societal cost resulting from polyurethane foam fires have been reported [12]. Statistics published by the United States Consumer Product Safety Commission (CPSC) in 2005 show that mattresses and bedding fires are the largest cause of the deaths as these items were often the first item to ignite during residential fires [13]. The report gave an estimated annual average of 9,000 fires, 520 civilian deaths, 1,040 civilian injuries and \$242 million dollars in property damage for the years 1999 to 2002 [13]. Another CPSC report estimated that in 1997, cigarette-ignited polyurethane foam fires alone caused about 880 deaths, 2120 injuries and over \$335 million worth of property loss [14]. Related statistics by Apte [9] also indicate that of the 14,850 fire deaths in 1,822,700 residential structures between 1994 and 1998 in the United States, 32% of the fires were caused by upholstered furniture ignition and 25% were caused by mattress/bedding ignition. Another CPSC report [15] indicates that among the causes of residential fires, open flame fires resulting from candles, cigarette

lighters and matches accounted for 33% of deaths and 55% of injuries. These statistics reveal the severe consequences of upholstered furniture and mattress/bedding in fires.

However, with advances in technologies, several initiatives have been taken by manufacturers to reduce fire deaths and injuries by producing combustion modified flexible polyurethane foams which are more resistant to ignition and fire growth [10, 16]. These fire protection characteristics are achieved by the addition of flame retardants which function to disrupt the reaction pathways of the polymer, which either terminate or extend the flaming ignition process [8].

The inclusion of these chemicals during production of polyurethane foams is aimed at reducing the rate of temperature rise, therefore producing a smaller fire. In situations where combustion occurs, the flame retardants suppress the production of combustible gases and enhance the production of non-combustible gases of high specific heats, which absorb the heat energy produced and consequently reduce the temperature rise in the flame [17]. This reduces the heat energy available for flame propagation and also provides a certain degree of fire protection when the foams form char and solid carbon, which help in preventing heat penetration to the unburned fuel substrate [8, 17]. When used in upholstered furniture and bedding, flexible polyurethane foams are also often protected by barrier fabrics. Despite the fire retardant technologies in modern polyurethane foams, most of the modified foams still lack the capacity to withstand a high heat source [10].

Thus, fire researchers and polymer engineers are committed to finding means of improving fire properties of polyurethane foam products as well as reducing their toxic effects due to the increased use of fire retardants in these polymeric materials [16]. An important part of this process is the development of standard fire tests for evaluating products containing flexible polyurethane foams. These tests are conducted by manufacturers and government agencies to determine the combustibility of the completed product and the component parts.

Flammability tests which involve assessment of the ease of ignition, the heat release rate (HRR) and the total energy release from polyurethane foam articles are designed to estimate the hazard level to end users. Often, this will involve testing a complete item which is very expensive. Alternatively, small-scale tests of these polymeric items can be conducted with the objective of identifying the fire characteristic of the component materials. These tests could be used as screening tools and to help predict the fire behaviour of the complete specimen.

A significant recent development is the new CPSC regulation for residential mattresses sold in the United States of America (16 CFR Part 1633) [15], which requires full-scale testing of mattresses and bedding using an open flame. This has intensified studies on the combustion behaviour of mattresses. As an extension of this open flame test, one of the objectives of the current research is to investigate the fire behaviour of polyurethane foam which is a major component of upholstered furniture and mattresses. The study will involve the investigation of the rate of heat release and the rate at which flame spreads on the surface of these items during fires. Small-scale tests of the polyurethane foams will be conducted and the information obtained will be used to predict the results of full-scale fire tests of the foams.

1.2 Combustion of Polyurethane Foams

Combustion is an exothermic chemical reaction of a fuel with oxygen which results in the production of heat energy, smoke, water vapour, carbon dioxide and toxic gases. Combustion of polyurethane foams involves the thermal decomposition of the substrate to yield low molecular mass products that can volatilise from the surface and form a flame [7, 18]. This decomposition process requires a critical heat flux (q_{cr}'') to break the chemical bonds of the foam. The heat flux is the convective and radiative heat fluxes produced by a flame. It may also be an external heat flux from a radiant source [19]. Janssens [20] gave an approximate relationship between q_{cr}'' and the ignition temperature

(Equation 1-1) assuming there is no conduction into the solid and that all of the heat striking the surface must be lost from the surface either by radiation or convection.

$$\alpha q_{cr}'' \approx \varepsilon q_{cr}'' = h(T_{ig} - T_{\infty}) + \varepsilon \sigma (T_{ig}^4 - T_{\infty}^4) \equiv h_{ig} (T_{ig} - T_{\infty}) \quad (1-1)$$

Where:

α = surface absorptivity (dimensionless)

ε = surface emissivity (dimensionless)

h = convective coefficient ($W / m^2 \cdot K$)

T_{ig} = surface temperature at ignition (K)

T_{∞} = ambient temperature (K)

σ = Stefan Boltzmann constant ($5.67 \times 10^{-8} W / m^2 \cdot K^4$)

h_{ig} = effective heat transfer coefficient at ignition ($W / m^2 \cdot K$)

$$= h + \varepsilon \alpha (T_{ig}^2 + T_{\infty}^2) (T_{ig} + T_{\infty})$$

This heat irradiance (Equation 1-1) must be high enough to overcome the thermal inertia ($k\rho c$) of the foam, which is an important material property that determines the rate of change of surface temperature, the ease of ignition and fire spread [8]. Since the density of flexible polyurethane foams are low which results in a low thermal inertia, the surface temperature of foams rises quickly when ignited. The quick rise in the surface temperature increases their ignition propensity which results to rapid flame growth. For this ignition to occur, however, the critical temperature of the surface (the ignition temperature T_{ig}) must be reached which then leads to sustained flaming depending on the size of the flame [21]. As the flaming combustion continues, the depth of the heated

layer $\sqrt{(\alpha t)}$ increases and heat is conducted into the foam. The subsequent fire growth will depend on how fast the flame spreads and involve more surfaces which are affected by the fuel's thermal inertia.

Polyurethane foam can behave as a thermally thin or thick material depending on the thermal conduction length $\sqrt{(\alpha t)}$, where α is the thermal diffusivity of the foam and t is the exposure time [8]. For polyurethane foams that can be treated as thermally thin materials, the velocity of flame propagation v has been found to be inversely proportional to the product of the fuels density (ρ), specific heat (c) and thickness (L_c) as:

$$v \propto \frac{1}{\rho c L_c} \quad (1-2)$$

Also, there is no temperature gradient within the bulk of the specimen's mass because the heat absorbed on the surface of the material penetrates very rapidly through the material [19, 22]. Aside from the condition that the physical depth of the material must be greater than the thermal conduction length (i.e. $L_c > \sqrt{\alpha t}$), the generalised criteria (Equation 1-3) used for classifying a thin material is that its Biot number must be less than 0.1 [23].

$$Bi = \frac{h L_c}{k} < 0.1 \quad (1-3)$$

where:

$$L_c = \frac{V}{A_s} \text{ is the ratio of the solid's volume to surface area for heat transfer (m).}$$

The surface temperature response of thermally thin foam materials is dependent on the characteristic thermal thickness $\rho c L_c$ expressed as [19, 22]:

$$T_s = T_0 + \left[\frac{q''}{h_{ign}} - (T_0 - T_\infty) \right] (1 - \exp(-h_{ign} t / \rho c L_c)) \quad (1-4)$$

where:

$T_0 = \text{Initial temperature (K)}$

$h_{ign} = \text{heat transfer coefficient (W / m}^2 \cdot \text{K)}$ (accounting for convective and radiative heat losses)

$\rho = \text{density of the specimen (kg/m}^3\text{)}$

$L_c = \text{thickness of the specimen (m)}$

$c = \text{heat capacity (J/kg} \cdot \text{K)}$

In most cases, however, polyurethane foams do not meet the criteria for thermally thin [24]. Thermally thick foams have a temperature distribution that is affected by its physical depth due to the prolonged time it takes heat energy to penetrate to the opposite side of the material [8]. For such foam specimens, the thermal penetration depth must be less than the physical depth so that increasing the physical thickness L_c of the specimen will not influence the time to ignition. Heat losses from the rear face of the material would be negligible if $L_c > 4 \cdot \sqrt{\alpha t}$ and the surface temperature response is dependent on the thermal inertia $k\rho c$ and is given as [19, 22]:

$$T_s = T_0 + \left[\frac{\dot{q}''}{h_{ign}} - (T_0 - T_\infty) \right] \left[1 - \exp\left(- \left(h_{ign} \sqrt{\frac{t}{k\rho c}} \right)^2 \right) \operatorname{erfc}\left(h_{ign} \sqrt{\frac{t}{k\rho c}} \right) \right] \quad (1-5)$$

For flame spread over thermally thick materials, the rate of spread (v) is inversely proportional to thermal inertia ($k\rho c$). This relationship shows that the rate of flame spread is strongly affected by density of the specimen. For polyurethane foam of low thermal inertia, flame spread can be initiated even if a very small portion of the specimen's surface is heated. Detailed analysis of the semi-infinite approximation is

found in Drysdale's Fire Dynamics Textbook [8]. Due to the air spaces in polyurethane foams, the combustion of these items involve both flaming and smouldering combustion [8, 25, 26].

1.2.1 Smouldering Combustion

Smouldering is a flameless combustion process that occurs in porous combustible fuels such as polyurethane foams. This flameless combustion constitutes a serious fire hazard as it yields a high amount of toxic gases due to incomplete combustion and also provides a pathway to flame propagation that can easily be initiated by low intensity heat sources, such as cigarettes [8, 26, 27]. The rate of heat energy generation, which characterises the intensity of smouldering and subsequent spread to the unburned fuel region, is dependent on the nature of the fuel such as the size and porosity of the particle aggregates to allow flow of oxygen.

As remarked by Ohlemiller [25], one characteristic that is common to most fuels that have the tendency to smoulder is the potential to form char which is preceded by melting. The char and tar formation in polyurethane foams are noted to inhibit smoulder propagation due to their insulating capabilities [8]. Other characteristics of polyurethane smoulder are the low smoulder temperatures (in the range of 350 to 700 °C) and low average smoulder spread rate (e.g., 0.01cm/s).

1.2.2 Flaming Combustion

Flaming combustion occurs when the fire itself, through feedback effects, supplies itself with heat by radiation as it spreads and grows. Often, flaming fires develop from smouldering combustion when a high energy source ignites the volatile gases that are produced during the thermal degradation (pyrolysis) process [8, 27]. The flow of volatiles from the decomposing fuel must exceed a critical value and a sufficient amount of oxygen must be available to ensure flame propagation. In most cases, flaming

combustion can occur spontaneously under quiescent conditions provided that a continuous flux of combustible gases is generated under a high energy heat source [8]. Also, the rate of flame growth and its propagation depends on the mixing rate of the pyrolysed or evaporated gaseous fuels from the burning area. Buoyancy effects due to the temperature gradient in the heated air often lead to turbulent mixing of the volatile gases with air which increases the burning rate and the flame height. Radiant heat flux from the flame ensures a continuous thermal decomposition of the fuel substrate ahead of the flame front which often results in spontaneous ignition.

1.3 Flame Spread

The rate of fire development and spread are processes which depend on how fast flame can propagate from the point of ignition to involve a large area of the fuel. The flame propagation is very significant in determining the rate of heat release from the burning foam specimen [8, 29].

The mechanism of flame spread involves the movement of flame wave and front (also called the flame base) which occurs at the interface between the burned and unburned fuel substrate where radiant heating produces sufficient combustible gases which act as fuel. In fire safety applications, one important consideration is to determine whether a flame initiated at one point will be limited to a localised, temporary burn or develop to become a large fire. Another consideration is to determine how fast the flame spreads to involve more burning surfaces. The spread rate can also be estimated by measuring the time taken for flame front to move from one point to another on the surface of a burning fuel which results in an increase in area involved in the fire and the heat release rate.

1.4 Compartment Fires and Polyurethane Foams

During fires, polyurethane foams undergo four burning stages after ignition has occurred. These stages include the spread, burn through, pool fire and burn out [9]. The spread phase is the time taken for the flame to engulf the entire surface of the polymer while burn through occurs when the foam begins to fail, forming and spilling the molten foam onto a surface that may be remote from their original location. During this stage, the molten foam burns at a steady rate with the generation of peak heat release rate (PHRR). The burn out phase is characterised by a gradual decay in the heat release rate and the depletion of the pool fire.

For polyurethane foam burning in an enclosure, the peak heat release rate is a basis for prediction of onset of hazardous conditions, property and structural damage, changes in burning rate, ignition of objects, and onset of flashover. As shown in Figure 1-1, fire development in an enclosure follows four stages. These include the growth and pre-flashover stage, flashover, fully developed fire and decay stages [8, 30]. The period during which the fire begins is the initial stage while the time lag from ignition to the moment when substantial growth begins is called the incubation time. Following ignition and depending on the fire response of the materials that are burning, the fire grows and develops in terms of its heat release rate and combustion product generation (early stages of fire), shown in Figure 1-2a.

However, the fire may burn itself out if there is inadequate ventilation (shown by the dotted line in Figure 1-1). With the generation of large quantity of energy and involvement of other combustibles within the compartment, the fire transits from a localized burning to a fully-developed fire at the point called flashover, shown in Figure 1-2b. In most cases, flashover may occur prior to the peak heat release rate. This instantaneous transition causes rapid thermal changes in the compartment environment and results when the effective temperature of the hot gas layer becomes sufficient to produce a radiant heat flux exceeding that required for the ignition of the other combustible products in the enclosure.

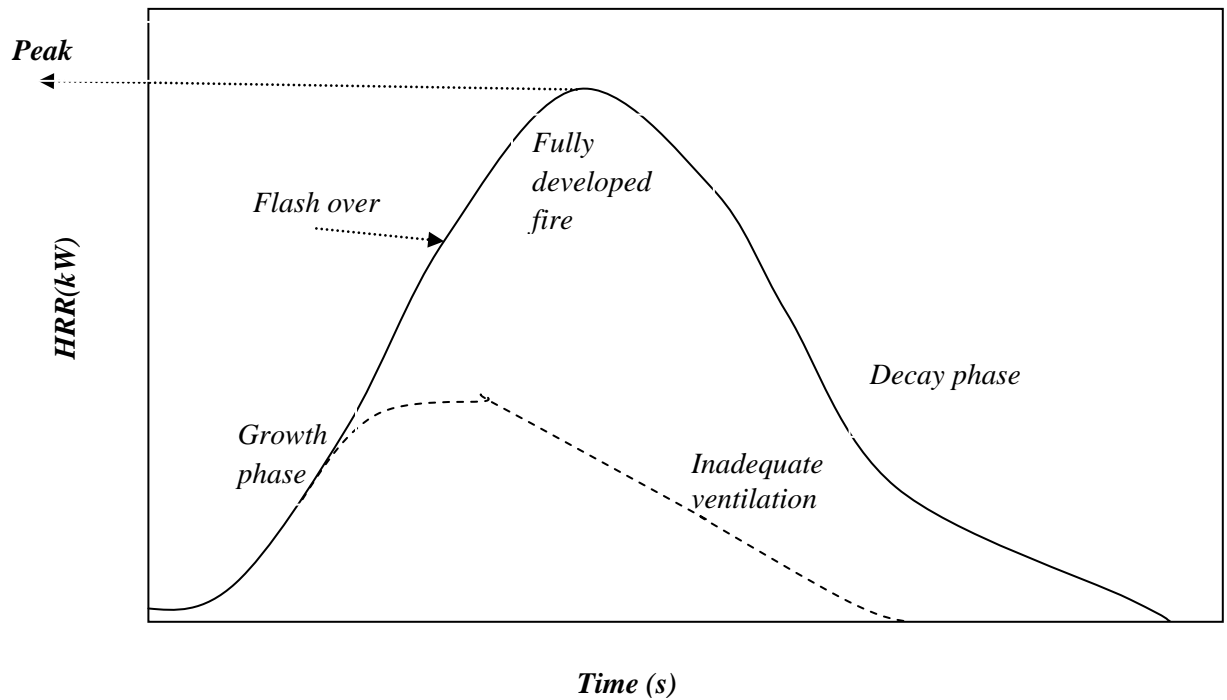


Figure 1-1. Idealized fire HRR profile [8].

For fires in a small room, flashover occurs at approximately 1,000 kW although the peak heat release rate may be as high as 2,000 kW or more. The temperature in the hot gas layer at flashover is within 600-1000°C during which flames exit through openings and spread to other spaces thereby making escape from the compartment impossible, as shown in Figure 1-2b. During this stage, depending on the size of ventilation openings in the enclosure, more fuel can be pyrolysed than can be burnt with the available oxygen which results in a condition called a ventilation-controlled fire. However, as the fuel becomes consumed and the heat generation reduces, the decay phase occurs and the fire becomes fuel-controlled [8].



(a)



(b)

Figure 1-2. Photographs at early stages of room fire (a) and at flashover (b).

1.5 Pool Fires

One of the consequences of polyurethane combustion is the potential for formation of pool fires which involve a horizontal, upwards-facing, combustible fuel in the liquid phase. Pool fires result when the polymer melts and forms a liquid-like fuel that flows, forming a pool of fire that may be remote from the original location of the fire [9]. Once the fire is established, gases evaporate rapidly from the liquid fuel as it is heated by radiation and convective heat transfer.

This re-radiation creates a feedback process whereby more gases become vaporized from the liquid surface. The surface flame increases in size in a continuing process of radiation and convection heating to the substrate area until almost the entire surface of the fuel is on fire.

In a fully developed pool fire, heat from the flames vaporises more fuel (substrate) which increases flame size and increases heat transfer to the fuel pool. The evaporation

rate eventually reaches a maximum depending on the intensity of the radiative and convective heat transfer from the flame [28]. The shape of the flame is generally dependent upon pool diameter (D), length or height of the flame (H_f), tilt (θ) and the stretching of its base (L) in the direction of the wind [28, 32].

Wind speed and air entrainment are significant variables in pool fires as they strongly affect the flame spread, flame tilt and length. The flame spread over a liquid pool is often rapid in the wind direction which increases pool diameter, rate of substrate (polymer) degradation, burning rate and heat release rate [33]. As the pool diameter increases, which suggests a large surface area for pool burning, the rate of heat release and burning rate become very high for a short duration whereas spills with a smaller surface area burn with a lower heat release rate for a longer duration [28, 33]. A more detailed treatment of pool fire modeling can be found in the following references [31, 32, 34-36].

1.6 Oxygen Consumption Calorimetry

The information obtained from standard tests of polyurethane foams and other products is used for comparing the expected fire behaviour of materials under conditions that are similar to the test scenario. Data includes the heat release rate, peak heat release rate, total heat release, heat of combustion, flame spread rate, time to ignition and smoke production rate. Of significant interest to fire researchers is the heat release rate (expressed in kW) which is the single most important flammability variable that represents the size and intensity of any fire [37-40].

A reliable technique for obtaining these fire variables, especially the heat release rate, is generally based on the principle of oxygen consumption calorimetry [41]. This principle holds that for a large number of organic liquids and gases, a nearly constant net amount of heat, 13.1 MJ/kg, is released per unit mass of oxygen consumed for complete combustion with an accuracy of $\pm 5\%$.

In using this technique, the amount of heat released by burning a specimen is estimated by measuring the reduction of oxygen in the fire. The basic objective for using the oxygen consumption technique is to account for all combustion products from a burning specimen assuming that the products underwent complete combustion. The principle of oxygen consumption calorimetry has led to the development of two general approaches for measuring heat release rates: full-scale fire test methods and small-scale fire methods [24, 27].

1.7 Large-Scale Fire Tests

Full-scale fire tests are used to evaluate the fire behaviour of products under conditions that are similar to those expected in a real fire scenario. There are a number of full-scale fire tests such as ASTM E 1590 [42], ASTM E 2067 [43] and ISO 9705 [44] that operate on the principle of oxygen consumption calorimetry. These laboratory-based full-scale fire tests are used to measure parameters such as the heat release rate, smoke production, temperature and ignitability [45]. Fire tests in full-scale are conducted in line with standardized regulations specified by organizations such as the American Society for Testing and Materials (ASTM), International Organization for Standardization (ISO) and Underwriters' Laboratory of Canada (ULC). Full-scale tests include furniture calorimeter tests, room tests and intermediate-scale calorimeter tests [43]. The major drawbacks associated with full-scale fire tests are that such tests are very expensive, there are limited test facilities and they take a long period of time to set up and run. However, advances in small-scale tests and computer fire modeling are reducing the use of full-scale fire tests.

1.7.1 Furniture Calorimeter

The furniture calorimeter equipment shown in Figure 1-3 was specifically designed for full-scale fire tests of furniture specimens such as mattresses, sofas and chairs while they are burning under open-air conditions [46]. To use the equipment, the specimen is

placed on a load platform to measure the mass loss rate during the test. An ignition source such as a propane burner is used and the products of combustion flow up and are collected in a hood. Instrumentation in the exhaust duct, gas analysis unit and a computer software are used to determine test results. ASTM test standards have been developed for chairs, mattresses and stacked chairs with the corresponding designations of ASTM E 1537 [47], ASTM E 1590 [42] and ASTM E 1822 [48] respectively.



Figure 1-3. University of Waterloo Furniture Calorimeter

1.7.2 Room Fire Tests

The room fire test is a full-scale test method designed to evaluate compartment-lining materials and fire-restricting materials [44]. The method evaluates the fire characteristics of the surface products (which cannot be tested in small scale, for

example thermoplastic materials) in a simulated room fire scenario. The typical room size measures 3.6 by 2.4 by 2.4 m (length, width and height respectively) with a doorway of dimension 0.8 by 2.0 m. Aside from measuring heat release rate, the total heat release and smoke production, the room corner test is designed to facilitate the study of room flashover.

During tests, a specimen is mounted inside the room, on the ceiling and / or on the walls. A propane gas burner is located in one of the corners and produces a specified heat release rate (e.g., 100 kW during the first 10 minutes, and then 300 kW the following 10 minutes). Combustion gases are collected through a hood where heat release rate and smoke production are measured and flame spread along the walls and ceiling are observed visually. The test is typically stopped at flashover, when flame emerges from the door opening or another flashover criteria is met [42].

1.7.3 The Intermediate-Scale Calorimeter

This test apparatus is a special type of furniture calorimeter which is required for use with composites and non-homogenous specimens which are small enough not to require testing of a complete full-scale product. It includes a large radiant gas panel which exposes a 1 by 1 m vertical specimen, with a thickness up to 150 mm, to a heat flux of 50 kW/m². The radiant heater panel and the test specimen are mounted on a load cell, under a hood so that parameters such as heat release rate, smoke production, ignitability and flame spread, and mass loss rate of the specimens can be measured. The ASTM Intermediate Scale calorimeter standard is designated ASTM E 1623 [49].

1.8 Small-Scale Tests

Babrauskas et al [50, 51] remarked that the measurements of fire growth and spread for large specimens are challenging, as it is very expensive to burn complete specimens and there is a need for sophisticated instrumentation for data acquisition. As a result, most

fire tests are carried out using representative specimens of the complete product which is less expensive than testing with a complete structure. Small-scale tests are also usually conducted in a laboratory setting where environmental conditions such as temperatures and humidity can be controlled and where the specimens can be tested with a small laboratory flame. However, one drawback associated with most small-scale tests is that they do not reproduce the actual heat and other burning behaviour that occur in real life scenarios [39, 40]. For instance, the flame spread, melting and pool fire development that can be observed in large-scale tests of polyurethane foams are difficult to achieve with the bench-scale testing. Another drawback is that items may not completely represent an actual item (e.g., inner spring mattresses). These limitations contribute to challenges in predicting the complex full-scale or real life fire scenario from small-scale data. However, one small-scale test apparatus which is widely used in standard fire tests is the cone calorimeter.

1.8.1 Cone Calorimeter

The cone calorimeter, shown in Figure 1-4 (top), is a versatile bench-scale fire testing equipment that appears in test standards such as ISO 5660-1 or ASTM E 1354 [52]. It is used to determine the fire behaviour of specimens of a reduced size. Some of the measurements that can be made using this apparatus include heat release rate, heat of combustion, smoke production and mass loss rate.

As shown in Figure 1-4 (bottom), at the core of the instrument is a radiant electric heater in the shape of a truncated cone (from which the name is derived) which is capable of providing heat fluxes to the specimen up to 100 kW/m^2 . The heater temperature is measured as an average of the readings from thermocouples that are in contact with the heating coil.

Calibration of heat flux as a function of heater temperature is carried out using a Schmidt-Boelter heat flux sensor. The heating element irradiates a horizontal or vertical specimen of dimension 10 by 10 cm placed beneath it. Ignition is provided by an

intermittent spark igniter located above the specimen which is removed as soon as the pyrolysis products produced by the specimen are ignited. The combustion stream is captured through an exhaust duct system, consisting of a centrifugal fan, a hood, and an orifice plate.



Figure 1-4. The cone calorimeter (top) and combustion chamber (bottom).

There is a load cell for continuous monitoring of the mass of the test specimen as combustion takes place. The oxygen, carbon dioxide and carbon monoxide concentrations in the exhaust stream are measured with gas analyzers. Smoke measurements are also made in the exhaust duct by a helium-neon laser system.

The cone calorimeter and the gas analyser are connected to a data acquisition system and a computer, which records data at a fixed interval while the test is being conducted.

1.9 Standard Fire Tests For Mattresses

Several standard fire tests of upholstered products and mattresses have been established with the aim of obtaining quantitative values that describe and represent their fire behaviour under varying test scenarios [27]. The majority of standardized tests were formulated due to the need to regulate and reduce the fatalities caused in residences and public occupancies when these materials are engulfed in fire. Moreover, these fire tests are designed to facilitate the comparison of materials based on their responses to high heat fluxes and also for screening of these materials on a pass or fail basis when subjected to controlled test conditions. For instance, the standard full-scale test referred to as the Code of Federal Regulations (CFR) 1633 was introduced in July 2007 in the United States to provide a means of determining the burning behaviour of mattresses when they are subjected to open flame [53].

The California Technical Bulletin 117 is another test standard which uses only individual components of the upholstered furniture such as the fabric and padding materials in a small-scale test that exposes the specimen to a small laboratory flaming and smouldering ignition source [54]. Other small scale tests of individual components of mattresses include ASTM E 1474 [55] and the California Technical Bulletin 106 [56] used for investigating the effects of exposing a padding material to a burning cigarette in order to assess its resistance to a smouldering ignition source.

There are also standards for mattresses used in other occupancies, such as in prisons, as opposed to standards for residential mattresses. In general, the standard tests of a

mattress or mattress pad are based on full-scale and small-scale open flame ignition or the smouldering cigarette test [27].

1.9.1 Open Flame Tests

As modified cigarettes have been developed that have less ignition potential [57], current fire incident reports have shown that an increasing number of fire fatalities are due to small open flames such as candle flames, lighters and matches that are used in homes [15]. As a result, the United States Consumer Product Safety Commission (CPSC) issued a flammability standard CFR1633 under the Flammable Fabric Act which addresses the performance requirements for mattresses when exposed to open flames [15].

The primary objective of the CPSC's mattress performance standard was to regulate the size and growth rate of fires involving mattresses, which will reduce the possibility of room flashover occurring and thus reduce death and injuries [15]. The initiative was made on October 11, 2001 when the CPSC issued a legislative proposal regarding open flame ignition of mattresses. The "rulemaking" led to joint research by the California Bureau of Home Furnishings, National Institute of Standards and Technology (NIST), CPSC and the upholstery industry to develop a test standard that would regulate mattress ignition characteristics. The law also specified the quality assurance for mattress components that will not generate heat and temperatures sufficient to cause room flashover.

Prior to establishing the mattress fire criteria, two mattress sets were tested using the NIST fire test protocol which involves exposing the specimen to a pair of T-shaped propane burners and allowing the mattress specimens to burn free for a period of 30 minutes. Heat release rate and total energy generated from the specimen were measured. A peak heat release rate of 2,000 kW produced in less than 5 minutes was measured, which was in excess of the heat release rate (1,000 kW) necessary for flashover of a small room.

Based on these results, the Commission established two test criteria which every mattress set must meet. The first criterion is that mattresses should be designed such that when they are involved in fires or screened for flammability, the peak heat release rate generated will not exceed 200 kW within the first 30 minutes of the test time. Limiting the peak heat release rate to 200 kW was to ensure a safe flammability design which will allow occupants more time to discover the fire and escape, especially during the early stages of fire development. Secondly, the total heat release must not exceed 15 MJ for the first 10 minutes of the tests. The results of the CPSC legislative proposal and flammability criteria for mattresses will likely lead to new mattress safety standards and regulations in many other parts of the world. This rule became effective in the U.S on July 1, 2007.

1.10 Previous Research

Various experimental studies relating to mattress fires have been by conducted by researchers. Publications by these authors are the foundation for the experimental work in this project, while the models which focus on predicting full-scale fire behaviour of polyurethane foams from small-scale data are based on fire growth principles from previous research. Examples of previous studies that are most relevant to this project will be discussed in the following sections and in Chapter Two.

1.10.1 Combustion Behaviour of Upholstered Furniture (CBUF) Project

In 1993, the European CBUF research group made of many laboratories investigated methods of using small-scale fire test results to predict full-scale fire behaviour of upholstered materials [24]. The research was the most extensive of its kind on the combustion of upholstered furniture and mattresses. The research group developed test protocols and the structure shown in Figure 1-5 to enable the assessment of the burning behaviour of upholstered furniture and mattresses.

The project structure, was designed so as to use cone calorimeter data for individual components of upholstered furniture materials to predict cone calorimeter results of composite specimens. This is represented as process (a-b). In process (b-c), furniture calorimeter results were in turn predicted based on data from bench scale tests of composites consisting of various layers of fabric, interliners and padding used in the construction of the furniture. Finally, conditions occurring in the room scenario due to burning of a piece of furniture were predicted based on results of large scale testing of the specimen in the furniture calorimeter, represented by process (c-d).

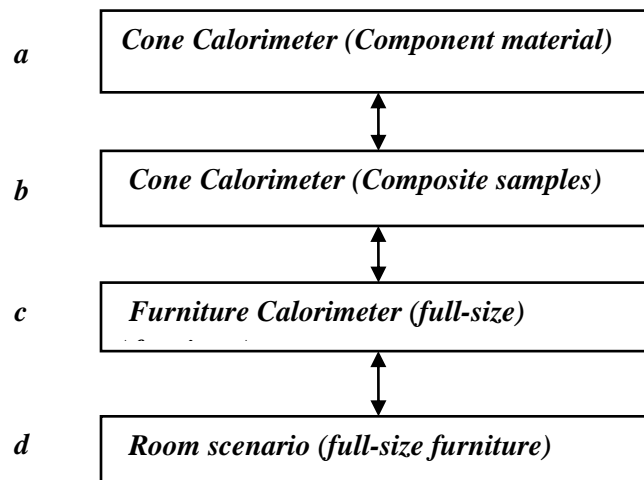


Figure 1-5. The CBUF project structure [24].

The most outstanding achievement of this program was the development of three predictive models identified as Models I, II and III which use cone calorimeter input data for full-scale prediction of upholstered furniture and mattress fires. The research group used the models to identify items that can propagate fire rapidly as well as those that did not burn on their own.

Model I is a ‘factor’ based method, based on statistically correlated factors derived from a large number of tests. This model can be used to predict the peak heat release rate,

time to peak release rate, total energy release, smoke production and the time to reach untenability in an ISO 9705 room test [44]. Model II is based on area convolution where expressions of burning area versus time are sought for various furniture geometry. The heat release rate of the burning furniture item is thus obtained by a convolution product of the cone calorimeter data and the burning area. Of interest to the current project is Model III, developed specifically for predicting the heat release rate and concurrent flame spread in mattresses which are based on a convolution integral. The fire spread model was a modification of an earlier physical model developed by Wickstrom and Goransson for upward flame spread [58, 59].

In applying Model III, CBUF researchers stated that for sustained flame propagation along a surface, the transient heat flux incident at every point for preheating must be known. The total heat release rate from the burning area was obtained by integrating the heat release rate density from the cone calorimeter obtained using an incident heat flux of 35 kW/m^2 and the flame area $A_f(t)$ obtained from the full-scale test.

In one of the CBUF experimental investigations, two mattress specimens made of the same materials but of different design were tested. One specimen was made of solid foam while the other specimen was of inner spring construction. They were chosen to represent different fire behaviours of mattresses. A square propane gas burner that was regulated to generate 35 kW of heat was used to produce flaming ignition for 2 minutes. The mattresses were ignited at their geometric centers (center ignition). The solid foam showed flame propagation and burnt totally while the innerspring mattress did not propagate fire, rather it smouldered for a while and self-extinguished due to reduced combustible mass. Visual observation of the flame front and geometry showed that the flame area or burning area $A_f(t)$ was circular in geometry with the fire spreading radially outwards. The flame plume was approximated as a cylinder. These flame geometries were used for obtaining flame area and heat flux distribution on the mattresses.

In the analysis of their experimental and numerical results, the CBUF research group reported that Model III did a reasonable job of predicting the full-scale fire behaviour of the tested mattresses. The predicted and measured heat release rate curves showed a fair agreement especially at the early part of the curve and at the peak. The investigators stated that the model is valid as a good predictive tool for mattress fires where no burn-through of the foam has occurred. Detailed discussion about this model will be made in Chapter Two.

1.10.2 Consumer Product Safety Commission (CPSC) Project

Another experimental study of mattress fires was conducted by the CPSC group made up of NIST, California Bureau of Home Furnishings and the upholstered furniture industry [15]. Their test protocol and flammability standard referred to as Code of Federal Regulations (CFR) 1633 (open flame) provided the foundation for screening and assessing the fire hazard associated with mattress fires, especially residential fires involving mattresses ignited by open flame sources. The goal of the CPSC project was to develop performance requirements which all mattress sets must meet before being introduced to the public.

The Commission tested two different mattress sets using NIST's full-scale test protocol [24]. The specimens were conditioned to a temperature range of 18°C to 25°C and a relative humidity below 55%. The test environment temperature ranged from 15°C to 27°C and relative humidities were less than 75%. The specimens were tested within 20 minutes after removal from the controlled storage conditions. T-shaped propane burners with burner-hole diameter of 1.17 mm were used to ignite the top and side (edge ignition) of the mattress for 70 s and 50 s respectively. Burners with smaller hole diameters were also used from trial to trial to compare the effects of different ignition sources on the experimental results.

In most of the trials, a peak heat release rate of 2,000 kW was generated in less than 5 minutes, which was higher than the heat release rate (1,000 kW) necessary for flashover

of a small room. Based on this result, the Commission established two test criteria that commercial mattresses must meet to pass the screening as discussed in section 1.9.1. Also, in assessing the effects of the different burner sizes on the fire behaviour of the mattresses, CPSC reported that the results due to using different burner diameters showed significant variations, with burners of larger hole size doing a better job of meeting the target peak flux levels than do the burners with smaller holes. The significance of this project is to ensure that mattress manufacturers meet the safety standard by adopting a less flammable mattress design. The project was a major initiative towards screening of upholstered materials for fire.

1.10.3 Previous Research at the University of Saskatchewan

Full-scale mattress tests were conducted by Threlfall [60] in Edmonton, Alberta, in September, 2004 in an abandoned office building. The primary purpose of the investigation was to measure temperatures and heat fluxes during a set of three mattress fires in the abandoned office building. The tests were conducted in a room with dimensions of 3.7 m by 4.3 m and a ceiling height of 2.7 m. Two sides of the walls were lined with dry wall while the other two sides were lined with metal sheet. There was a door-sized opening with dimensions of 0.8 by 2.0 m high. Two mattresses made from polyurethane foam and one other made from fibre and rayon were tested in the room. Several thermocouples and heat flux sensors used to measure temperatures and heat fluxes were located over the mattress on the ceiling and from the ceiling to the floor at an interval of 0.6 m.

During the test, the mattresses made of polyurethane foam burned completely while the other made from fibre and rayon smouldered without sustained flaming combustion. The tests were captured using infra-red and regular video cameras. Peak temperatures measured during the test of the completely burned polyurethane mattresses varied while there was no significant temperature increases in the room during the test of fibre and rayon mattress. Using several fire protection engineering correlations such as the Alpert

ceiling temperature correlation and the t-squared fire growth model [60], the measured temperatures were compared with predicted temperatures. The comparison showed better agreement at early stages of the test for mattress 1 than for mattress 2, as shown in Figure 1-6. These differences were due to the difficulty in estimating the appropriate fire growth coefficient for those mattress specimens. Also, flame spread rates for the specimens were not considered.

As an advancement of the Edmonton 2004 project, the fire research teams at the Universities of Saskatchewan and Waterloo conducted a study of solid-core mattresses (polyurethane foam) in July and November, 2006 using cone and furniture calorimeters. The study was designed to provide data on the fire response of various mattress specimens which would be used for developing correlations between small-scale and full-scale tests, and ultimately to predict real-life/room fire scenarios.

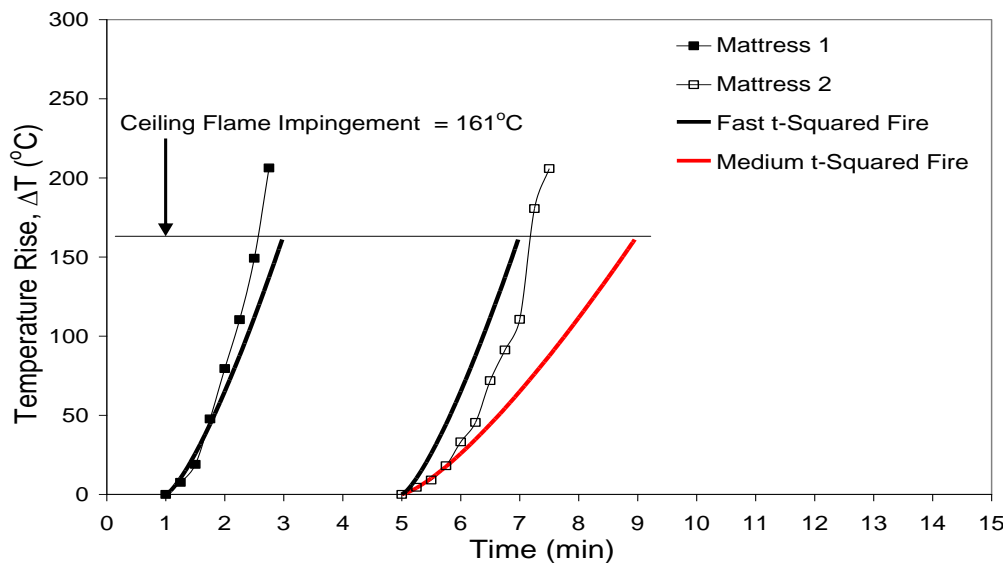


Figure 1-6. Comparison of measured and predicted temperatures [60].

At the University of Waterloo, three foam sizes of 0.6 by 1.2 m by 5 cm, 0.6 by 1.2 m by 10 cm and 1.2 by 1.2 m by 10 cm were tested. Before being ignited with a small hand-held propane torch, the top of the specimens were marked in a grid pattern of 10 by 10 cm squares similar in size to cone calorimeter specimens as shown in

Figure 1-7. The flame area spread $A_f(t)$ were determined from video records and digital photos. The results of the tests showed that heat release rate varied with dimensions of each specimen as shown in Figure 1-8.



a) Ignition $t = 0$.

b) Elapsed Time = 126 s ($A_f = 0.4 \text{ m}^2$)

Figure 1-7. Photographs of furniture calorimeter test of 1.2 by 1.2 m by 10 cm foam specimen [61].

For cone calorimeter tests conducted at the University of Saskatchewan, 10 by 10 cm by 5 cm thick specimen of the same polyurethane foam were conditioned in a container at 20°C and 80% relative humidity for 48 hours with the objective of providing data at similar conditions to the full-scale tests at the University of Waterloo in July 2006. Cone calorimeter tests of the foams were conducted using an incident heat flux of 35 kW/m². The average heat release rate density for the first 60 s of the cone calorimeter test was approximately 280 kW/m² as shown in Figure 1-9 [61].

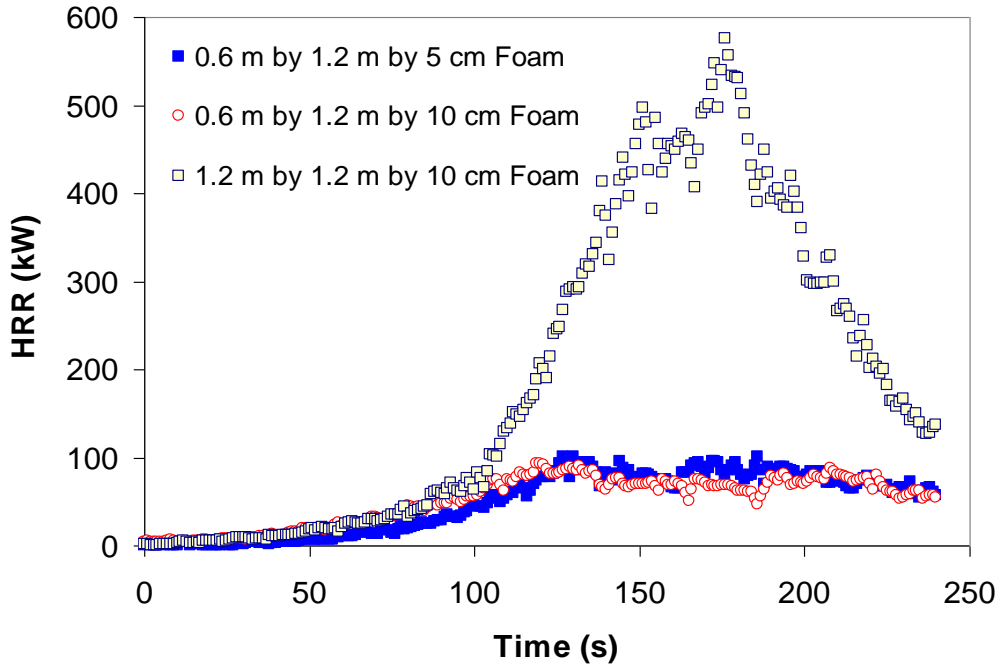


Figure 1-8. Comparison of HRR curves measured in furniture calorimeter tests of various pieces of polyurethane foam [61].

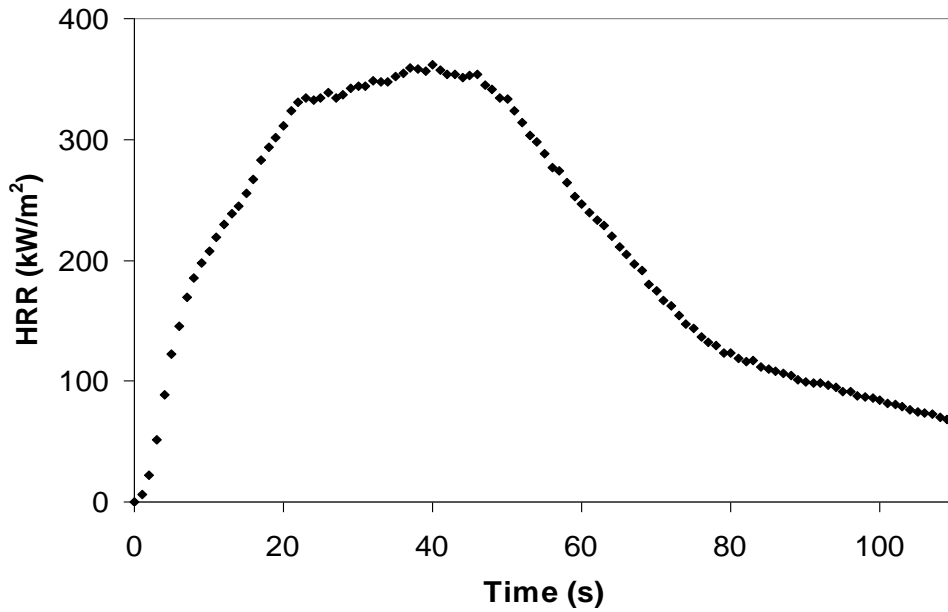


Figure 1-9. HRR density from cone calorimeter tests of 5cm thick pieces of polyurethane foam [61].

Two modeling techniques (t-squared model and time-dependent fire area models $A_f(t)$) were used to predict full-scale fire behaviour of the mattresses from cone calorimeter data. As shown in Figure 1-10, the predictions using the two models were similar to full-scale measurements. However, the flame spread model over-predicted the heat release rate early in fire, due to using the average heat release rate density in the model which was higher than the heat release rate density values for about the first 20 seconds of the cone calorimeter test.

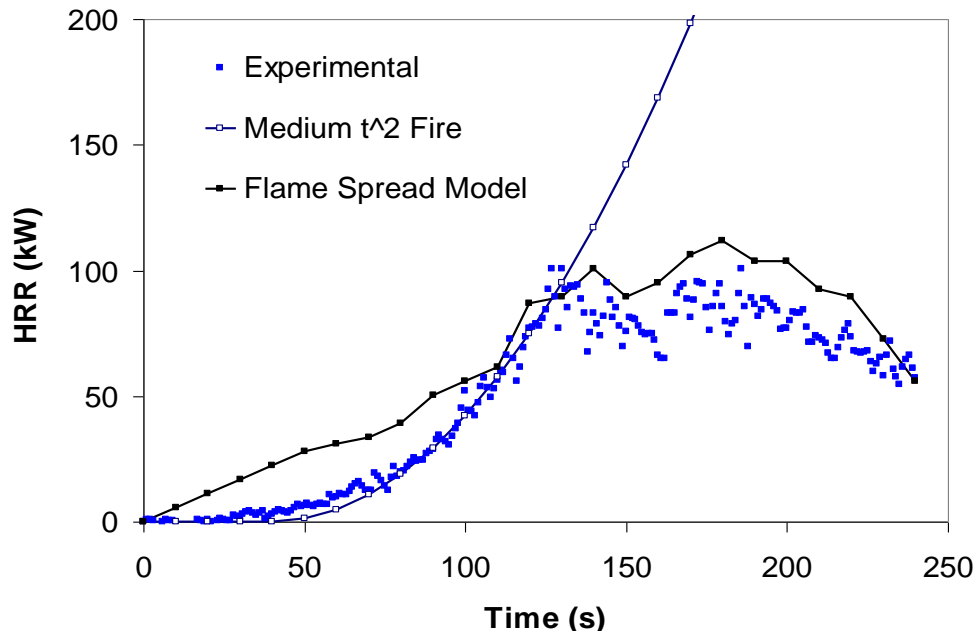


Figure 1-10. Comparison of HRR measured during test of 0.6 by 1.2 m by 5 cm specimen and predicted using medium t^2 fire and flame spread model [61].

The drawback associated with the flame spread model is that it assumes that the fire of the small scale specimen is stationary and an average HRR density is used in the model. The use of a constant HRR density in the prediction does not represent the transient fire behaviour, thus, the model may not be an efficient predictive tool which is evident in the variation of the predicted of HRR profile especially at the growth. This is shown by the over-prediction of the early stages of the fire in Figure 1-10. For the t -squared fire

model, the predicted fire growth was achieved by using a suitable fire growth coefficient that could fit the measured HRR curve.

Thus to overcome this shortcoming and reduce the uncertainty in the heat release rate values, finer modeling techniques are needed. Certainly, if accurate predictions of large-scale tests and real life fire behaviour are to be made from small-scale experimental data, then an accurate and reliable representation of fire growth and spread in a given fire scenario must be made. Hence, a more sophisticated model is needed which will generate more dependable data for full-scale fires, which is an area of focus in the current project.

1.11 Research Objectives And Scope

1. The major objective of this project was to investigate the use of several fire protection engineering correlations and models that can be used to predict the heat release rates and flame spread rates for full-scale tests of polyurethane foam specimens, based on information obtained from cone calorimeter tests.
2. A related objective was to gather cone and furniture calorimeter test data for polyurethane foams under more tightly controlled environmental conditions than in previous studies conducted by the research group, so that these data could be used to evaluate the fire protection engineering correlations and models.
3. One secondary objective was to use the furniture calorimeter data to compare the effects of ignition location on heat release and flame spread rates in full-scale fire tests.
4. Another secondary objective was to look at the effect of thickness and different testing arrangements on cone calorimeter results.

As the University of Saskatchewan does not have a furniture calorimeter and the gas analyzer unit on the fire research group's cone calorimeter was not functional during this research project, the cone and furniture calorimeter tests described in this thesis were

conducted at the University of Waterloo by personnel in their laboratory. The author of this thesis participated in the design of the experiments and was responsible for analyzing all of the test data and image analysis, and then used this test data to evaluate the fire models that are discussed in this thesis. Separate cone calorimeter tests were also conducted by the author for investigation of vertical flame spread rates.

1.12 Thesis Outline

The thesis is presented in six chapters. Chapter one provides an overview of combustion of flexible polyurethane foams and the economic and societal concerns relating to their flammability. Some of the works and regulatory standards involving the fire behaviour of polyurethane foams are discussed. Thermal models and various predictive techniques for fire growth and flame spread in polyurethane foams are detailed in Chapter Two. The convolution integral formulation which connects the small-scale and full-scale polyurethane fires is established. Chapter Three will provide the experimental methodologies and instrumentation for the full-scale fire tests of the polyurethane foams, and present and discuss the results from the experimental investigation. The small-scale tests of the polyurethane foams will be discussed in Chapter Four. Chapter Five will discuss the results from the numerical models and fire protection engineering correlations. Numerical and experimental results will be compared in Chapter Six. Conclusions and recommended future work will be presented in Chapter Seven.

CHAPTER TWO: MODELS FOR POLYURETHANE FOAM FIRES

Fire is a complex phenomenon that involves a series of chemical and physical processes that are dependent on the nature of fuel, ignition source and air supply [8]. The complexities associated with fires in real life makes their modeling a difficult task [63]. As a result, mathematical models which predict fire behaviour of materials in an approximated form such as the heat release rate curve of a fire from ignition to a peak value and the decay are needed. Predictions using the mathematical models are usually based on experimental data that are gathered from fire test apparatus such as the cone calorimeter and the furniture calorimeter. The information that is acquired from these laboratory equipment serve as input data for validation of fire models [20].

The subject of this chapter is to outline various fire models that predict the consequences of a fire scenario. The models are essentially fire protection engineering models and correlations which are used for calculation of heat release rates as opposed to detailed, research type models such as Computational Fluid Dynamics (CFD) models. Heat transfer, which is fundamental to flaming combustion and the subsequent flame spread mechanism, will first be discussed. Models that can be used to model flame spread are then discussed. Various techniques of calculating the heat release rate such as the convolution integral model, flame spread model and the t-squared fire growth model will also be discussed.

2.1 Heat Transfer Model

Heat transfer is the driving force for ignition and development of fire on any combustible fuel including the polyurethane foams. Heating is important in fire modeling as it is one of the important parameters that determine the flammability behaviour of a material. This is because the incident heat flux determines whether ignition and sustained flaming combustion on materials are feasible as most materials will not burn in air without an external heat flux [8]. Most importantly, the level of heat irradiance is very significant in determining the rate of heat release from fuels during

fires [32]. Examples of heat irradiance include the heat flux from electric pilot igniter and irradiant heater in the cone calorimeter, small burner flames or a propane torch used in furniture calorimeter tests or radiant heat from large flames, which are composed of both convective and radiative components [8,19, 22]. Leung [64] presented the generalised expression for the effective heat flux as:

$$q_t'' = q_e'' + q_c'' + q_f'' \quad (2-1)$$

where:

q_t'' = total heat flux conducted into the fuel (W/m^2)

q_e'' = the total heat flux incident on the fuel (W/m^2)

q_f'' = the radiative feedback from the burning area of the fuel (W/m^2)

q_c'' = the convective and radiative heat loss from the fuel which is expressed as

$$q_c'' = -h_c(T_s(t) - T_\infty) - \varepsilon\sigma(T_s^4(t) - T_\infty^4) \quad (2-2)$$

$$q_c'' \cong -h_{eff}(T_s(t) - T_\infty) \quad (2-3)$$

where:

h_c = convective heat transfer coefficient ($W / m^2 \cdot K$)

ε = surface emissivity

σ = Stefan Boltzmann constant ($5.67 \times 10^{-8} W / m^2 \cdot K^4$)

h_{eff} = effective heat loss coefficient due to convective and radiative heat transfer
($W / m^2 \cdot K$)

$T_s(t)$ = transient surface temperature of the fuel assumed equivalent to flame temperature (K)

T_∞ = ambient temperature (K)

From heat transfer principles, the heat conduction in the fuel can be represented by the Fourier field equation in Cartesian coordinates given by [23]:

$$\rho c \frac{\partial T}{\partial t} = \frac{\partial}{\partial x} \left(k \frac{\partial T}{\partial x} \right) + \frac{\partial}{\partial y} \left(k \frac{\partial T}{\partial y} \right) + \frac{\partial}{\partial z} \left(k \frac{\partial T}{\partial z} \right) \quad (2-4)$$

where:

T = temperature (K)

t = time (s)

c = specific heat capacity of the foam (J / kg · K)

ρ = density of the foam (kg/m³)

k = thermal conductivity (W / m · K)

Assuming heat penetration occurs only in the vertical direction y, the Fourier field equation can be simplified as one dimensional heat conduction equation in the y direction, given by:

$$\rho c \frac{\partial T}{\partial t} = \frac{\partial}{\partial y} \left(k \frac{\partial T}{\partial y} \right) \quad (2-5)$$

Assuming that the thermal properties (k, c, ρ) do not vary with temperature, the equation becomes:

$$\frac{\partial T}{\partial t} = \frac{k}{\rho c} \frac{\partial^2 T}{\partial y^2} \quad (2-6a)$$

$$\frac{\partial T}{\partial t} = \alpha \frac{\partial^2 T}{\partial y^2} \quad (2-6b)$$

where:

$$\alpha = \frac{k}{\rho c} \text{ is the thermal diffusivity (m}^2\text{/s).}$$

At the surface of the fuel ($y=0$), the effective heat irradiance is the conduction heat flux given as [64]:

$$q_t'' \equiv -k \frac{dT}{dy} \quad (2-7)$$

Equation (2-7) is the net heat irradiance that initiates pyrolysis, ignition and flaming combustion. During preheating prior to flaming combustion, the radiative heat flux term in Equation (2-2) is very small since the flame size is small and then is assumed to be negligible. However, with continuous heating, the surface temperature T_s increases to ignition temperature T_{ig} at which point sufficient volatile gases are produced to cause flaming combustion. This flame from the burning surface produces a radiant heat flux represented by [24]:

$$q'' = \Phi \varepsilon_f \sigma T_f^4 \quad (2-8)$$

where:

T_f = flame temperature (K)

Φ = view factor which is a function of the flame height (z) and radial position (r)

$\varepsilon_f = \text{flame emissivity (dimensionless)}$.

The heat flux from the flame causes an increase in the flame spread as fuel ahead of the burning area is pyrolysed. The radiative feedback effect enhances the rate of burning which causes an increase in heat release rate. Subsequent heat flux incident at any point on the fuel surface is dependent on the size and shape of the flame from the burning area [24]. However, the radiant heat flux decreases in intensity with increasing radial distance from the flame front. The radial distance away from the flame front where the heat flux is assumed to be independent of flame size and shape, is called the exposure range (r_p), which is heat release rate dependent. It is expressed as [24]:

$$r_p = k_f \dot{Q}^n \quad (2-9)$$

where:

$\dot{Q} = \text{HRR from the fire (kW)}$

$n = 0.62$

$$k_f = f(\dot{Q}(t) / A(t)) \cong 30.7 \left[m(kW m^{-2})^{1-n} \right] (\dot{Q} / A_p)^{-0.88} \quad (2-10)$$

The height of the flame cylinder above the burning surface is given as:

$$z_f = -1.022r_f + 0.0235\dot{Q}^{2/3} \quad (2-11)$$

and the flame emissivity is given as:

$$\varepsilon_f = 1 - \exp(-k_m r_m) \quad (2-12)$$

where:

$r_f = \text{flame front (m)}$

$k_m = \text{flame absorption coefficient assumed to be } 1m^{-1}$

$$r_m = \text{the optical mean beam length given as } 3.5V_f / A_f \quad (m)$$

$$V_f = \text{volume of flame column } (m^3)$$

$$A_f = \text{area of flame } (m^2)$$

2.2 Flame Spread Models

A number of flame spread models have been developed for description and prediction of fire growth on combustible materials. One remarkable feature common to most flame area models is that they have the ability to predict a power law, such as the t-squared fire model (which will be discussed in section 2.3.2), that guides the growth of the fire from ignition to a peak burning area [65, 66]. As most combustible products are easily ignited, one important objective for developing flame area models is to determine if a fire grows (self propagating fire) after flaming ignition has occurred. Another purpose is to determine the flame spread rate which is used to characterize how rapidly the fire propagates on the burning fuel. For instance, Figure 2-1 shows an idealised flame propagation pattern on the surface of a thin polyurethane foam ignited at the edge.

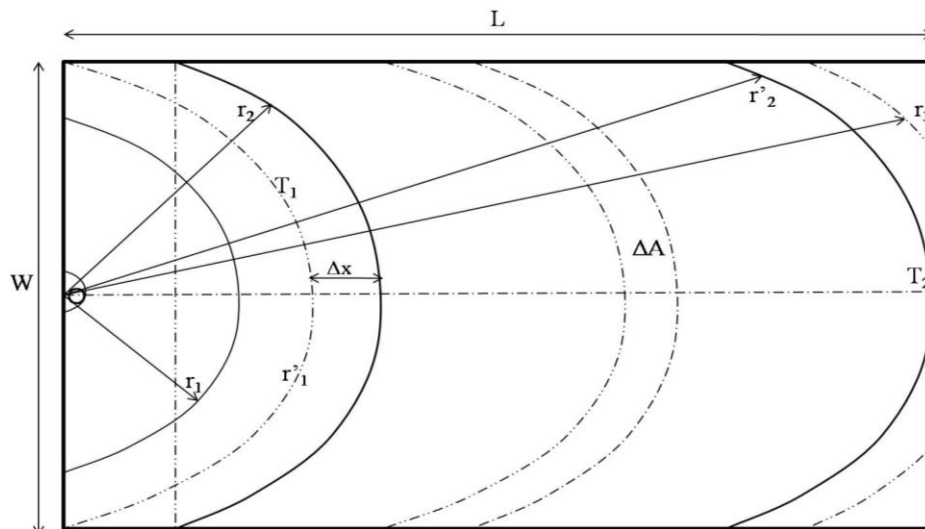


Figure 2-1. Idealized flame spread mechanism for an edge-ignited specimen.

As shown in the sketch (Figure 2-1), the flame spread initiates from the point of ignition and propagates across the width (W) of the specimen at a uniform rate \dot{r} , maintaining a semi-circular pattern. As the flame front reaches the edge of the specimen (transition point T_1), there is a sudden change in the spread pattern and then the flame front assumes a different profile and spreads at a uniform rate until the entire surface (L) is engulfed in flame. Using this idealised flame spread pattern, the flame area and spread rates can be estimated with reasonable accuracy.

2.2.1 CBUF Flame Spread Model

Babrauskas et al. [24] developed and implemented flame spread models which are used for assessing the burning of upholstered furniture as part of the CBUF research programme. A specialised thermal model for flame spread incorporated in CBUF Model III accounts for flame spread for a burning mattress [24]. One significant purpose for developing the flame model was to identify the breakpoint between propagating and non-propagating mattress fires as occurring between a three-minute average heat release rate density of 90-125 kW/m², as measured in the cone calorimeter using a 35 kW/m² heat irradiance.

The one dimensional differential equation for upward flame spread modified by the CBUF group for horizontal flame spread on mattresses is given by [24]:

$$\frac{dr_f}{dt} = \frac{r_p - r_f}{\tau_{ig}} \quad (2-13)$$

where:

r_f = flame radius (m)

r_p = exposure range which varies with heat release rate from the burning area

as given in Equation (2-9). It is the radial distance from center of flame to

any point away from the flame front (m)

τ_{ig} = a time constant referred to as ignition time (s).

At the time of ignition, $t = 0$, the initial flame radius $r_f(0) = r_{fo}$ and for a propagating fire, Equation (2-13) is written as:

$$\frac{dr_f(t)}{dt} = \frac{r_f(t) - r_p(t)}{\tau_{ig}} > 0 \quad (2-14)$$

For a fire that does not grow after ignition (non-propagating fire), Equation (2-14) becomes:

$$\frac{dr_f(t)}{dt} < 0 \quad (2-15)$$

Assuming a polyurethane specimen of length L and width W as shown in Figure 2-1, the flame spread will be limited to the dimensions of the specimen and the flame growth will terminate when $r_f \geq L$. At this instant, Equation (2-14) becomes:

$$\frac{dr_f}{dt} = 0 \quad (2-16)$$

However, when flame radius r_f is within the boundaries of the specimen ($R < r_f < L$), especially for a center-ignited specimen, the flame spread rate is assumed to be constant, thus Equation (2-14) becomes:

$$\frac{dr_f}{dt} = \dot{r} \equiv r_f(t_R) \quad (2-17)$$

where :

\dot{r} = linear regression rate or flame spread rate (mm/s) until the maximum flame radius R is attained.

2.2.2 Burning Area Model for Combustible Lining Materials

Wickstrom and Goransson [58, 59] developed an area growth model based on observations of flame spread on wall and ceiling materials during a room/corner test. The model was intended to be used to predict four phases of fire growth. Wickstrom remarked that the flame growth model gives realistic results of flame development observed for thin materials and that the prediction (flame area growth) obtained using the model is proportional to the ease of ignition and heat release properties of the specimen in the cone calorimeter. In using the model, Wickstrom and Goransson [58] assumed that the heat release rate history for each burning point on the specimen's surface in the full-scale has the same history as the cone calorimeter specimen when tested at a heat flux of 25 kW/m². Thus, the total heat release for the product is obtained by summing the contributions from each part of the total burning area.

The area growth function is given as:

$$A(t) = A_0 \left[1 + a \frac{(t - t_x)^2}{t_{ign}} \right] \quad (2-18)$$

where:

A_0 = Initial burning area assumed as the area behind the burner (m²)

a = empirical constant representing the fire growth constant. For the specimen used by Wickstrom, the constant was found to be 0.025 s⁻¹.

t_{ign} = time to ignition of the specimen on the cone calorimeter.

t_x = value chosen in relation to the burning area growth.

Taking the time derivative of Equation (2-18) gives the differential burning area (m²) of the specimen as:

$$\Delta A = \left(\frac{2A_0 a}{t_{ign}} \right) (t - t_x) \Delta t \quad (2-19)$$

Equations (2-18) and (2-19) indicate an inverse relationship between flame area and the ignition time in the cone calorimeter test. Equations (2-18) and (2-19) can be used for full-scale heat release rate prediction models as will be discussed in the next section. For self propagating fires typical of polyurethane burn, the area growth curve follows a rapid growth pattern as shown in Figure 2-2.

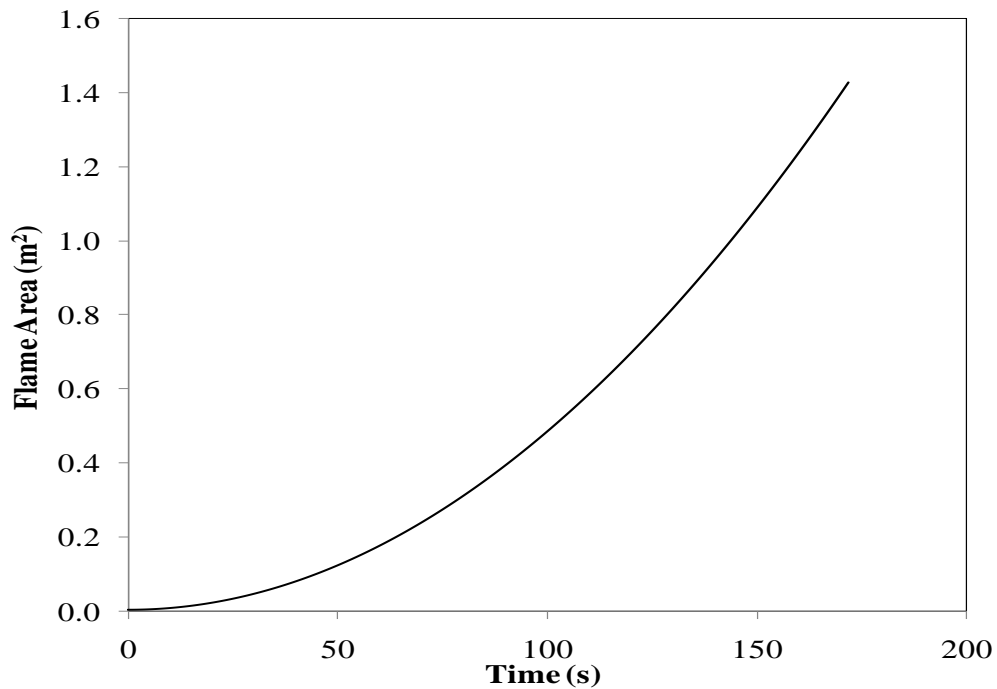


Figure 2-2. Example of ideal flame area growth showing an exponential profile.

For materials of high ignitability, the flame area growth follows an exponential curve with time. The idealised flame area growth shown in Figure 2-2 was produced using an ignition time of 2 s from a cone calorimeter test of a foam specimen, and an initial burning area of 0.00321 m^2 as determined during full-scale specimen tests for this project. An empirical constant ($a = 0.025 \text{ s}^{-1}$) for propagating fire and $t_x = 0.2 \text{ s}$ were adopted from Wickstrom and Goransson's work. A major drawback with using this

model in the current research is that the model was originally developed for homogenous wall and ceiling linings such as wood, which have considerable larger values of thermal inertia ($k\rho c$) than polyurethane forms.

2.2.3 Single Burning Item (SBI) Model

Hansen [67] presented a modified predictive model for calculating flame area, which was also referred to as effective heat releasing area in the Single Burning Item (SBI) test. The SBI test was developed in Europe among laboratories for testing individual fuel items using an ignition source, such as a wastebasket, in a room/corner scenario. The test involved placing the fire source in a corner between two walls covered with the lining to be tested.

The model is based on Wickstrom and Goransson's model described in the previous section [58, 59]. The model was modified to predict the heat release rate a product will attain in the SBI test based on cone calorimeter test results. The flame area model is incorporated in the Fire Growth Rate Index (FIGRA) which is used for classifying products in Europe based on the maximum value of the ratio between heat release rate and the time the heat release rate is measured. As a burning area is the source of heat released, Hansen [67] remarked that the use of the time derivative of effective burning area in Duhamel's formula, as will be shown in the next section, is significant for full-scale heat release rate prediction. The expression for the effective heat release area model is given as:

$$A_{HRR,eff}(t) = A_{max,HRR} \left[1 - \left(1 + \frac{t - t_0}{2} \right) \exp \left(-\frac{t - t_0}{t_0} \right) \right] \quad (2-20)$$

where:

A_{max} = maximum area involved

$t_0 \cong t_{ign} = \text{time to ignition at } 40 \text{ kW/m}^2 \text{ in the cone calorimeter.}$

Hansen [67] remarked that the value of ignition time determines the effectiveness of the model as a predictive tool. An extended ignition time was reported to give a slow growth in flame area and a low heat release rate compared to predictions made using a short ignition time. Hansen [67] suggested the use of an ignition time ranging between 10 and 30 s for a more realistic prediction instead of using the apparent time to ignition from cone calorimeter tests, since most materials behave as thermally thick materials with extended ignition times. The apparent time to ignition is the time when the heat release density of 50 kW/m^2 is exceeded in a cone calorimeter test of a specimen.

Hansen also reported that the value of $A_{HRR,eff}$ is dependent on the total heat release rate from the product [67]. For a product with total heat release rate greater than 75 kW, Hansen proposed the use of 0.6 m^2 for $A_{HRR,eff}$. Analysing the results obtained by use of this area model, it was noted that flame spread for materials generally follows one of three routes. The first route accounts for materials of low combustibility with a low value of $A_{max,HRR}$ of 0.2 m^2 , the second route accounts for materials with $A_{max,HRR}$ values ranging between 0.35 and 0.6 m^2 , while the last route is for materials of high combustibility with high initial growth rate and an $A_{max,HRR}$ value of 0.6 m^2 . Perhaps, the most significant feature of the SBI area model is the ability to show more realistic flame development and area growth rate because the models were developed based on empirical observations.

Assuming an apparent time to ignition of 15 s and a maximum burning area of 1.45 m^2 for a 1.2 by 1.2 m full-scale specimen, an example of the ideal flame growth curve is shown in Figure 2-3. As the flame area profile indicates, the model assumes that specimens' burn out never occurs during the fire and treats the maximum burning area as a steady state condition.

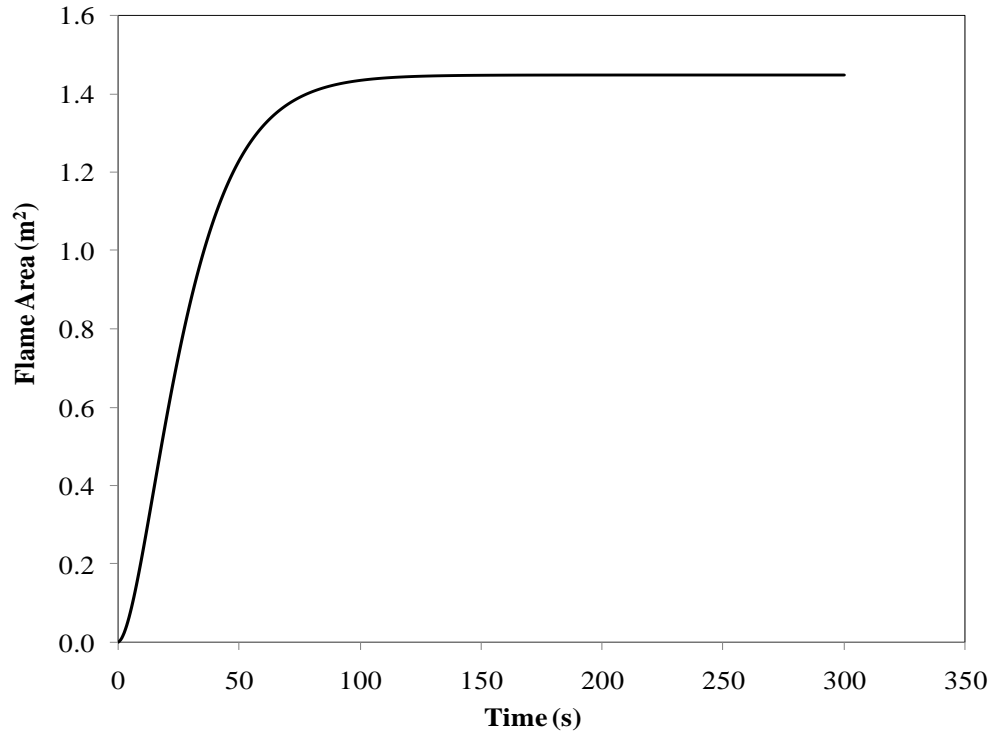


Figure 2-3. Flame area growth showing exponential and steady state profile.

This discussion of flame spread models is to illustrate the flame area growth patterns which are typical of combustible fuels. The Wickstrom and Gorrasson flame area model which will be used in the validation of the models in section 5-1, will be compared with the experimental flame areas to illustrate the correlation between the two results.

2.3 Heat Release Rate Models

2.3.1 Combustion Science Heat Release Rate Model

The generalized expression for calculating the heat release rate is the combustion science expression given in Equation 2-21. This expression has been used by fire researchers to determine the heat release rate in fire prior to the development of the oxygen consumption calorimetry which facilitated the measurement of heat release rate

and other fire variables as combustion takes place. The model assumes that heat release rate is dependent on the mass burning rate of the material, flame area of the fuel and the effective heat of combustion of the fuel [8].

$$\dot{Q} = x \cdot \dot{m}'' \cdot A_f \cdot \Delta H_{c,eff} \quad (2-21)$$

where:

\dot{Q} = heat release rate (kW)

x = factor accounting for incomplete combustion (<1.0)

\dot{m}'' = mass loss rate per unit area (kg/m²sec)

A_f = flame surface area (m²)

$\Delta H_{c,eff}$ = effective heat of combustion (kJ/kg).

Although the model is easy to apply, there is the challenge in obtaining an accurate mass loss rate per unit area and heat of combustion of a product, especially for a composite specimen such as foam and fabric composite. Another drawback of the model is the lack of reliable information relating to combustion efficiency for many combustible products. Therefore, the following sections will describe heat release rate models and correlations which can be implemented using more readily available empirical data.

2.3.2 CBUF Thermal Fire Spread Model For Mattresses

As mentioned in Chapter One, the rate of heat release is the most important variable used for characterizing fire [37], and one of the objectives of this project is to predict the heat release rates from various polyurethane foam specimens in furniture calorimeter tests based on results from the cone calorimeter. Wickstrom and Goransson's [58, 59] model for the heat release rate in the room corner test for upward flame spread on wall

linings is probably the most sophisticated model modified by the CBUF research group for use in calculating the heat release rates for mattresses using cone calorimeter data [24]. The model, referred to as Model III by Babrauskas et al. [24, 50, 68], described the physical processes of ignition, flame spread and heat release rate to predict fire growth in mattresses.

The basic assumption for using the model is that the heat release rate from each elemental burning area of the full-scale specimen surface has the same heat release rate time curve as the specimen tested in the cone calorimeter at an arbitrarily chosen heat flux of 35 kW/m² [24]. However, the model functions most efficiently for thin specimens and for materials that do not melt and form pool fire during combustion. Thus, the use of the model will be limited by the melting behaviour of the polyurethane foams as will be shown in Chapters Five and Six.

Since the burning area determines the amount of heat energy generation during fires, a convolution theorem known as the Duhamel integral was applied by the CBUF group to calculate the full-scale time-dependent heat release rate of a burning mattress. The model calculates full-scale heat release rate measured in furniture calorimeters as the convolution integral of the burning area rate $\dot{A}_f(t)$ in full-scale and the heat release rate density $\dot{q}''(r,t)$ from a representative specimen tested in the cone calorimeter. This is represented mathematically as [24]

$$\dot{Q}_f = \int_0^t \dot{q}''(t-\tau) \frac{dA_f(\tau)}{d\tau} d\tau \quad (2-22)$$

where:

$\dot{q}''(t)$ = Heat release rate per unit area time history (kW/m²) measured in the cone calorimeter

$A_f(t)$ = Effective area burning rate at time t (m²/s)

τ = Dummy variable (s).

The integral in Equation (2-22) can be written in summation formula given as:

$$\dot{Q}^N = \sum_{i=0}^N \Delta A^i \dot{q}_{bs}^{N-i} \quad (2-23)$$

where:

ΔA^i = differential burning area determined using a flame area model (e.g., Equation 2-18 or Equation 2-20) at the time increment i ,

\dot{q}_{bs}^{N-i} = Heat release rate density after $(N-i)$ time increments, recorded in cone calorimeter.

To use the integral model for full-scale heat release rate calculations, an analytical expression for the cone calorimeter heat release rate profile $\dot{q}''(t)$ and the effective burning area $A_f(t)$ in full-scale must be determined [24]. The effective burning area can be represented using an analytical flame area model as given in Equations 2-18 and 2-20. The integral model is a non-linear expression which has no closed-form solution due to the heat release rate profile $\dot{q}''(t)$. To simplify the model, Gregory [66] suggested the use of curve fitting techniques to generate a Gaussian profile as shown in Figure 2-4 that is an approximate representative of the heat release rate density $\dot{q}''(t)$ from the cone calorimeter tests. The approximate Gaussian profile generated by using Equation (2-24) is aimed at representing the accelerating growth and decay profiles typical of heat release rate curves. Gregory [66] gave a generalised Gaussian function for curve fitting of cone calorimeter data as:

$$\dot{q}''(t) = a \cdot \exp[-b(c-t)^2] \quad (2-24)$$

where:

$a = \dot{q}_{\max}''$, the peak heat release rate density measured in cone calorimeter
(W/m²)

b = an arbitrary variable that determines the width of the peak value (the larger the value of b , the sharper the peak)

c = a parameter that represents the time to peak heat release rate density.

For a given number of terms (N) performed using Equation 2-24, the entire heat release rate density expression is obtained using a summation formula:

$$\dot{q}''(t) = \sum_{i=0}^N \dot{q}''_{\max(i)} \cdot \exp[-b_i(c_i - t)^2] \quad (2-25)$$

where:

N = total number of terms in the series

i = counter.

The ideal heat release rate density shown in Figure 2-4, generated using Equation 2-24 is based on a peak heat release rate value ($\dot{q}''_{\max} = 410 \text{ kW/m}^2$), time to \dot{q}''_{\max} ($c = 75 \text{ s}$) and $b = 0.001$.

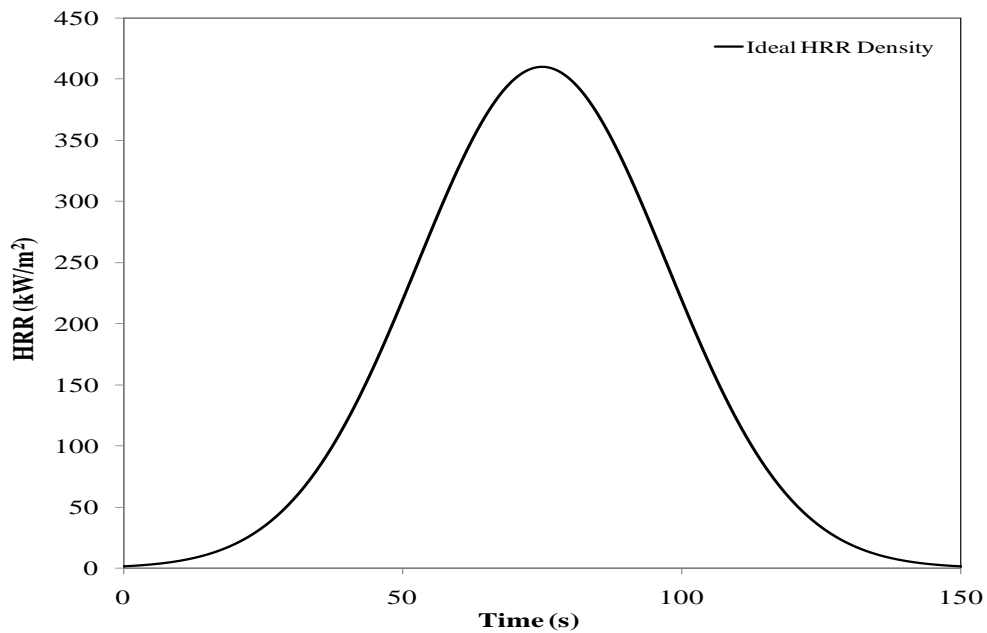


Figure 2-4. Gaussian function representing an idealized HRR density.

2.3.3 Time-Squared Heat Release Rate Model

With the use of computer fire models, it has become easier to predict several fire parameters such as the accelerative growth of the fire, rate of burning, time to room flashover, temperatures. The t-squared fire model is one of such model has become popular as a simple method for predicting the pre-flashover stage of fires.

Due to the parabolic fire growth of most combustibles, the t-squared fire model is used extensively to predict fire development, assuming that the heat release rate is equal to the product of a fire growth coefficient and the square of the elapsed time since the start of the fire [8, 69]. The model is used to classify fire growth of combustible items as slow, medium, fast and ultra fast developing fires depending on their speed of development from ignition point as shown in Figure 2-5. The model is given as [8]:

$$\dot{Q} = \alpha(t - t_0)^2 \quad (2-26)$$

Where:

\dot{Q} = Full-scale heat release rate (kW)

α = Fire growth coefficient which is dependent on the type of fuel (kW/s²)

t = Time(s)

t_0 = Incubation time (s) which is the time lag between ignition and the time the flame becomes significant.

The model requires only the fuel-specific fire growth coefficient to determine the heat release rate (e.g., Table 2-1). Grimwood [70] reported that an outstanding capacity of the t-squared model is its ability to predict how fire size doubles every 60 seconds in an optimally ventilated compartment where the air-fuel mixture is in adequate range. Grimwood [70] reported that slow developing fires double in size every 120 seconds, medium developing fires double every 60 seconds, while fast and ultra-fast developing fires double in size every 30 and 15 seconds, respectively.

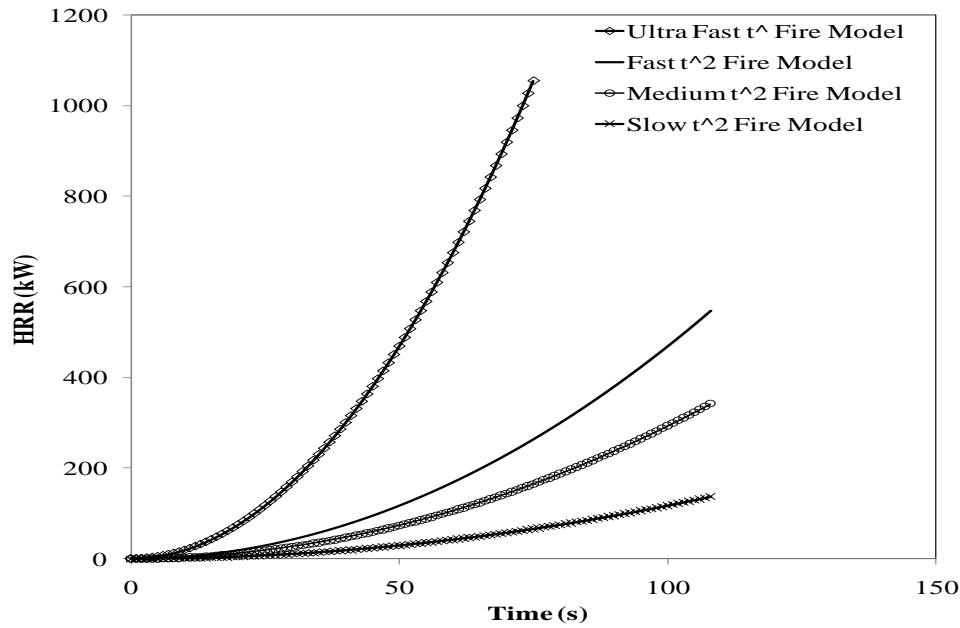


Figure 2-5. Set of t-squared growth curves.

Table 2-1. Different values of fire growth coefficient [8, 70].

Fire growth coefficient kW/s ²	Classification	Materials
0.00293	Slow	Solid wood cabinetry, densely packed paper.
0.01172	Medium	Upholstered furniture, traditional mattress/boxspring.
0.0469	Fast	Corrugated cardboard, cartons, thin plywood wardrobe, polyurethane foam mattress.
0.1878	Ultra fast	Methyl alcohol pool, high rack storage.

One significant limitation in using the t-square fire model is that the expression does not account for the decay stage of fire after attaining the peak heat release rate. Another drawback of the model is that it does not give information about the flame area which determines fire growth. Although Janssens [69] outlined a list of fire growth coefficients

for upholstery materials, there is the challenge of selecting the appropriate fire growth coefficients for non- polymeric products.

2.3.4 NIST-CBHF Heat Release Rate Correlation

Experimental research was conducted by the National Institute of Standards and Technology (NIST) and California Bureau of Home Furnishings (CBHF) to screen and classify upholstered furniture products based on their fire performance during laboratory tests. The study showed that the ability of upholstery materials to propagate fire is dependent on the heat release rate density during the first three minutes of a test in the cone calorimeter. The magnitude of three-minute average cone calorimeter heat release rate density from products was set as cut-off criteria to classify products as to whether they can self-propagate fire or not [71].

The heat release rate determined from the cone calorimeter at 35 kW/m^2 heat irradiance was used as input data for predicting the full-scale peak heat release rate of the upholstered products. In analysing their empirical results from upholstered products, the NIST and CBHF groups noted that a three-minute average heat release rate density less than 100 kW/m^2 was not sufficient to generate enough heat energy to cause self flame propagation in the upholstery materials. A three-minute average heat release rate density greater than 200 kW/m^2 was noted to generate enough energy to cause self propagating flame and fire growth in actual furniture. As a result, they distinguished three regions a combustible material may be identified with. The first region accounts for non-self propagating fire which is characterized by an average bench-scale heat release rate density of less than approximately 100 kW/m^2 . The second region which describes a self propagating fire is characterized by average bench-scale heat release rate density of approximately 200 kW/m^2 . The last region was identified as intermediate region between 100 and 200 kW/m^2 where the full-scale fire behaviour is uncertain.

The equations developed for the peak full-scale heat release rate for propagating and non-propagation fires are given as [71]:

$$\dot{Q}_{FS} = 0.75 \cdot \dot{q}_{SC}^* \text{ \{Non-propagating\}} \quad (2-27a)$$

$$\dot{Q}_{FS} = 4 \cdot \dot{q}_{SC}^* + 800 \text{ \{Self- Propagating\}} \quad (2-27b)$$

where:

\dot{Q}_{FS} = Full-Scale Peak Heat Release Rate (kW)

\dot{q}_{SC}^* = Three-minute average cone calorimeter Heat Release Rate (kW/m²)

obtained at 35 kW/m² heat irradiance.

Although the correlations have been proven to predict full-scale peak heat release rates of upholstered materials from cone calorimeter data, a significant limitation with the models is that they do not have the capacity to predict the entire heat release rate-time history in full-scale and the time to peak heat release rate. Another difficulty associated with the models is that they do not account for the intermediate range of heat release rate density between non-propagating and self-propagating fires.

2.4 Burning Rate and Duration

In pool fires, the two most important indicators of the flame behaviour are heat release rate and the mass burning rate [34, 35, 72]. The mass burning rate is the mass of fuel supplied to the flame per second per unit area of the pool which determines the rate of heat release from the fire.

Babrauskas [72] gave the following expression (Equation 2-28) for mass burning rate of liquid pool fires with a diameter greater than 0.2 m:

$$\dot{m}'' = \dot{m}''_{\infty} (1 - \exp(-k\beta D)) \quad (2-28)$$

where:

\dot{m}'' = mass burning rate of fuel per unit area ($kg / m^2 \cdot s$)

\dot{m}''_{∞} = maximum mass burning rate of fuel per unit area ($kg / m^2 \cdot s$)

$k\beta$ = empirically determined mean beam length corrector extinction coefficient product (m^{-1})

D = pool fire diameter (m).

Rew [32] presented the following correlation for calculating the maximum mass burning rate \dot{m}''_{∞} :

$$\dot{m}''_{\infty} = \frac{0.001\Delta H_c}{\Delta H_v} \quad (2-29)$$

where:

ΔH_c = net heat of combustion of the fuel at its boiling point (kJ/kg)

ΔH_v = modified heat of vaporization of the fuel (kJ/kg), which is equal to heat of vaporisation of the fuel above its boiling point, expressed as:

$$\Delta H_v = \Delta H_v + c_p(T_b - T_0) \quad (2-30)$$

where:

ΔH_v = heat of vaporisation of the fuel at its boiling point (kJ/kg)

$c_p = \text{specific heat capacity of the liquid (kJ/kg K)}$

$T_b = \text{liquid boiling temperature (K)}$

$T_o = \text{initial temperature of the fuel (K)}$.

Drysdale [8] gave a simplified expression (Equation 2-31) for the burning rate as a function of linear regression rate:

$$\dot{m}'' = \frac{\rho_l \cdot \dot{R} \cdot 10^{-3}}{60} \quad (2-31)$$

where:

$\rho_l = \text{density of the liquid (kg/m}^3\text{)}$

$\dot{R} = \text{linear regression rate (m/s)}$.

Note: the regression rate is equivalent to the volumetric loss of liquid per unit surface area of the pool in unit time [8]. With the mass burning rate per unit area and the effective heat of combustion of the fuel determined, the heat release rate can be determined using the expression given as [28]:

$$\dot{Q}_f = \dot{m}'' \Delta H_{c,eff} A_f (1 - \exp(-k\beta D)) \quad (2-32)$$

where:

$A_f = \text{flame area (m}^2\text{)}$

As the heat release rate from a liquid pool fire is dependent on the flame area A_f which is a function of pool diameter D , Babrauskas et al. [45, 72, 73] reported that the radiative and convective heat transfer modes in pool fires are distinguished by the pool diameter. Table 2-2 illustrates the variation of burning mode with increasing pool diameter.

Table 2-2. Heat transfer mode dependent on pool diameter [72].

Diameter (<i>m</i>)	Burning mode
<0.05	Convective, laminar
0.05-0.2	Convective, turbulent
0.2-1.0	Radiative, optically thin
>1.0	Radiative, optically thick

Drysdale [8] also reported that for laminar flames with a pool diameter less than 0.03 m, which are characterised by a low Reynolds number of 20, the rate of burning (regression rate) decreases with increasing pool diameter. For fully turbulent flames with pool diameter greater than 1 m, the burning rate becomes independent of diameter. Rew [32] reported a similar observation “as the flame grows it reaches a characteristic size at which it is said to have become optically thick and any further increase in size does not produce an increase in emitted radiation”.

Another remark by Drysdale [8] is that transition from a laminar to turbulent flame occurs when the pool diameter is between 0.03 m and 1.0 m. Within this range of pool diameters, any increase in pool diameter will cause a proportional increase in the burning rate of the fuel with Reynolds number ranging from 200 to 500. Another significant remark by Drysdale is that the rate of evaporation is more pronounced at the edge of the liquid fuel than at its center as flames above small pools are predominantly convective in nature. Conversely, increasing the size of the pool diameter causes the heat transfer process to become predominantly radiative which increases the rate of burning.

Babrauskas [33, 72] noted that a pool fire that is burning at a constant heat release rate consumes fuel mass at a constant rate, however, as the fuel is consumed, its thickness decreases. Also, for a large pool fire with a small flame area, the burning duration is

reported to be long and vice versa [28]. The expression for the burning duration is given as:

$$t_b = \frac{4V}{\pi D^2 \dot{R}} \quad (2-33)$$

where:

V = volume of liquid (m^3)

\dot{R} = regression rate ($\dot{R} = \dot{m}'' / \rho$ (m/s))

D = pool diameter (m)

2.5 Flame Pulsation

The fuel vapour leaving the pool is rapidly heated by re-radiation from the surrounding flame. As the rate of air entrainment into the flame becomes high, a turbulent mixing process occurs which brings together air, volatile gases and combustion products and subsequently changes the burning rate [8]. As the turbulent mixing increases with the diameter of the pool, the fire plume becomes unsteady which results in a pulsating flame. Another contribution to the pulsating behaviour of a pool fire is the heat conduction losses into the liquid which vary in space and time [33]. Drysdale [8] gave an expression for the pulsating frequency of a flame as a function of diameter as:

$$f = (0.05 \pm 0.04)(g/D)^{1/2} \quad \text{Hz} \quad (2-34)$$

where:

g = the acceleration due to gravity (m/s^2)

D = the flame diameter (m).

The effects of turbulence in the flame resulting from an increased pool diameter generally lead to temperature fluctuations which vary across the width and height of the flame and most significantly around the edges and near the top of the flame [8, 32].

Since it is very hard to determine the exact flame temperature due to the pulsating effect, Rew [32] noted that approximate flame temperatures can be obtained by measuring average temperatures at different locations within the flame.

2.6 Fire Scaling

Due to the complexity of fire, the use of mathematical models which give approximate description of thermophysical processes of fire in real life are not sufficient for fire analysis. As a result, Quintiere's [63] examination of the mass, energy and momentum conservation equations indicates that fire scaling which involves the use of dimensional analyses is an excellent supplementary tool for establishing correlations between small-scale and large-scale fires. The scaling techniques which are based on Froude modeling, Reynolds modeling and pressure modeling are significant for generating dimensionless parameters for flame spread and large-scale fire dynamics such as natural convection conditions and transition from laminar to turbulent flow [63, 74].

2.7 Summary of Chapter

The various physics-based mathematical models which describe the fire behaviour of polyurethane foams have been highlighted. Thermal processes such as the heat transfer mechanisms, pool fire models, flame spread and fire growth models for polyurethane foams in full-scale were illustrated. While the heat transfer and pool fire models described in sections 2.1 and 2.4 respectively will not be implemented in the modeling section of this project, they are intended to show the physics of the combustion process in the full-scale tests of the polyurethane foams. The models will also be used to help explain the full-scale results in Chapter Three.

Fire protection engineering correlations and models which are used for predicting large-scale fire test behaviour of combustible substances based on information obtained from small-scale tests were discussed. These models, however, have inherent assumptions

which limit their accuracy due to the complexities of fire. Although there is computational fluid dynamics fire modeling software developed for the calculation of fire variables, the integral convolution model will be used for most of the heat release rate predictions. Flame spread and t-squared fire models will also be used.

To use these models, the input data are obtained from small and full-scale tests of the specimens. Thus, the next Chapter will focus on the full-scale tests of the specimens from which the flame areas needed for the convolution model will be determined. The Chapter will also give detailed information on the heat release rate-time history of the specimens based on ignition locations.

CHAPTER THREE: FULL-SCALE TESTS OF POLYURETHANE FOAMS

3.1 Introduction

Full-scale flammability studies of polyurethane foams were conducted by fire research groups at the Universities of Saskatchewan and Waterloo in 2006 to investigate the fire behaviour of polyurethane foam specimens of various thicknesses and surface area [61]. The studies were aimed at assessing the fire performance of the foams when ignited at the edge using an open flame from a small propane burner. However, those tests did not consider the effects of igniting the specimens at the center. As an extension of the previous work, this study undertakes to investigate the effects of using both edge and center-ignition locations to estimate the sensitivity of flame spread and heat release rate from polyurethane foams to different ignition locations. Cone calorimeter test data for the polyurethane foams will also be gathered and then used with the flame areas to predict the heat release rate for full-scale test of the specimens. The cone calorimeter tests are described in Chapter Four.

3.2 Materials

The polyurethane foams selected for the furniture calorimeter tests were lightweight foams purchased from different branches of a Canadian retail chain in Kitchener-Waterloo and Saskatoon between July, 2006 and May, 2008. The specimens are flexible domestic foams available to consumers for various purposes including camping. However, they are not intended for upholstered furniture and mattress manufacture.

The dimensions of the foams were chosen to be consistent with sizes of the specimens tested in 2006. Three different sizes of the foams measuring 61 by 61 cm (two specimens), 61 by 122 cm (two specimens), 122 by 122 cm (three specimens), all having a thickness of 10 cm were tested in May 2008 at the University of Waterloo's full-scale test facility. The specimens were non fire-retardant foams with average

density of 17.3 kg/m³ and standard deviation of 1.8 kg/m³. The wide variation in nominal densities (ranging from 15.55 kg/m³ to 20.67 kg/m³) was due to the fact that the foams did not expand uniformly after being unwrapped for several days. The density would have dropped from 20.6 to 18.1 kg/m³ if it had expanded to its nominal thickness of 10 cm. Table 3-1 gives a summary of general characteristics of the foams.

Table 3-1. Furniture calorimeter test specimens and test dates/environmental conditions.

Test Specimen	Test Date (Temp. & Relative Humidity)	Ignition Location	Dimensions (cm)			Mass (kg)	Density (kg/m ³)
			Width	Length	Thickness		
C1	May 15, 2008 (17 °C, 38%)	Center	60	62	9.3	0.58	16.8
C2	May 15, 2008 (18 °C, 36%)	Center	60	62	9.5	0.58	16.4
C3	May 16, 2008 (18 °C, 36%)	Center	121	124	9.7	2.31	15.9
E4	May 15,2008 (14 °C, 72%)	Edge	61	126	10.0	1.23	16.0
E5	May 15,2008 (16 °C, 41%)	Edge	61	126	9.3	1.38	19.3
EE3	May 15,2008 (18 °C, 35%)	Edge	125	122	8.8	2.76	20.6
EE4	May 16,2008 (14 °C, 45%)	Edge	125	122	9.8	2.43	16.3

3.3 Experimental Procedure

3.3.1 Specimen Preparation

As the foams were packaged in rolls at the point of purchase, the specimens were unwrapped, cut to size and allowed to expand. This was followed by marking-out of square cells measuring 10 by 10 cm each across the surface of the specimen as shown in Figure 3-1. The grid cells were aimed at simulating the specimen surface areas used in cone calorimeter tests.

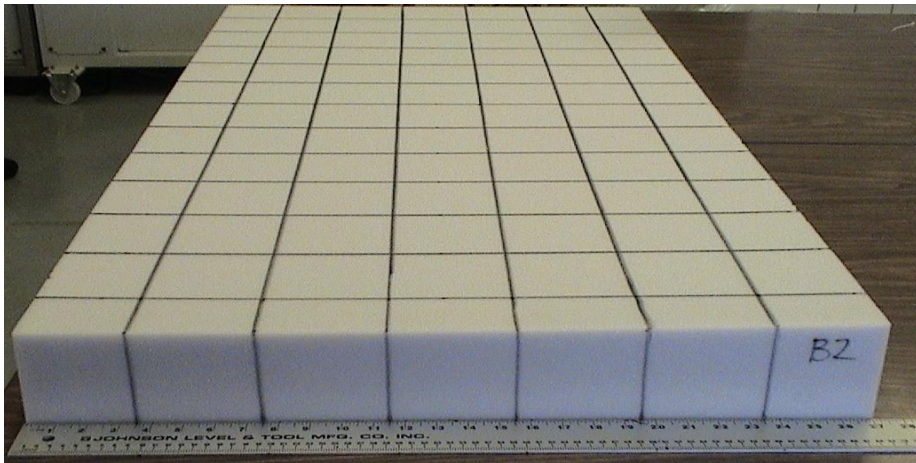


Figure 3-1. Grid marking of a 10 by 10 cm cell on a foam specimen.

A 6.4 cm diameter hole with a depth of 1.3 cm was cut at the geometric centers of center-ignited specimens to ensure a consistent ignition point during the tests. This was also done to prevent preferential flame spread at ignition. The edge-tested specimens were marked at half the width to indicate the ignition point.

Conditioning was carried out for at least 24 hours at the cone calorimeter laboratory at the University of Waterloo in May 2008. The temperature and relative humidity in the cone calorimeter laboratory are controlled during the day using an air handling system and, if necessary, a dehumidifier. The dehumidifier is not run at night. The temperatures

and relative humidity in the cone calorimeter laboratory during the test period were between 22 and 23°C, and 32 and 46%, respectively.

3.3.2 Furniture Calorimeter Calibration

The calibration of the entire furniture calorimeter, based on heat release rate, was done using propane gas which burned in a diffusion burner at standard atmospheric pressure and temperature in the range of 75 and 200 kW. One reason for the calibration was to ascertain the performance level and possible errors with the apparatus. The burner was positioned at the center of the calorimetry hood at a height above the test frame as shown in Figure 3-2. The calibration was carried out using a similar procedure to that outlined in ASTM E 1590 [42]. The calibration was repeated once a day to ensure repeatability of results throughout the tests.



Figure 3-2. Furniture calorimeter HRR calibration using a propane burner.

3.3.3 Photography

Cameras were positioned to capture the burning behaviour and flame spread patterns of the specimens during the tests. The camera instrumentation included a digital Panasonic DMC-LZ10 still camera (Panasonic Canada Inc., Mississauga, ON), a Sony MiniDV camcorder (Sony of Canada, Toronto, ON), and a FLIR ThermaCAM® S60 infrared camera (FLIR Systems, Burlington, ON) with a spectral range of 7.5 to 13 μm . Lights were set such that sufficient illumination was provided on the test area. To obtain a full view of the test specimens, the camcorder and infrared cameras were mounted on tripods (Figure 3-3).

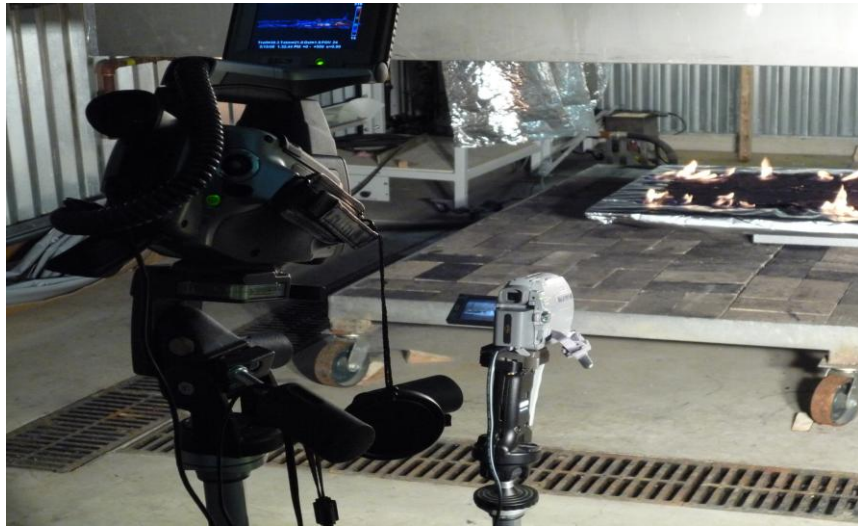


Figure 3-3. Infra-red camera and camcorder positions.

3.3.4 Test Procedure

Specimen preparation and testing techniques were based on standard open flame mattress tests such as ASTM E 1590 and CFR 1633 for edge ignition while the center ignition tests were consistent with the CBUF test method [24]. Prior to ignition, each of the specimens was positioned on top of the ceramic protective sheet which covered the load cell. During the tests, the foams were ignited using a small hand-held propane torch positioned at 45° to the specimen and at pre-determined ignition locations. The

burner position was such that flame directly impinged on the specimen (Figure 3-4). This position was chosen to reduce uncertainties with ignition. The burner was regulated to produce heat flux high enough to cause sustained ignition, and once a flaming ignition was established, the specimen was allowed to burn to completion on its own.



Figure 3-4. Flame impingement at the ignition point on edge of foam.

Two ignition locations (edge and center locations) were chosen for the flame impingement. The choice for the two ignition locations was to enable the comparison of flame growth patterns, flame spread rates and the heat release rate dependence on the different ignition locations. Four of the specimens E4, E5, EE3 and EE4 were tested using edge-ignition. During the edge tests, flame impingement was made at the center of the edge of each specimen to ensure symmetry of flame growth. Specimens C1, C2 and C3 were ignited at the 6.4 cm diameter hole cut at the geometric center.

During ignition, it was observed that flaming combustion commenced easily once there was flame impingement. As the tests progressed, heat release rates and other combustion variables were measured in the data logging system at 1s intervals. The camera instrumentation also captured the video, thermal and photo images of the flame propagation.

3.4 Determination of Flame Spread

This section provides a description of the techniques that were used to measure and obtain the flame spread / flame areas for the furniture calorimeter tests of polyurethane foams. The analyses were made based on the video records and photographs. This section will also discuss some of the drawbacks associated with using the various video imaging techniques.

Generally, the analyses were carried out based on the principle that the flame spread rate is dependent on the times at which the flame front (the base of a glowing foam specimen ahead of the fire plume) reaches given locations on the specimen. The flame areas were evaluated by estimating the region of the specimens engulfed by flame. All the visual observations and measurements were based on the images (videos and photos) that were displayed on the computer screen. However, as the images on the screen are not the same size as the actual specimen, a scaling factor was used.

The distances measured from the computer screen were multiplied by scaling factors to produce an approximate flame area. For more complicated flame spread patterns, flame areas were obtained by estimating the effective number of cells (with a unit dimension of 10 by 10 cm) that were burning. In most cases, the total burning area was obtained by summation of rectangular and semi-circular flame areas for ease of analysis.

Assuming that flame growth over the specimens is symmetric, estimates were made to account for the fire history likely to be occurring at the opposite sides of the specimens which could not be seen in the video images captured by the cameras. For the most part, the flame front development followed a purely radial pattern which spread outward from the point of ignition to engulf the whole specimen as shown in Figures 3-5 and 3-6. The flame areas were thus estimated by measuring the diameter (as in center-ignition analysis) or radius (for edge-ignition analysis) of flame at predetermined time steps, and then using the scale factor.

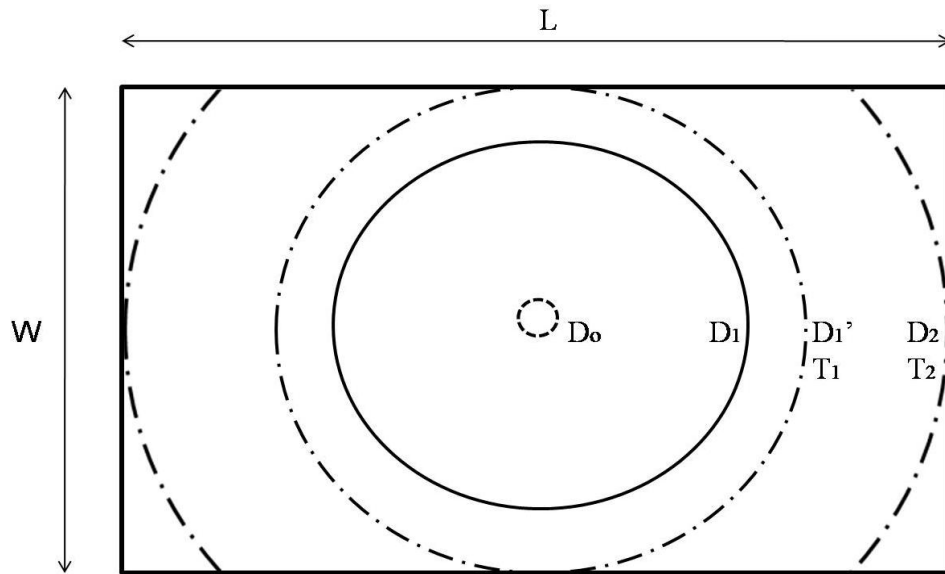


Figure 3-5. Schematic of ideal radial flame spread over a center-ignited specimen.

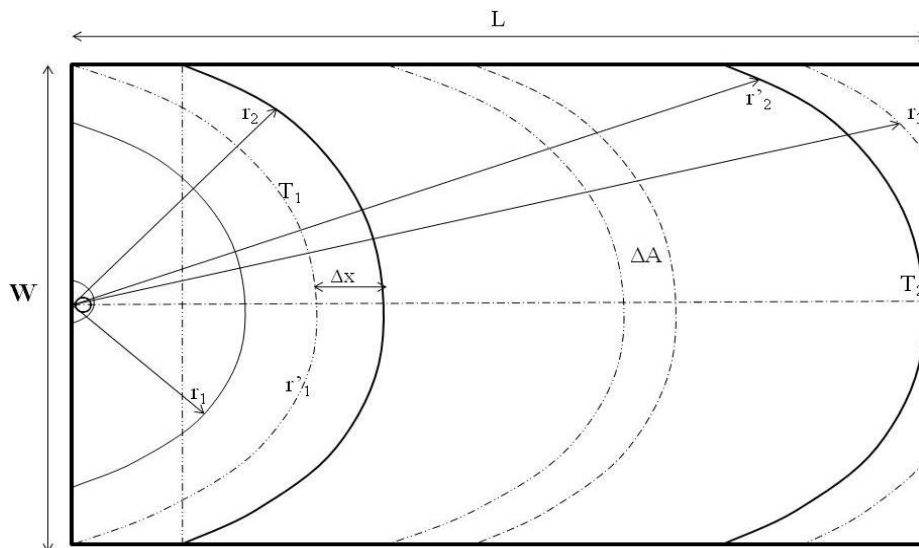


Figure 3-6. Schematic of ideal radial flame spread over an edge-ignited specimen.

The radial growth pattern was more prevalent in center-ignited specimens than in edge-ignited specimens as shown in Figure 3-7. However, one common challenge was encountered at transition points T1 and T2 (shown in Figures 3-5 and 3-6) where the flame fronts (or arcs of the flame ring) reached the edges / boundaries (at D_2 and r'_2) of

the specimens, which caused truncation of the radial flame spread pattern. Once this situation occurred, the flame area estimation technique was modified by calculating the difference between the total number of cells of the specimen and the number of non-burning cells, and then multiplying this difference by 10 by 10 cm (the area of a unit cell) to obtain the total burning area.



Figure 3-7. Radial flame growth over a center-ignited specimen (top) and elliptic flame growth over an edge-ignited specimen (bottom).

Edge-ignited specimens, however, showed flame growth that was consistent with the radial flame growth observed in the center-ignited specimens especially at the early stage of flame development when the flame front had not reached the width W of the specimen. The flame spread for the edge-ignited specimens was analysed by assuming that the flame front spreads radially outwards as a semi-circle from the ignition point O towards the length L of the specimen as shown in Figure 3-6. When the full width was completely engulfed in flames, the flame front continued in a parabolic pattern along the length of the specimen until the whole specimen was burning.



Figure 3-8. Flame spread across the length of the specimen.

However, this growth pattern constituted a challenge in the course of evaluating the flame areas. One of the challenges was that the semi-circular spread was not universal to the entire surface of a specimen as the radial flame front was not uniform across the length of the specimen. For instance, the 122 by 122 cm (4 by 4 ft.) edge-ignited specimens showed a semi-circular pattern at the early stage of the flame development, and prior to the flame reaching the width of the specimen, the flame front assumed an elliptical shape as shown in Figure 3-7. This scenario, however, was less prevalent in the 61 by 122 cm (2 by 4 ft.) specimens where the flame fronts were relatively semi-circular in shape until the flame reached the width of the specimen. The decay phase of the

flame spread was also calculated. This was achieved by estimating the total number of cells that have been burned out and then subtracting the area from the surface area of the specimen.

3.4.1 Infra-red Camera

The flame spread measurements using the infra-red images (viewed using Microsoft® Windows® MovieMaker) were based on observing the location of the flame front where there is a demarcation between the glowing foam boundaries and the unburned regions of the specimen. The distinct flame front contour facilitated the measurements of the flame diameter with reasonable accuracy. Most importantly, the infra-red view provided information relating to the temperature distribution across the specimen. One significant drawback with the infra-red video was its inability to show outlines of each cell which made estimation of the number of burning cells challenging.

In order to illustrate the procedure used to analyze the infra-red video records, results from the test of specimen C3 (122 by 122 cm, center ignition) will be discussed. For center-ignited specimens, a ratio of dimensions of the real-scale specimen to dimensions of the specimen images measured from the computer screen was established to determine a scale factor. Using the scale factor, real-scale flame diameters at 5 s time-steps were estimated.

The initial time was based on when flaming ignition was established and burning area (Figure 3-9) at this time was calculated based on the 6.4 cm diameter cut at the center of the specimens. Subsequent total burning areas were evaluated as the infra-red video was stopped every 5 s.

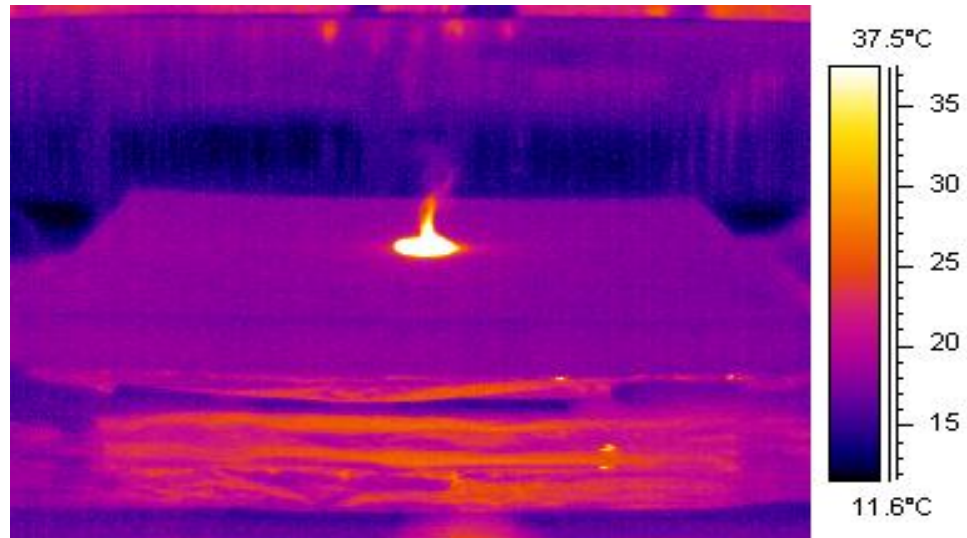


Figure 3-9. Infra-red image of the initial burning area for specimen C3.

Once the radial flame front reached the edges /corners of the specimen, the flame front became truncated as shown in Figure 3-10. At this point, obtaining the flame area was achieved by estimating the difference between the surface area of the specimen and the approximate area of non-burning section of the specimen. This approximation of the effective flame area was based on visual estimates as there were no outlines for the cells which could have facilitated a more accurate calculation.

However, once the whole specimen was engulfed in flame, the flame area became equivalent to the entire specimen surface area (122 by 122 cm). As the entire surface was burning, it was observed that the flame started to spread vertically downwards at the sides while the flame was starting to decay at the central section of the foam as shown in Figure 3-11. The contribution of vertically burning sides to the total burning area was accounted for by estimating the area of the burning sides of the specimen. The reference point for estimating the burning region was the flame base (flame front) shown on the infra-red image as an isothermal outline on the burning foam.

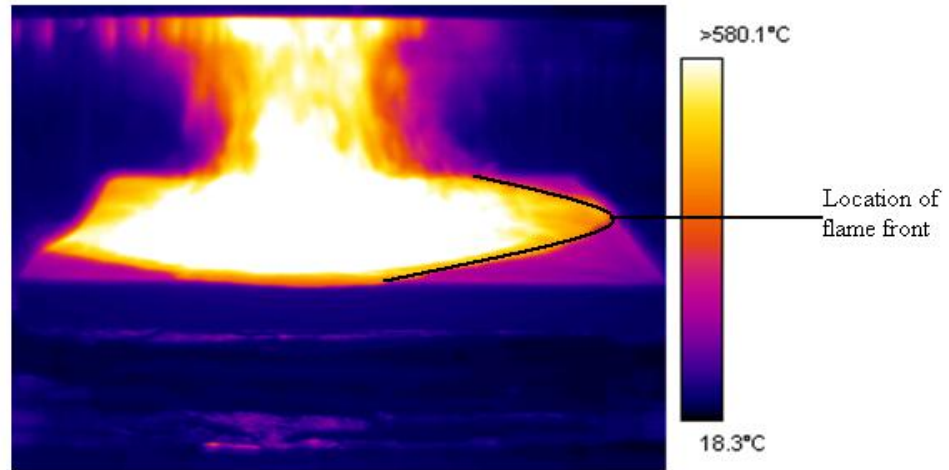


Figure 3-10. Infra-red image showing truncated flame front for specimen C3.

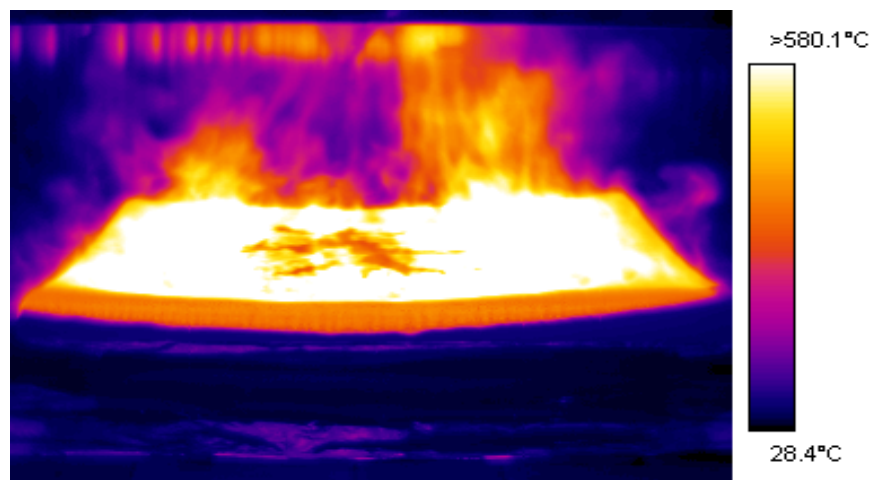


Figure 3-11. Vertical flame spread and onset of burn-out for specimen C3.

As the vertical spread progressed, it was observed that specimen burn-out became significant and continued toward the corners of the specimen. Visual estimates were used to approximate the effective burning areas as there were no distinctive outlines of the flame front in that region. As the specimen burn-out increased, the remaining burning area became confined to a small portion of the specimen as shown in

Figure 3-12. The process continued until the specimen was completely burned out. This stage accounts for the decay phase and the eventual termination of the fire.

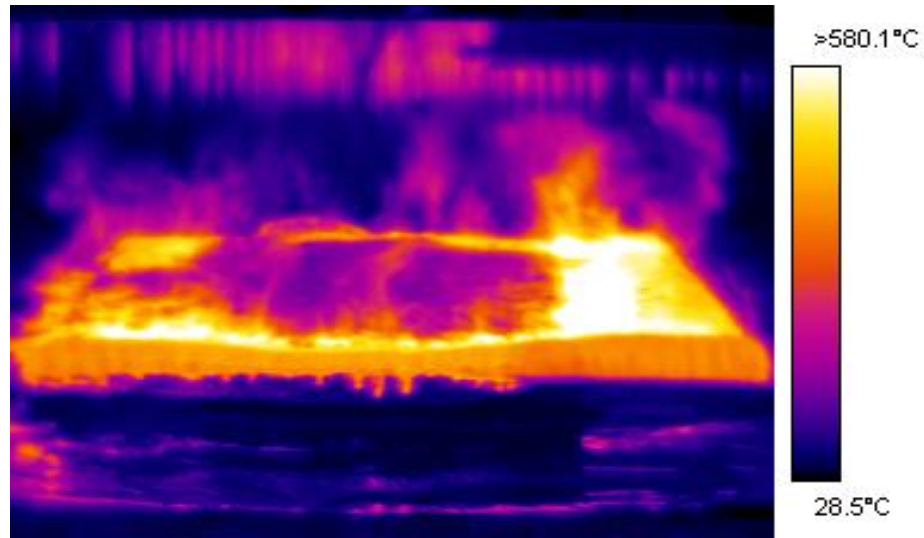


Figure 3-12. Well developed burn-out section and flame decay for specimen C3.

Flame spread measurements for edge-ignited specimens from the infra-red video images were carried out by assuming semi-circular flame growth. During the measurements, the flame front continuously fluctuated from semi-circular to parabolic and elliptic shape. The scaling factor used for the analyses was calculated in the same way as for the center-ignited specimens. Measurements from the screen were made once flaming ignition was established on the specimen.

These measurements were carried out every 5 s until the flame front reached the width of the specimen. However, once the flame reached the width of the specimen, the flame front pattern changed and then flame spread continued across the length of the specimen as shown in Figures 3-13 and 3-14, which are for the test of specimen EE3 (122 by 122 cm, edge ignition).

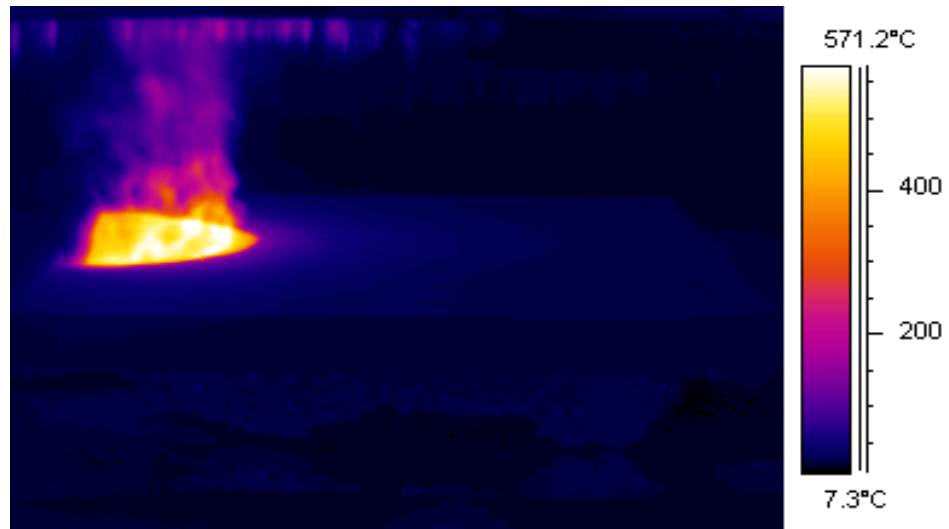


Figure 3-13. Flame growth towards the edge of specimen EE3.

Measuring the flame area after the flame front had reached the width of the specimen and then started to propagate along the length of the specimen involved two techniques. First, the rectangular burning section directly behind the parabolic flame region was determined as shown in Figure 3-15. This rectangular flame area was then approximated by multiplying the real-scale length by the width of the real-scale specimen. Second, the radius of the parabolic / semi-circular flame arc which started at the end of the rectangular section was measured. The total flame area is then the sum of the rectangular and semi-circular flame areas. This process was carried out at 5 s intervals until the flame front reached the end of the specimen. At this instant, the flame arc became truncated.

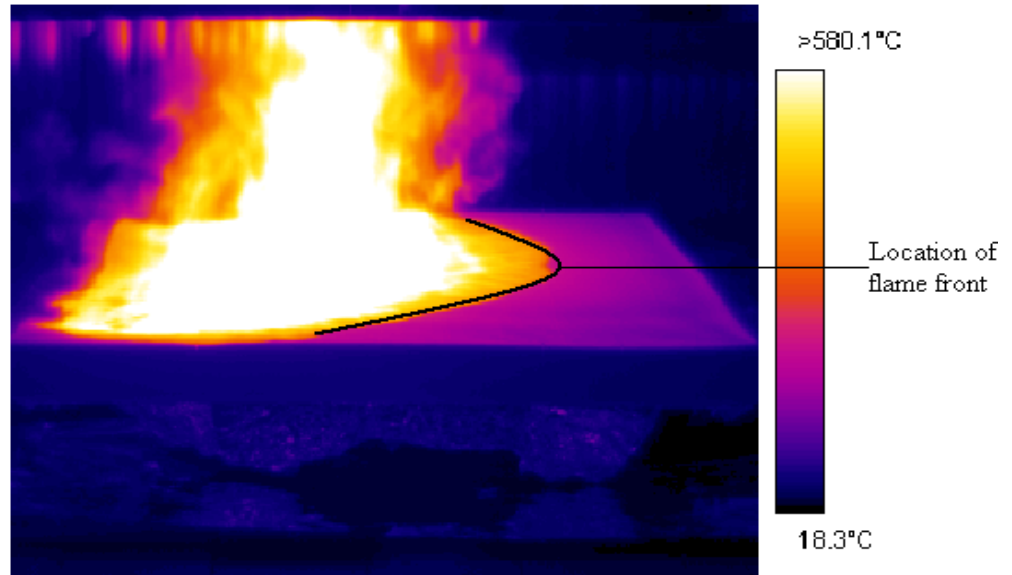


Figure 3-14. Flame growth across the length of specimen EE3.

The effective burning area was thus estimated by the difference between the entire specimen surface and an approximation of non-burning region. Regions with flame decay were successively subtracted from the total surface area as the effective burning area was being estimated.

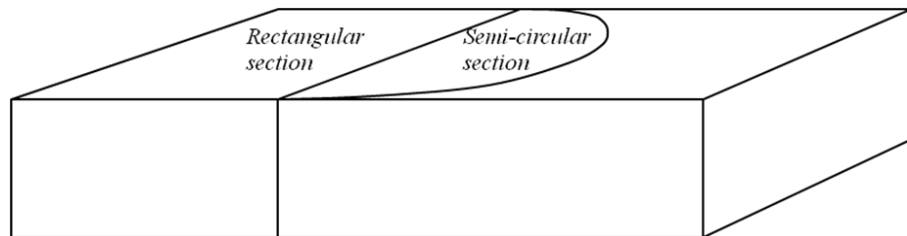


Figure 3-15. Schematic showing the rectangular and semi-circular burning sections of a foam.

3.4.2 Video Camera

For the measurements using the video files, the procedures used were similar to those used for infra-red analyses for both the center and edge-ignition tests. A scaling factor was also established. For center-ignition analysis, the time at which ignition occurred on the video was recorded and the initial burning area (Figure 3-16) was calculated based on the 6.4 cm diameter hole at the center of the specimen surface. Using 5 s intervals, successive flame diameters were determined and the real-scale flame areas calculated.



Figure 3-16. Initial burning area for specimen C3.

When the flame front reached the edge of the specimen and changed its spread pattern (Figure 3-17), flame area was then estimated by obtaining the difference between the surface area of the specimen and the area of the non-burning cells. The number of cells was estimated on the basis of assumed symmetry of burning sections as the video images did not show the back of the flames.



Figure 3-17. Truncated flame front at the edge of specimen C3.

Once the entire surface was engulfed in fire, the flame spread vertically downwards at the sides of the specimen (Figure 3-18) while specimen burn-out began to occur at the center which gradually continued toward the edge. The area of the vertically burning section was estimated and added to calculate the effective horizontal flame area. This process continued until the foam was completely burned.



Figure 3-18. Vertically-downwards flame spread at the sides of specimen C3.



Figure 3-19. Flame tilting and pulsation for specimen E4.

The techniques used for analyzing the video records of edge-ignited specimens were exactly the same as the infra-red measurements. An advantage of the video images was the ease of estimation of burning and non-burning regions of the specimens as the cells have visible outlines in most of the specimens. The infra-red video / image analyses were dependent on thermal contours (isotherms) which describe flame temperatures of the specimens. Cell outlines for one of the 61 by 122 cm specimens (E4) were, however, blurred due to inappropriate camera settings. Another challenge was the considerable flame tilting and pulsation (Figure 3-19). These effects caused ambiguity in measuring the flame spread rates for specimen E4. Therefore, flame areas were not measured for this test.

3.4.3 Still Camera

Visual observations and measurements of the digital photo images were straightforward as there was no need to intermittently stop the video files during data analyses. These photos were mainly intended to supplement the images captured by infra-red and video cameras for flame spread analyses. The time at which ignition occurred was determined based on the time that the photo of ignition was created on the memory card in the

camera. The time at which subsequent files were created on the memory card were used to determine the time intervals between photos.

3.5 Flame Spread Rates

3.5.1 Center Ignition Tests

Figure 3-20 shows the comparison of video, IR and photo-determined flame area for specimen C1. The two profiles (determined from IR and video cameras) representing the flame growth show a high degree of consistency especially at the developmental stage of the fire, and a reasonable agreement at the decay stage of the fire. However, one remarkable feature of the Figure 3-20 is the gap existing between the growth curves for the video and IR-measured flame areas. One reason for this gap is due to the difference in camera resolution of the flame fronts during flame propagation. The IR camera captured more exact flame front outlines than the video camera. As noticed during data analyses (e.g., Figure 3-20), the video camera-determined flame areas lie above the IR-determined flame areas.

This is because the exact flame fronts were not readily assessed in the video files due to blurred interface between the flame front and the unburned portion of the specimen which limited measurements and as a result led to errors in the estimated the flame growth. For measurements obtained using the digital photos, the inconsistent time steps made the flame area curve have a significant divergence from the IR and video-determined flame areas as shown in Figure 3-20. For the IR video file, the temperature difference between burning and non-burning sections of the specimens facilitated a more exact measurement of flame fronts. As the IR video file gave finer results, the rest of the discussion will be based on IR determined data.

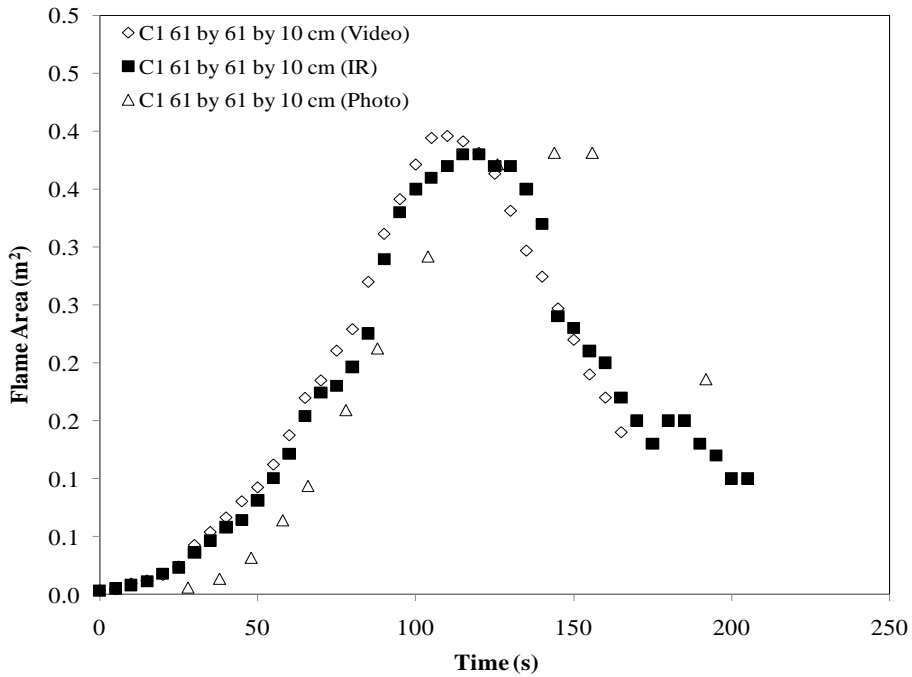


Figure 3-20. Comparison of video, IR and digital photo-determined flame spread rates for specimen C1.

Figure 3-21 shows the infra-red results for time-dependent flame spread $A_f(t)$ for center-ignited specimens C1 and C2 (61 by 61 cm by 10 cm) and specimen C3 (122 by 122 by 10 cm). The flame area profiles illustrate the surface burning characteristics of the specimens which include the growth stage (burn-through and accelerative growth), peak flame area and the decay stages. As Figure 3-21 indicates, the results obtained for specimens C1 and C2 showed a high degree of repeatability as the flame spread profiles for both specimens are similar.

Also, the flame development for the larger specimen C3 showed similar growth pattern as the smaller width specimens. For the three specimens, the flame development stages followed linear and exponential growth patterns after ignition until the maximum burning areas were attained. The initial flame growth stages occurring within 30 s after ignition account for onset of burn-through in the thickness direction (after sustained flaming ignition) due to conduction heat transfer (with a considerable temperature

gradient) from the surface to the interior of the foams. This stage involved extended burning duration as the specimens behaved as thermally thick materials. This was followed by accelerative flame spread across the surface resulting from the low thermal inertia of the foams due to their low density.

At 80 s, the flame spread reached a transition point when the flame front hit the width / edge of the specimens C1 and C2. This is identified as a shift in the growth profile.

After this transition point, flame growth occurred at a relatively slower rate until the peak flame areas (the entire surface and a portion of the sides of the specimens) were attained at approximately 110 s. For the larger size specimen C3, different observations were made during the flame development. At 50 s after ignition, the initially quiescent and laminar radial flame pattern developed to a flickering, pulsating plume with an onset of pool fire. This is consistent with Drysdale's [8] report that most flaming ignition processes follow a short period of laminar burning which quickly develops to turbulence as the flame size increases. During these events, the flame spread preferentially in one direction due to circulation patterns under the hood and at 100 s, the flame front hit one edge of the specimen and spread more rapidly across the length of the edge due to edge effects as shown in Figure 3-17. Part of the reason for the rapid flame spread was that at the edge of a specimen, the fuel assumes thin-fuel behaviour with minimal heating length and reduced thermal inertia [8].

At 130 s, flame front truncation became very considerable and the spread continued until the entire surface and sections of the sides of the specimen (accounting for peak flame area) were engulfed in flame at 155 s.

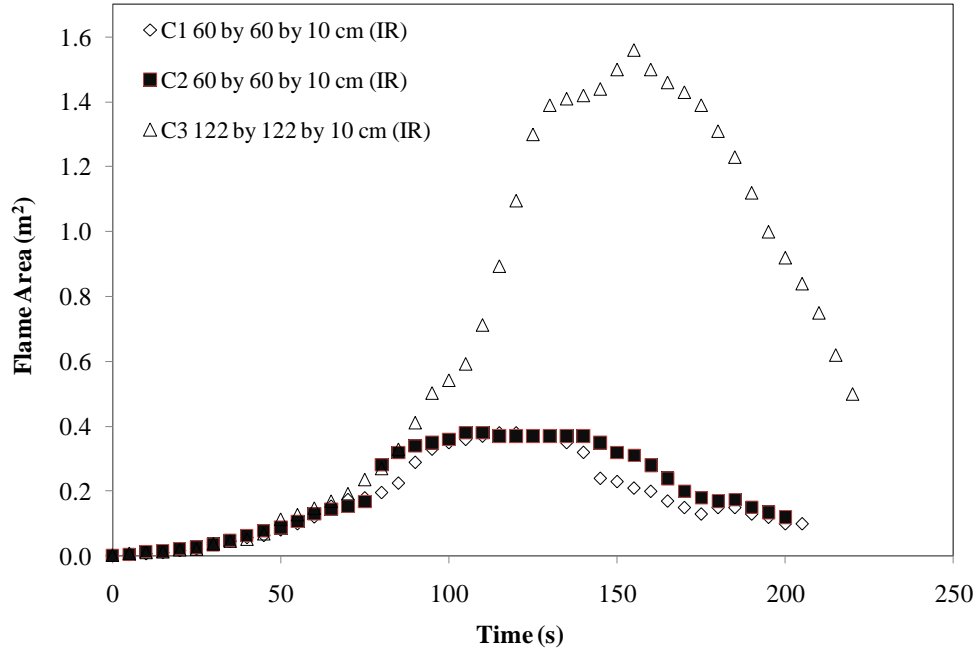


Figure 3-21. Flame areas determined using IR video for specimens C1, C2 and C3.

While measurements were based on the surface of the specimens, it is noteworthy that the flames also burned along the sides of the specimens. Therefore, flame areas were corrected by adding the total top surface burning area and the areas of the vertically burning sections. For the smaller width specimens C1 and C2, the vertically downward burned section was approximately 3% of the peak flame area of 0.38 m^2 . Similarly, the contribution of the vertical burn was 5% of the peak flame area of 1.56 m^2 for specimen C3.

As evident in Figure 3-21, the effect of different specimen sizes on flame areas is quite pronounced. For each size of foam, the flame area varies with the dimensions of the specimen. For instance, the peak flame area of specimen C3 is 310% higher than those of specimens C1 and C2 which is as expected as the surface area (1.49 m^2) for specimen C3 is 303% larger than the area (0.37 m^2) for specimens C1 and C2. Beyond the peak flame areas, the effective flame areas decay exponentially with time which was due to specimen burn-out occurring as time elapsed. The decay stages showed a significant

discrepancy especially for specimens C1 and C2 (Figure 3-21). This resulted from the inability to accurately determine the burned-out areas of the specimens. However, as hazards posed during the decay phase are often insignificant when compared to hazards resulting from the fully developed phase, the decay phase is often neglected during analysis.

The estimated time dependent flame radius was used to determine linear flame spread rates (linear regression rates) across the surface of the specimens. As is evident in Figure 3-22, although the flame spread rate changed with time, the linear flame spread rate was relatively constant within 60 to 90 s of ignition for each test when the flame propagated from ignition point to the edge of the specimens. The expression for the linear dependence of flame growth on time is given as:

$$r(t) = \alpha t \quad (3-5)$$

where:

α is the radial growth constant or the linear regression rate (mm/s).

For specimens C1 (Figure 3-22) and C2, the average value of the linear regression rate during the initial flame spread was 3.1 mm/s. As is evident in the curve, at 80 s there is an abrupt deviation in the spread rate which accounts for the transition from a pure radial spread to preferential spread when the flame front reached the edge of the specimens and assumed a slightly different spread rate due to edge effects. However, beyond the transition point, the surface flame spread rate was observed to occur at a slower rate.

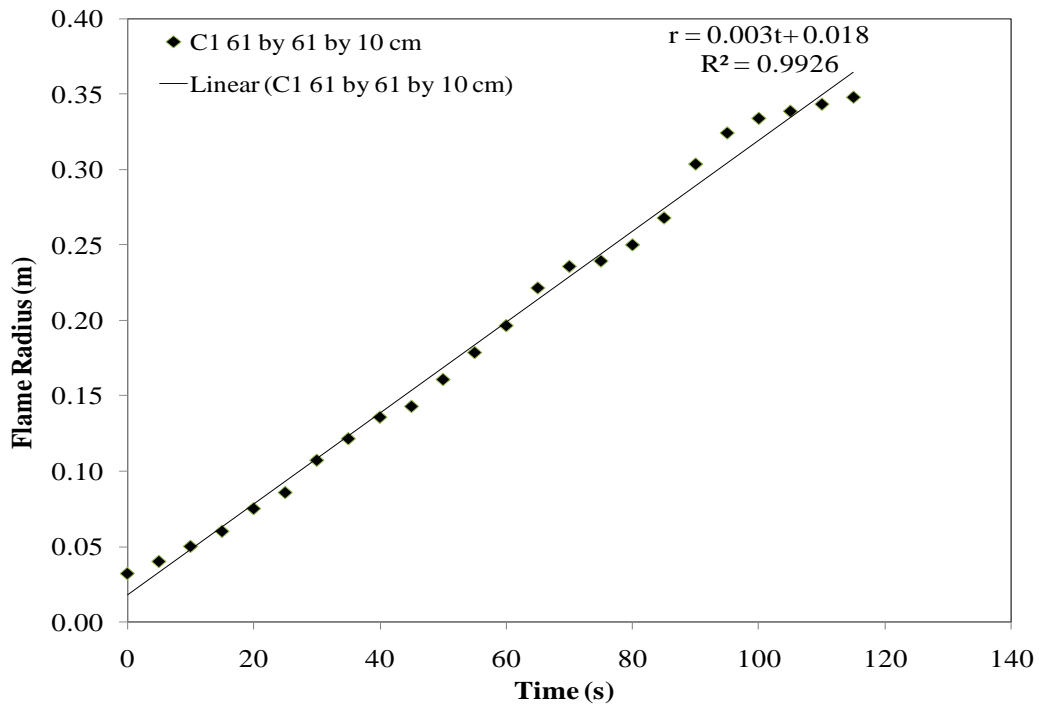


Figure 3-22. Linear regression rate for specimen C1.

With reference to Figures 3-21 and 3-23, the flame area varies exponentially with time:

$$A(t) = A_0 \exp(\lambda t) \quad (3-6)$$

where:

λ is the flame area growth constant in unit of s^{-1} .

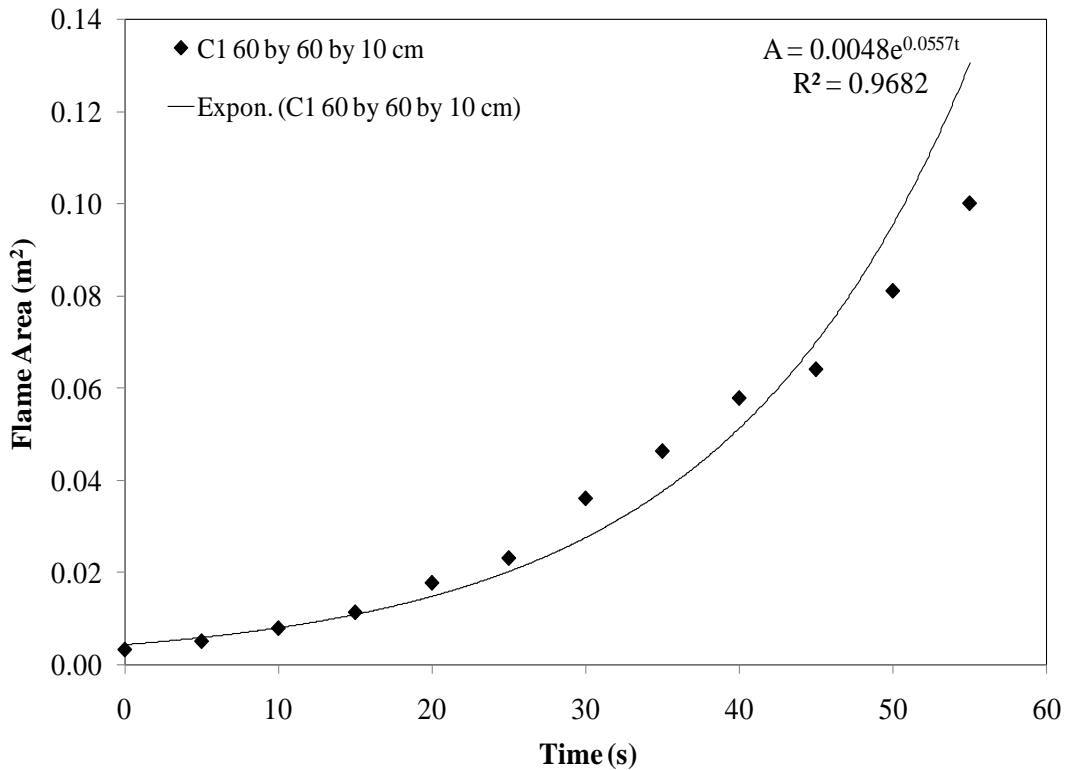


Figure 3-23. Exponential flame area growth curve for specimen C1.

As determined from Figure 3-23, the flame area growth constant for specimen C1 was 0.056 s^{-1} . For specimen C2, the growth constant was 0.051 s^{-1} . The best fits ($R^2 = 0.968$ and 0.938) were obtained with coefficients of 0.0048 and 0.0064 respectively.

Generally, the linear and exponential flame growths for specimen C1 are 3 and 9% higher than those of specimen C2. The variation in the growth constants can be attributed to the random mechanism of the fire plumes during the pool fires.

For each size of foam, the flame spread rate and growth vary with dimensions of the specimen. For specimen C3, the average horizontal surface spread rate value of 4.2 mm/s (determined using the same technique as specimen C1) was relatively higher than those of specimens C1 (3.0 mm/s) and C2 (2.9 mm/s). Part of the reason for this difference was due to larger dimensions of the specimen C3 which enhanced the rate of horizontal flame spread as fuels with substantial surface areas are characterized by

significant burning rate [8]. This is consistent with the visual observation of flame propagation across the two sizes of specimens where the flame spreads more rapidly over the specimen C3 after 80 s and reached the peak at 155 s due to the significant radiative heat transfer resulting from large fire plume which caused a greater spread rate.

3.5.2 Edge Ignition Tests

A comparison of flame areas estimated using the video file from the camcorder, infra-red video and digital photos for edge-ignited specimen E5 is shown in Figure 3-24. The flame area showed consistent exponential growth during the early flame development. As the graph illustrates (more pronounced with the infra-red curve), there is a deviation between curves at 100 s due to abrupt changes in the geometric flame spread pattern observed when the flame hit the edge of the 122 cm wide specimen.

For this specimen, the fluctuations from semi-circular to parabolic flame front occurred at 50 s after ignition due to considerable air entrainment from the ignition end of the foam. The parabolic spread continued and then changed to an elliptic spread pattern which progressed until the flame reached the edge of the specimen. Due to complexity of the flame spread at the transition point (edge of specimen), there is, however, a remarkable discontinuity in the flame area growth estimated using the three measurement techniques between 100 and 120 s of the tests. This was due to differences in camera resolution and estimation of burning cells at the transition point. Since the infra-red video produced sufficiently clear burning outlines (with the infra-red curve slightly below those of video and photo files as observed for center ignition tests), the analyses of the flame spread were based on data obtained from infra-red measurements.

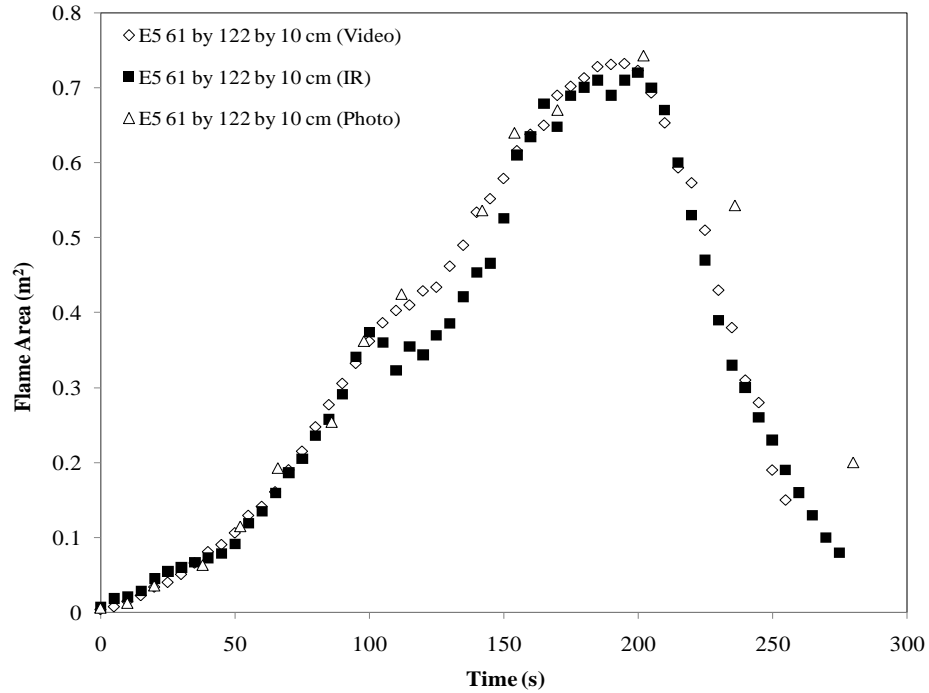


Figure 3-24. Flame areas estimated using camcorder, IR camera and digital photos for specimen E5.

The results of the flame areas estimated using the infra-red video record for edge-ignited specimens E5, EE3 and EE4 are shown in Figure 3-25. As noted earlier for specimen E4, flame area data could not be determined due to unclear images captured in the camera. As evident in Figure 3-25, the flame growth for the three specimens are similar, especially at the early stage of flame development when the flame fronts changed from a pure radial pattern to parabolic and then elliptic patterns until a considerable area of the specimen was engulfed in flame. Flame spread was similar for all specimens for approximately the first 100 s of the tests, after which flames reached the sides of the 61 cm specimen and then flame area increased at a slower rate. After 100 s, flame areas increased at higher rates for the 122 cm wide foams which reached the sides of the specimens at 154 and 133 s for EE3 and EE4 respectively (as observed from video recordings).

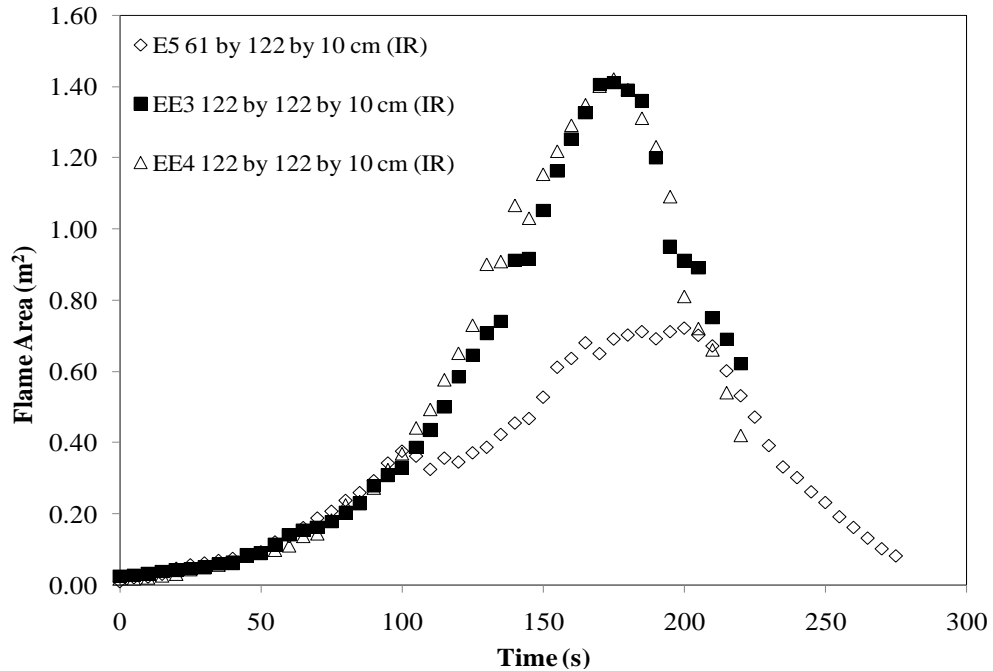


Figure 3-25. Flame areas estimated from IR video of edge-ignition tests.

The pure radial flame growth, however, was more dominant in the 122 cm wide specimens EE3 and EE4 as indicated by the relatively smooth exponential growth curves from ignition to a peak flame area of 1.42 m^2 attained at approximately 172 s. This is, however, different than for 61 cm wide specimen E5 where a more distinct transition point occurred at 100 s when the flame front reached the width of the specimen. The truncation of the flame growth and fluctuations in the spread pattern resulted in a deviation in the later part of the flame growth curve for specimen E5.

Flame areas for each size of specimen varied with physical dimension of the foam. As expected, the peak flame area of 1.42 m^2 for 122 cm wide specimen EE3 and EE4 is approximately 97% higher than that of specimen E5 since the nominal surface area of 1.49 m^2 for specimen EE3 (also for EE4) is 101% larger than that (0.74 m^2) for specimen E5. Moreover, these peak flame areas for the two sizes of specimens were attained at approximately the same time. As opposed to center ignition tests, the peak flame areas for E5 and EE3/EE4 are approximately 4 and 5% less than the physical

areas of the specimens. This accounts for the specimen burn-out that occurred at the initially burning portion of the foams before the flame engulfed the entire specimen. The decay phases of the flame areas showed a high level of agreement, as the three decay curves have similar profiles.

Figure 3-26 shows the radial spread rate for edge-ignited specimen E5. The graph illustrates the various flame front developments observed for the 61 cm wide specimen. At ignition, the flame radius $r_f(t=0)$ of 0.07 m was approximately 119% higher than the radius (0.032m) of the burner flame as illustrated in Figure 3-22 for specimen C1. This difference can be attributed to the tilted flame impingement on the specimen during ignition which over-engulfed the marked portion of the foam before flaming ignition was established.

During the first 100 s, the undulating nature of the data points (which is partly due to uncertainties in the measurements) represents the various fluctuations from semi-circular to parabolic and then to elliptic spread patterns. At 100 s, the sudden jump in the curve is due to the change in spread rate when the flame hit the width of the specimen and then progressed at a slower rate. Generally as the graph shows, the linear spread rate within the first 100 s occurred at an average value of 3.7 mm/s which is approximately 12% higher than the spread rate (3.3 mm/s) during the later part of the spread.

For the wider specimens EE3 and EE4, the linear spread pattern was more uniform during the first 100 s with average values of 3.4 and 3.6 mm/s respectively. For flame areas, specimens EE3 and EE4 had a growth constant of $0.029 s^{-1}$ while specimen E5 had $0.036 s^{-1}$ as shown in Figure 3-27.

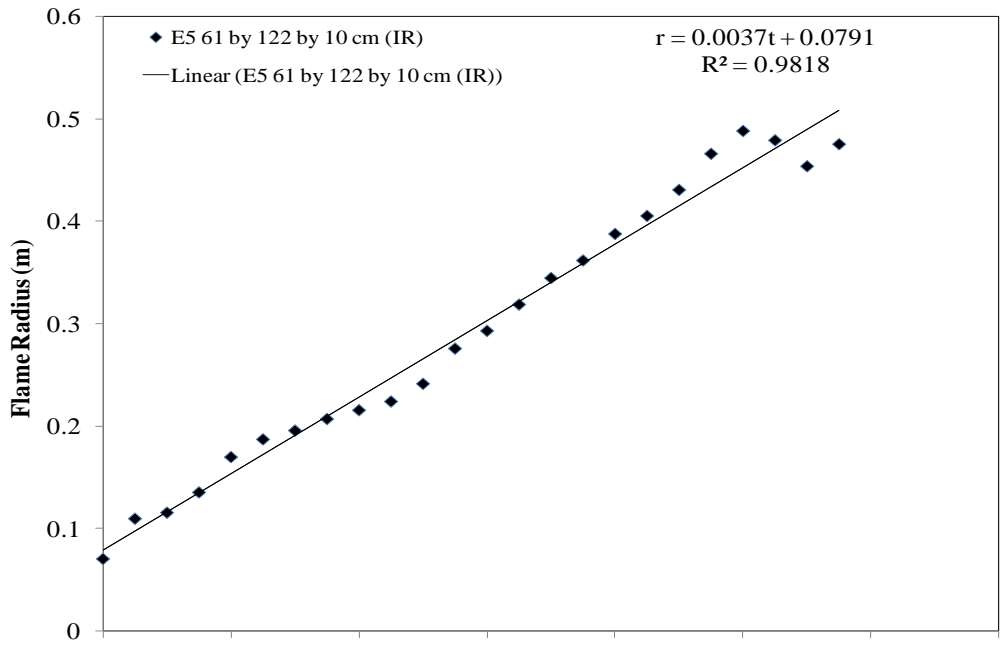


Figure 3-26. Linear regression rate for specimen E5.

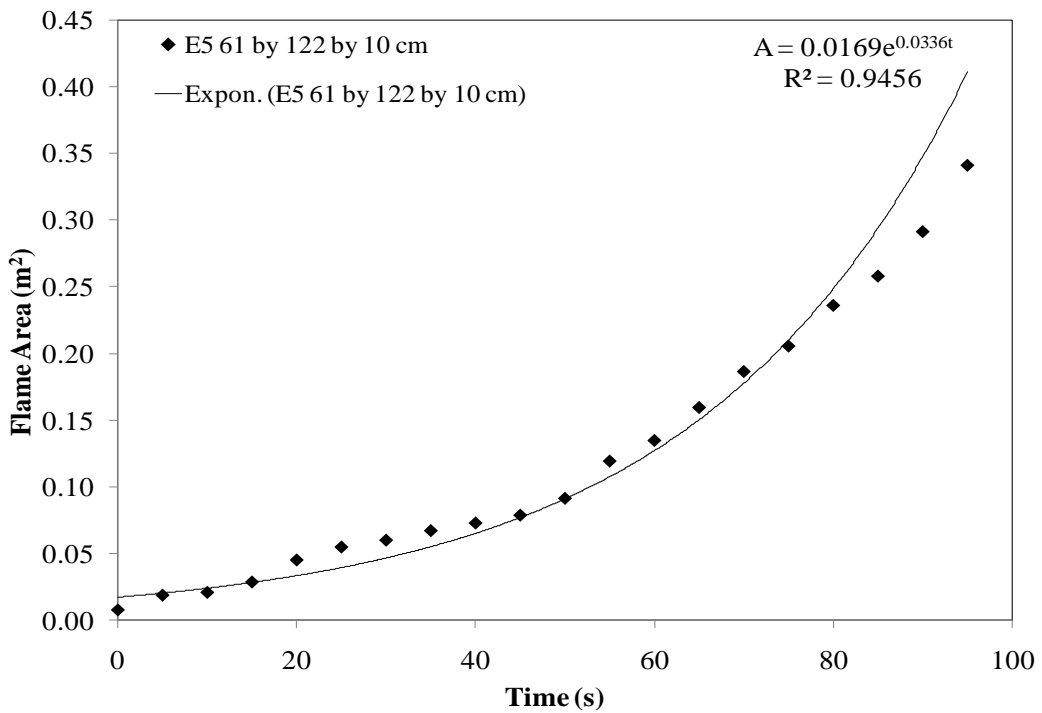


Figure 3-27. Flame area growth rate for specimen E5.

3.5.3 Comparison Of Center And Edge-Ignition Tests

The peak flame areas and flame spread rates for each test are given in Table 3-2. These parameters were found to be similar for specimens with the same physical dimensions and varied considerably with ignition location. As calculated from Table 3-2 for the six specimens with average density of 17.6 kg/m^3 , the average linear spread rate was 3.4 mm/s with a standard deviation of 0.42 which is in good agreement with flame spread rates of 3.7 mm/s and 2.5 mm/s for polyurethane foams of densities 15 and 22 kg/m^3 respectively, reported by Drysdale for horizontally burning foams [8].

Table 3-2. Summary of peak flame areas and spread rates of polyurethane foam specimens.

Test Specimen	Peak Flame Area (m^2)	Linear Regression Rate (mm/s)	Flame Growth Constant (s^{-1})
C1	0.38	3.0	0.056
C2	0.38	2.9	0.051
C3	1.56	4.0	0.042
E4	N/A	N/A	N/A
E5	0.72	3.7	0.036
EE3	1.41	3.4	0.029
EE4	1.42	3.6	0.029

Figure 3-28 compares the flame area time histories of center-ignited specimens C1 and C2 and edge-ignited specimen E5. As shown in the graph, the flame areas for the three specimens have approximately similar curves until the peak flame areas were attained at roughly 110 s . For specimen E5, there is an abrupt deviation in the growth curve at 100 s which resulted from sudden changes in the flame front geometry when the flame reached the width and started to spread across the length of the specimen at a reduced

rate until reaching the peak value after roughly 200 s. The peak flame area for E5 is 95% higher than for specimens C1 and C2 as the dimensions of E5 are 100% larger than for C1 and C2.

As given in Table 3-2, the average linear spread rate for specimen E5 is approximately 17% higher than those of C1 and C2. This is as expected since the overall size of flames (which determine the fire spread rate [8]), despite higher heat losses is larger for specimen E5 than for C1 and C2, as observed in the video records.

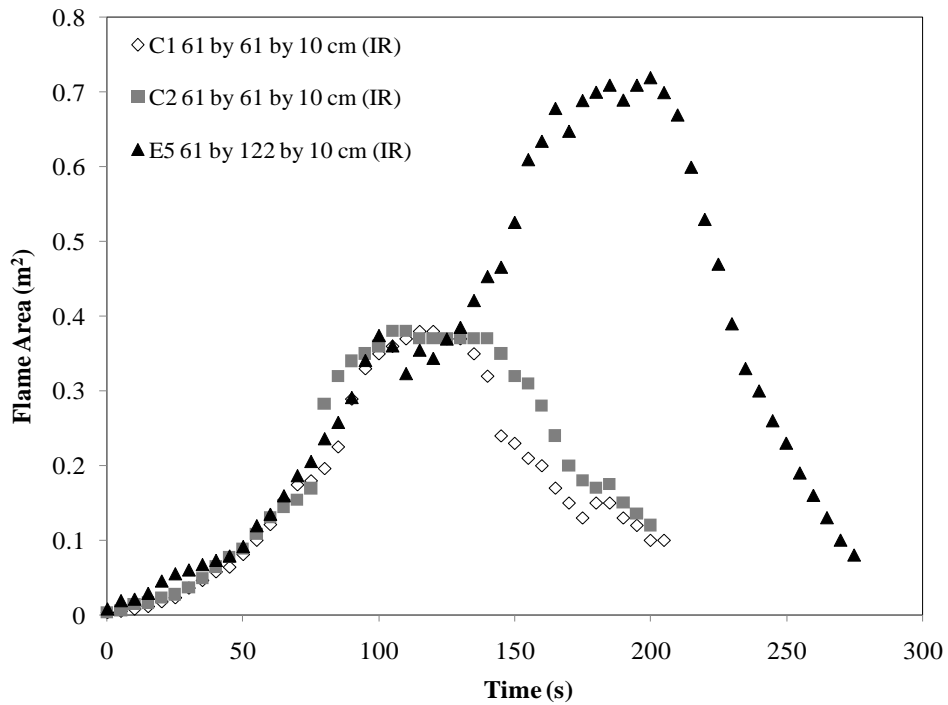


Figure 3-28. Comparison of flame areas estimated using IR video of center-ignited tests C1 and C2 and edge test E5.

For the wider specimens C3, EE3 and EE4 with similar physical dimensions of 122 by 122 by 10 cm (Figure 3-29), there is a significant difference in flame growths on the basis of the ignition locations with the center-ignited specimen C3 developing more

rapidly than those of edge-ignited specimens EE3 and EE4. As shown in Table 3-2, the estimated flame area growth constant for C3 (0.042 s^{-1}) is approximately 31% higher than those of EE3 and EE4. Similarly, the average linear regression rate for C3 (4.0 mm/s) is roughly 13% higher than those for edge-ignited specimens EE3 and EE4. These differences in the spread rates between the two ignition tests account for the gap in the flame area profiles shown in Figure 3-29. In terms of heat transfer, the more rapid increase in flame area for center ignition test C3 is as a result of less convective heat losses associated with pure radial flame growth typical of center-ignited specimens where the radiative feedback effect was considerable. The significant radiative feedback effect resulted in a rapid and more uniform flame spread across the surface.

For the edge-ignited specimens, considerable air entrainment from the ignition edge due to buoyancy effects caused a significant loss of heat energy. The energy losses reduced the radiative feedback loop which affected the flame spread rate. These scenarios are evident in the video files whereby the flame development in the edge-ignited specimens was characterised by significant flame tilting due to influx of air from the ignition edge of the specimens. The air influx also caused a considerable turbulence in the fire plume with associated heat losses.

Although the three specimens (C3, EE3 and EE4) have the same physical dimensions, the peak flame area for C3 is approximately 10% higher than the peak flame area for EE3 and EE4. This can be explained by recalling that specimen burn-out occurred at the ignition region of the edge-ignited specimens before the flame had engulfed the entire length of the specimens. For the center-ignited foam, specimen burn-out did not occur until the entire surface and parts of the sides were burning. Generally, as Figures 3-28 and 29 indicate, there was a reasonable degree of repeatability in the flame area estimates of specimens with similar dimensions and ignition location.

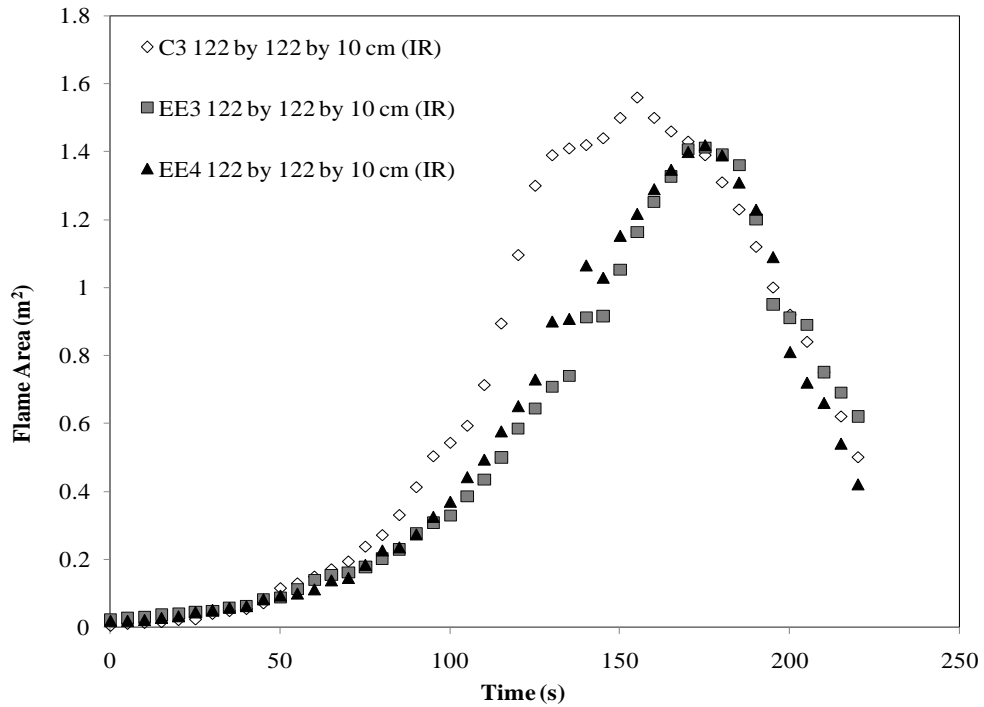


Figure 3-29. Comparison of flame areas estimated using IR video of center-ignited test C3 and edge tests EE3 and EE4.

3.5.4 Vertical Flame Spread Rates

Flame spread rates along the vertical surface of the specimens were also estimated in a similar fashion to the horizontal flame spread. The vertically downward flame propagation was measured at 5 s intervals at different locations (third, sixth and ninth cells) of individual edge-ignited specimens, based on the leading edge of the flame, shown in Figure 3-30.

It was determined that the vertical spread rate was much slower with an average value of 1.76 mm/s and standard deviation of 0.3 versus the spread of 3.4 mm/s along the horizontal surface. This was partly due to upward air flow into the flame which caused a counter-current spread. The vertical spread rate for the foams is in fair agreement with the value of 1.3 mm/s reported by Drysdale for the downward spread rate over computer cards [8], although these cards are made of a different material.

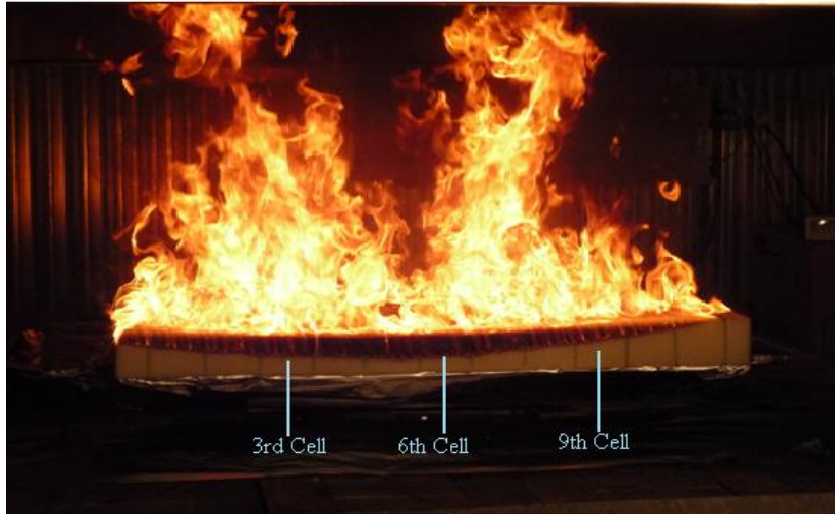


Figure 3-30. Locations of vertical flame spread rate measurements for specimen EE3.

As shown in Figure 3-31, the top vertical surface at different locations on the specimens burned almost instantaneously and developed fire more rapidly within the first 20 s of the vertical spread. The rate of vertical burn decreased as time elapsed until the entire depth of the specimen was burned out. The varying stages of burn account for the different behaviour of the specimen in fire.

Instantaneous flame spread rate at each location for edge-ignited specimens E5, EE3 and EE4 is shown in Figure 3-32. As the figure illustrates, the average spread rate was most intense at the top surface of the specimens (within 3 cm depth) which is the result of the rapid growth pattern of the spread rate versus depth of specimen curve. The high rate of flame spread within the first 3 cm of the specimen thickness can be attributed to the fact that the top and outermost layer of the specimens are very porous (with low density), which burned as thin fuels (thermally thin material) [8].

As the depth of heating increased, the spread rate decreased when the foams melted and formed a liquid pool which prevented heat penetration. During this stage, the burning rate and spread rate occurred at a relatively constant rate until the specimen thickness was gradually consumed. It is also observed that the inner bulk of the foams burned at a

slower rate than at the vertical surface. The inner burning rate was not estimated due to difficulties in tracking the flame front.

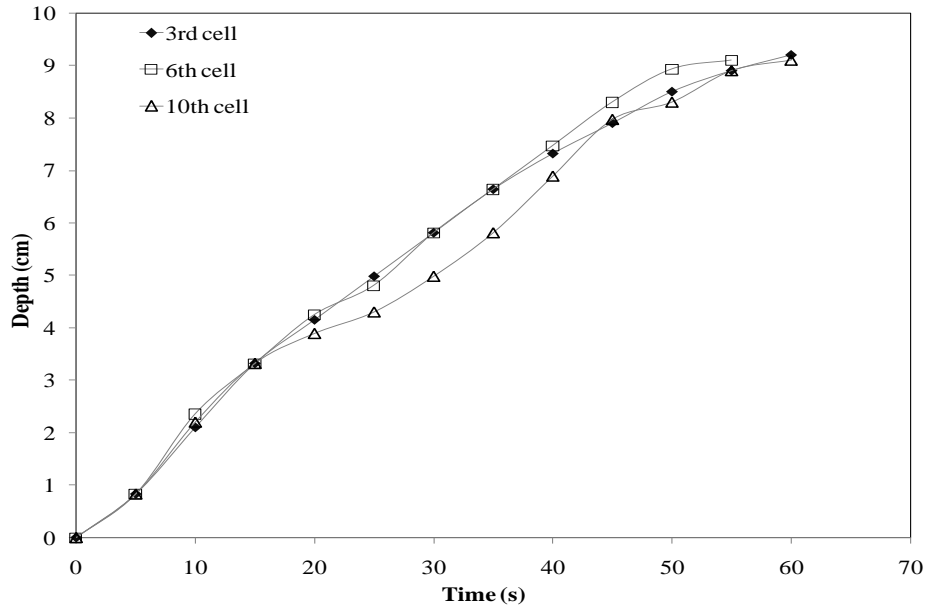


Figure 3-31. Average depth of vertical burn at different locations for specimens E5, EE3 and EE4.

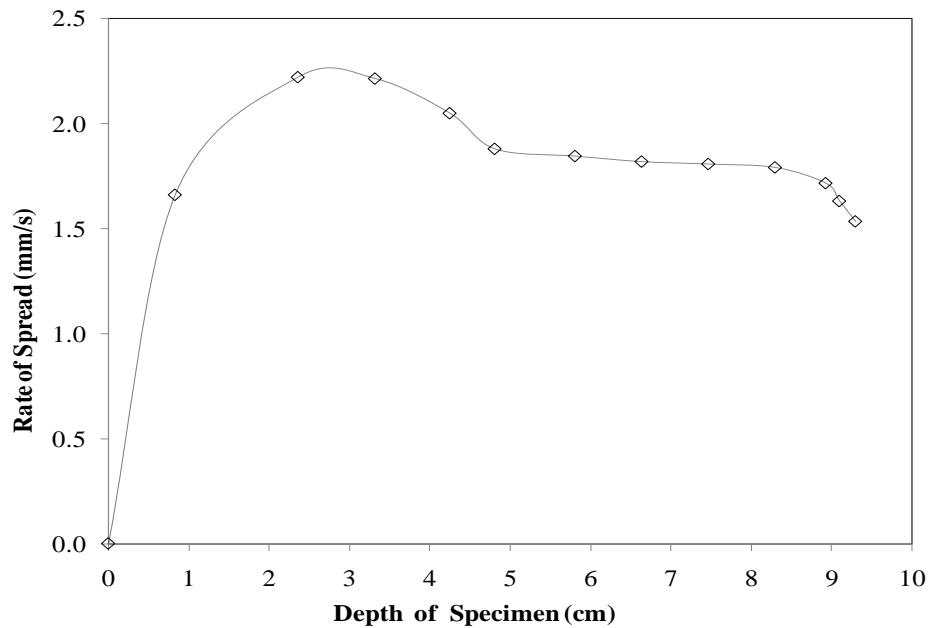


Figure 3-32. Instantaneous flame spread rate at each location (average value for specimens E5, EE3 and EE4).

3.6 Heat Release Rates

As noted earlier, the analysis of heat release rate (HRR) is the most important parameter in full-scale fire tests as it represents the size and hazard level of a complete specimen. The features of interest for these analyses will include the accelerative and decay phases of the HRR curves. The HRR-time curves will be used to analyse effects of ignition location. Other important features such as the peak HRR and time to peak HRR, total heat release (THR) and mass loss rate (MLR) will be used to compare the burning characteristics of the foams.

The selection of a uniform reference time for the plots of flame spread, HRR, MLR and other variables is important as the times in the data files generated by the furniture calorimeter system were not automatically synchronized with the video records and photographs. As the software allows the user to record an ignition time by manually pressing a button, the ignition event was used to adjust the data so that a common start time was used. Using the time correction technique, all the plots were adjusted to begin from a common starting point with the assumption that the specimens started to burn at the same time. The time correction was very important in establishing correlations between the HRR curves and the flame area curves.

A summary of the HRR data for the polyurethane foam specimens is given in Table 3.3. The ratios between peak heat release rate and peak flame area for center-ignited specimens are generally higher compared with those for edge ignition tests due to differences in energy loss between the two types of tests.

Table 3-3. Summary of heat release rate test results of polyurethane foam specimens.

Test Specimen	Peak Heat Release Rate (kW)	Time to Peak Heat Release Rate (s)	Percentage Loss in Mass (%)	Ratio of Peak Heat Release Rate and Flame Area (kW/m ²)	Total Heat Release (MJ)
C1	174	94	93	458	14.3
C2	170	95	95	447	14.7
C3	612	125	N/A	392	57.3
E4	222	145	89	N/A	27.8
E5	241	170	N/A	335	33.5
EE3	503	167	97	357	60.5
EE4	509	162	95	358	59.8

3.6.1 Center-Ignition Tests

Figure 3-33 shows the HRR-time histories for the 61 cm wide specimens C1, C2 and C3. Three features which represent the burning stages of each specimen can be identified from the graph: growth stage (burn-through and rapid growth stage), peak HRR and the decay stage. These observations are similar to those for flame spread, as flame area growth and HRR for each of the specimens show exponential growth and decay stages in a similar pattern.

As can be seen from Figure 3-33, significant fire growth started after a time delay of 30 s, which depends on the thermal inertia ($k\rho c$) of the foam and the total heat flux to the surface [8]. During this time delay, burn-through in the thickness direction occurred which established sufficient heat transfer from the flame before the rapid flame spread/growth commenced. As the burn-through was necessary to overcome the thermal

inertia, a considerable amount of energy was transferred into the specimen, which contributed to a delay in the flame growth and a negligible HRR. The rapid flame spread represents the exponential rise in the HRR-time curve.

Similar to flame areas, the center ignition specimens follow the same growth pattern at the initial stage of the tests but the curves showed a clear departure from each other at approximately 80 s of the tests.

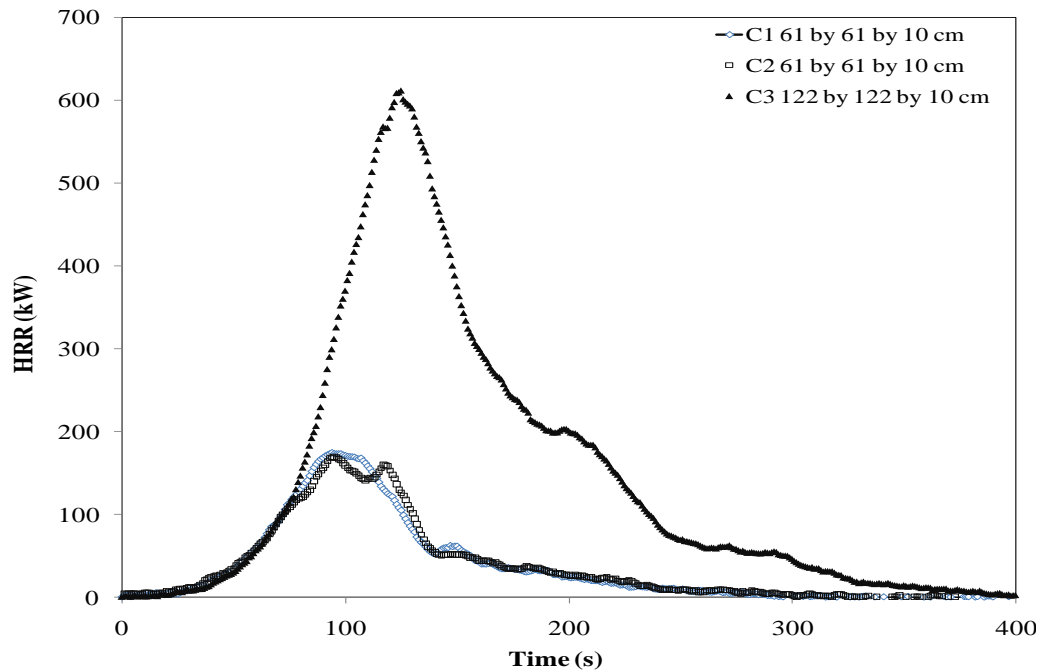


Figure 3-33. HRR-time histories for specimens C1, C2 and C3 during center ignition tests.

The curves for specimens C1 and C2 reached the peak HRR of 174 and 170 kW respectively at approximately 95 s of the tests while specimen C3 increased rapidly from 80 s until a peak HRR of 612 kW was reached at 125 s. Although the 61 cm wide specimens C1 and C2 showed a high degree of repeatability, a distinguishing feature is evident at the peak and decay stages of the curves. For instance, specimen C2 had two peaks (170 and 160 kW attained at 95 and 117s respectively) and one trough (144 kW at 107 s) as opposed to a single peak for specimen C1. For specimen C2, the decrease in HRR to the trough was due to onset of specimen burn-out at the middle of the specimen

where ignition started as observed in the video record. The quick recovery to the second peak resulted when the edges of the specimen were engulfed in flames (Figure 3-34). Beyond this second peak HRR, the fire decays exponentially with time for all the specimens until a steady state condition was reached.

Comparing the different sizes of specimens, the peak HRR of specimen C3 is approximately 256% higher than those for C1 and C2. This is as expected since the surface area of specimen C3 is 300% larger than those for specimens C1 and C2. As explained in section 3.3.1, the flame front propagated radially from the ignition point and advanced towards the sides of the specimen until the whole surface was engulfed in flame. The flame propagation across the surface of specimen C3 was faster than in specimens C1 and C2. Thus, when the entire surface of C1 or C2 was burning (with a peak HRR of 174 kW and 170 kW respectively), the larger surface area specimen was already engulfed in flame (with the production of peak HRR of 612 kW).



Figure 3-34. Burning of portions of the specimen at the four edges of specimen C1.

An example of the dependence of HRR on flame area is shown in Figure 3-35 for specimen C1. The HRR versus flame area time histories showed a good agreement as both parameters grew exponentially with time. A striking feature of the two variables is

the consistency at which the flame area profiles progressively tracked the HRR curves. This agreement in the two growth curves indicates that flame spread is a dominant fire variable which determines the fire growth for a burning fuel [8]. As evident in the two growth curves, any point on the flame area profile represents an amount of heat energy released. For instance, the peak flame area of 0.38 m^2 corresponds to the peak heat release rate of 174 kW. The HRR and flame area curves are typical of the center ignition specimens C2 and C3.

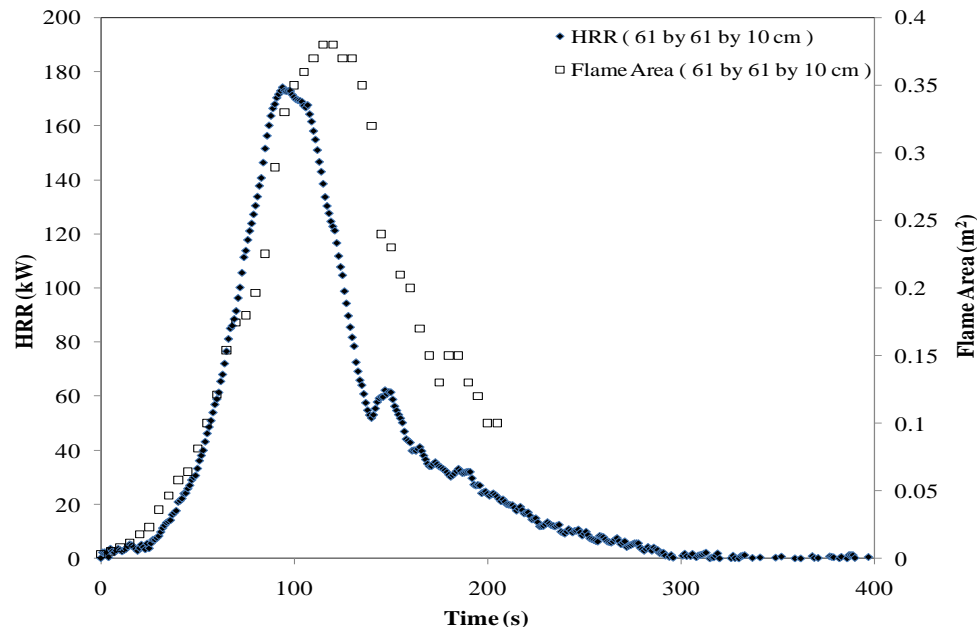


Figure 3-35. Relationship between HRR and flame area growth for specimen C1.

3.6.2 Edge-Ignition Tests

The burning behaviour of edge-ignited specimens E4, E5, EE3 and EE4 is shown in Figure 3-36. The HRR-time curves of these specimens have features typical of center-ignited specimens in terms of repeatability and similar fire growth pattern. For the four specimens, the HRR growth occurred almost at a uniform rate until approximately 80 s when the departure in growth curves became significant. For specimens E4 and E5, this represented the moment the flame front reached the width of the foams and then

progressed across the length of the surface with a rapid increase in size of the fire. After the first 100 s of the tests, the two growth curves for specimens E4 and E5 showed further departure from each other.

As observed in the video image, the flame front for specimen E4 propagated a longer distance across the surface than in the test of specimen E5 before the width was engulfed in flame. Similar observations for specimens E4 and E5 were made for both specimens EE3 and EE4 which accounted for the fast growth in the fire at the moment the peak HRR values for E4 and E5 were reached.

A unique feature of the 61 cm wide specimens is the uniform recession from peak HRRs of 222 and 241 kW to the second peak value of 182 and 198 kW respectively for specimen E4 and E5. There is also a difference in the areas under the curves indicating a difference of 17% in the THR between the two specimens which is expected since the mass difference between the specimens is approximately 11%.

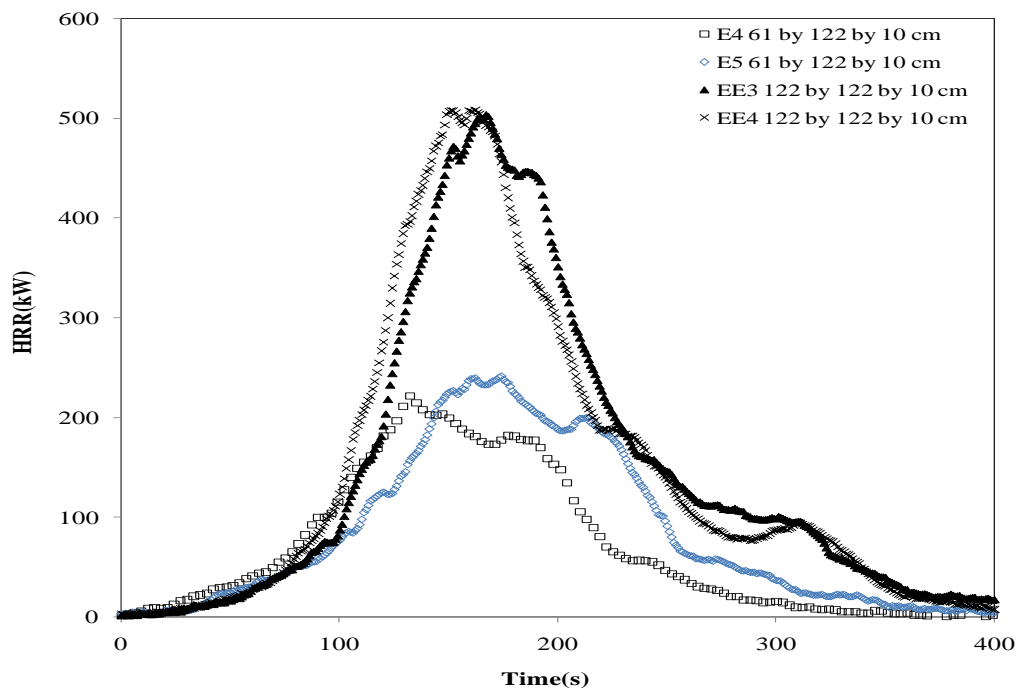


Figure 3-36. HRR-time histories for edge-ignited specimens E4, E5, EE3 and EE4.

For specimens EE3 and EE4, the peak HRR values are within 2% of each other while those for E4 and E5 vary by 8%. Comparing the different size of the specimens, the average peak HRR for specimens EE3 and EE4 is more than double that of specimens E4 and E5. The relationship between the HRR and flame area is shown in Figures 3-37 for specimen EE4. Both parameters grew and declined exponentially with time in a similar fashion as the center-ignited specimens. The two growth curves show the interdependence between the HRRs and flame areas. The growth in flame area results in increase in the HRR and as the specimen is consumed, the flame area diminishes with a decrease in the HRR.

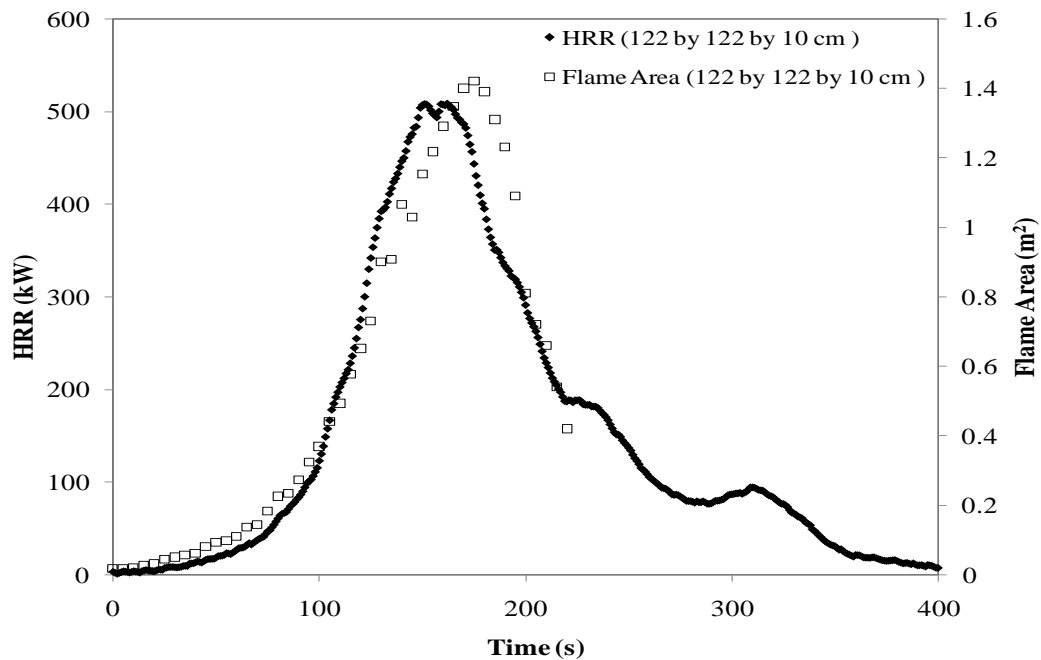


Figure 3-37. Relationship between HRR and flame area growth for specimen EE4.

3.6.3 Comparison of Center and Edge-Ignition Tests

As Figure 3-38 shows, there are clear differences in the burning behaviour of the center and edge-ignited specimens despite having approximately the same mass and surface areas. Specimen C3 attained a peak HRR of 612 kW early in the fire which is approximately 17% higher than those attained by specimens EE3 and EE4. Aside from

the higher peak HRR, the fire from specimen C3 grew more rapidly than those from specimens EE3 and EE4, which is evident in the gaps existing in the three growth curves. One reason for the gap is that the pool fire was more pronounced in specimen C3 than in specimen EE3 and EE4. Another reason is due to the higher convective heat losses associated with edge-ignition tests than in center-ignition tests.

As observed during the tests, the center-ignited specimens maintained a more laminar flame structure with pure radial flame fronts especially at the early stage as opposed to the pulsating flame structure observed in edge-ignited specimens. Although flames from the two ignition tests (specimens C3 and EE3/EE4) flickered significantly when the fire was well developed, the flame from specimen C3 had a more uniform plume and less air influx than the edge specimens EE3 and EE4. Hence, the laminar flame structure and the uniform air entrainment accounts for the smoothness of the curve for specimen C3.

The higher radiative feedback from the large pool fire contributed to the higher HRR from specimen C3 than from EE3 and EE4. The considerable specimen burn-out which occurred at the ignition section for edge-ignited specimens EE3 and EE4 affected the flame size (and thus the HRR) behind the leading edge as opposed to stronger flames from specimen C3 which had a more persistent burning area. The specimen burn-out that occurred during the edge tests created an imbalance in the natural buoyancy of the flame as air flowed into the flame preferentially from the ignition side, thereby causing a somewhat counter-current fire growth than in the center tests [8].

The HRR for center (C1 and C2) and edge-ignited (E4 and E5) specimens with a width of 61 cm are shown in Figure 3-39. However, different surface areas of the specimens make it difficult to examine the effects of ignition locations on the HRR.

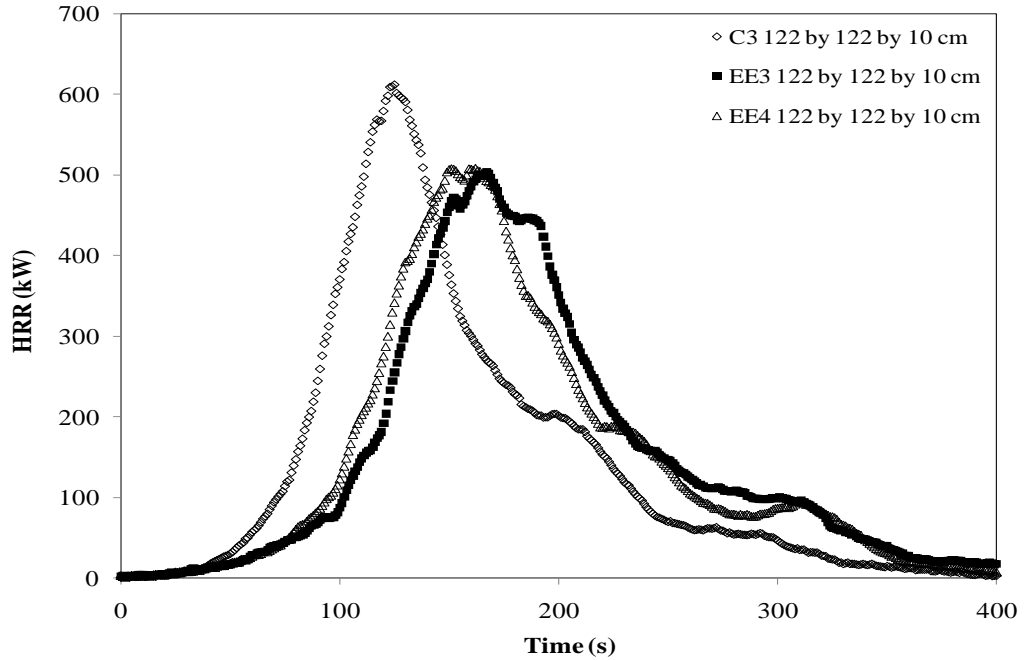


Figure 3-38. Comparison of HRR for center (C3) and edge-ignited (EE3 & EE4) specimens.

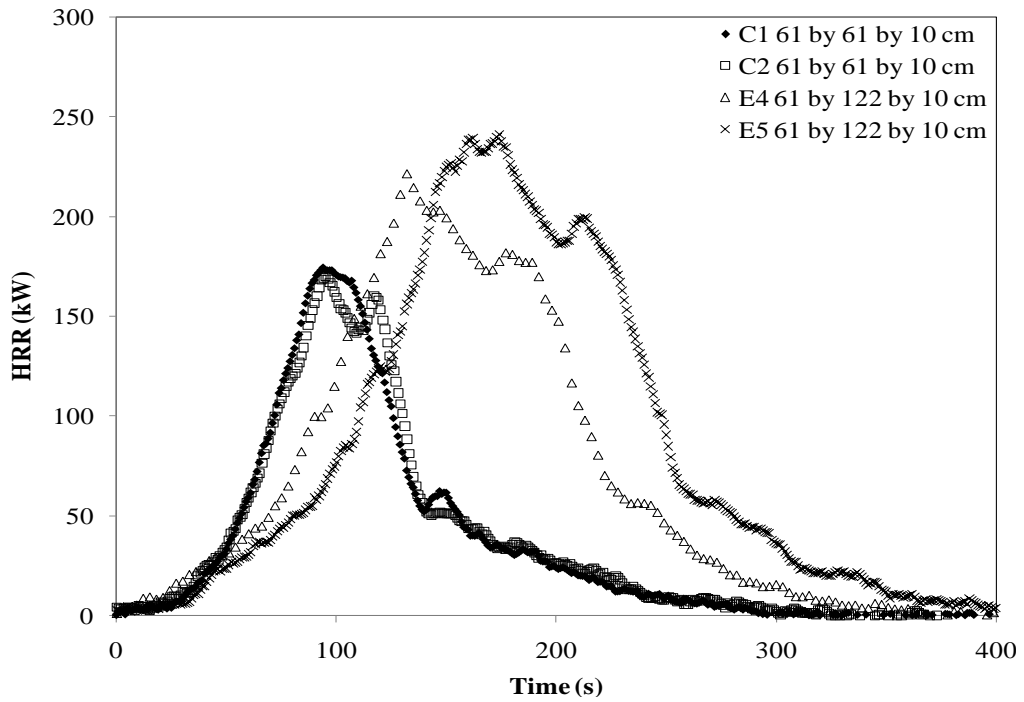


Figure 3-39. Comparison of HRR for center (C1 & C2) and edge-ignited (E4 & E5) specimens.

3.7 Mass Loss Rates

The mass loss rates for each of the specimens can also be used to characterise the fire behaviour of the foams as they determine the rate of energy release in fire. This is because the rate at which the mass of a fuel decomposes and eventually volatilizes under heat irradiance is a strong determinant for flame spread rate and rate of fire growth as given in Equation 2-32. In fire hazard assessments, fuels which produce gaseous combustibles very rapidly have the tendency to generate greater amount of heat energy and increase in flame spread. Thus, the pyrolysis rates of the foam specimens will also be used to compare fire behaviours during the center and edge ignition tests.

As shown in Figure 3-40, the pyrolysis-time history for specimens C1 and C2 increased and decreased in a similar pattern as the corresponding heat release rate. A significant feature of the MLRs is the agreements in the peak values between similar specimens. As shown in Figure 3-40, a 0.4% difference in the peak MLRs (7.18 and 7.15 g/s) for specimens C1 and C2 produced a 3% difference in peak HRRs.

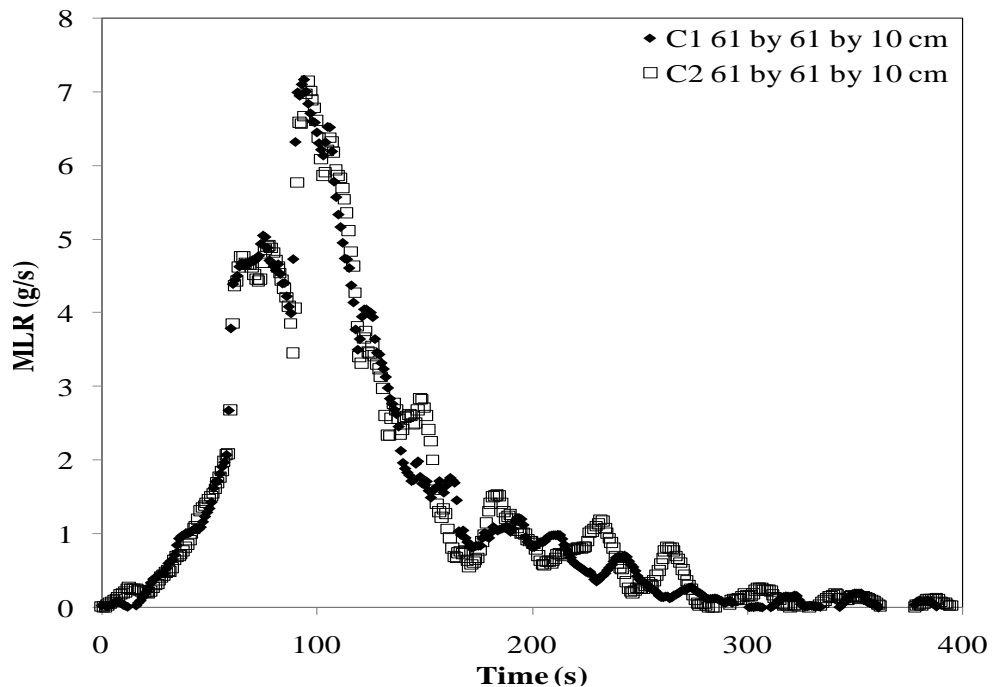


Figure 3-40. Comparison of mass loss rates during center-ignition tests of specimens C1 and C2.

For edge-ignited specimens EE3 and EE4 shown in Figure 3-41, peak MLRs differed by 0.09% with a corresponding 1% difference in peak HRR. For different sizes of specimens, the peak MLRs varied proportionally with dimensions of the specimens. For instance, the peak MLR from specimen E5 is 19% higher than those for specimens C1 and C2. Also, the peak MLR from C3 is 67 and 58% higher than the peak MLR from C1 and C2. Aside from having greater fire load, the wider specimens produced sufficiently large fires such that flames with stronger radiative feedback caused increased production of volatile gases which resulted in high heat release rates. Furthermore, the time to peak MLRs and peak HRRs are essentially the same for similar specimens which indicate that peak HRRs result at the instant the pyrolysis rate is maximum.

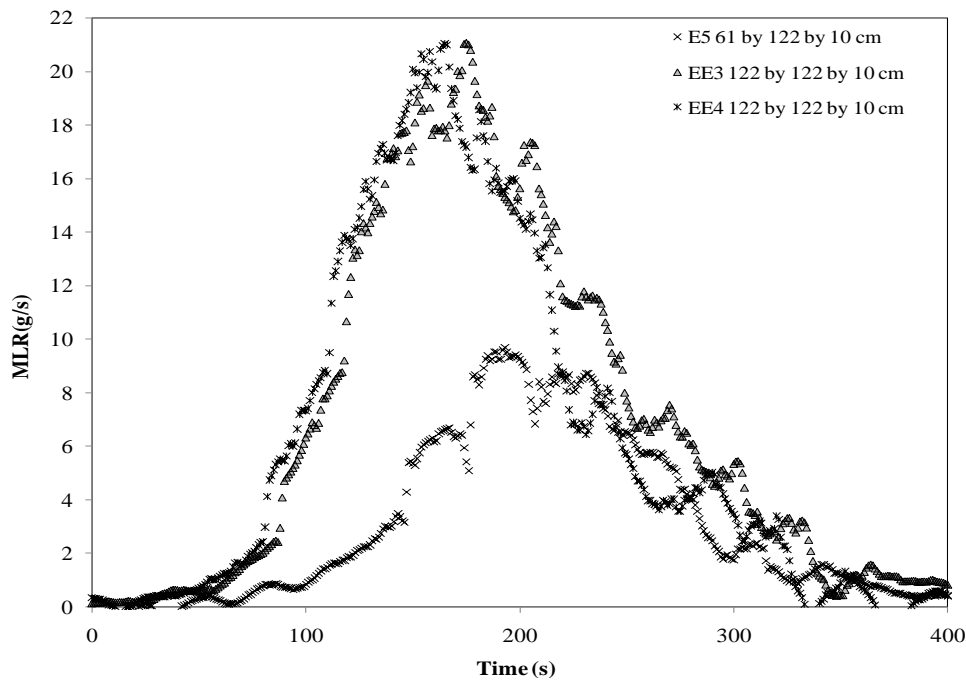


Figure 3-41. Comparison of mass loss rates during center and edge-ignition tests of specimens E5, EE3 and EE4.

3.8 Summary of Chapter

The motivation for the present chapter was to investigate the fire test behaviour of polyurethane foams based on their ignition locations. The estimated flame areas and flame spread rates, based on the visual observation of the video records, varied significantly with dimensions and ignition locations of the specimens. Flame spread patterns for both ignition tests developed in a similar fashion at the early stages of flame development and then assumed different geometry when the flame front reached the width of the specimens. For specimens of the same size, center-ignited foams produced flame areas which were 10% larger compared to edge-ignited specimens. Peak values of the flame areas were attained more rapidly in center ignition tests. The average horizontal and vertical flame spread rates for the entire specimens showed good agreement with the literature.

The examination of the furniture calorimeter data for the specimens shows that fire growths are sensitive to the ignition location. For instance, the center ignition tests produced higher rates of heat release than edge ignition tests. Peak heat release rates were approximately 20% higher in center ignition tests than for the edge ignition tests. Also, the ratios of the peak heat release rate to peak flame area were larger in center tests compared to edge ignition tests. The total heat release rate was independent of the ignition location but increased with the physical dimensions of the specimens.

Chapter Four will focus on the cone calorimeter tests of the representative foam specimens. Results from the cone calorimeter tests will also be used in combination with the flame areas determined in this Chapter in the modeling section of this project.

CHAPTER FOUR: SMALL-SCALE TESTS OF POLYURETHANE FOAMS

4.1 Introduction

The small-scale tests of the polyurethane foam specimens were conducted on the 6th and 10th November, 2008 using the FTT (Fire Testing Technology, East Grinstead, UK) cone calorimeter at the University of Waterloo. The tests were primarily intended to measure HRR densities (kW/m^2) of various thicknesses of polyurethane forms which are required as input data for modeling of full-scale fire behaviour of the specimens. The small-scale tests are also important for investigation of thickness effects, effects of ignition source and testing procedure of the specimens on the rate of heat release.

Vertical flame spread tests were also conducted on the 12th November, 2008 using the University of Saskatchewan FTT cone calorimeter. This equipment is identical to the University of Waterloo cone calorimeter. The tests were conducted using different thicknesses of polyurethane foams in single and composite forms. Data obtained from the video records were also used to assist in modeling the fire behaviour of each individual foam as a layered specimen, as will be discussed in Chapter Five.

4.2 Specimen Preparation

Four different thicknesses of polyurethane foam specimens were selected for the cone calorimeter tests: 2.5 cm (1 in), 5 cm (2 in), 7.5 cm (3 in) and 10 cm (4 in) thick. These foams were the same foams described in section 3.2 (but here the other three thicknesses were also used). The surface area of each of the specimens measuring 10 by 10 cm was in line with the standard test specimen dimensions for the cone calorimeter as stated in ASTM E 1474 [55].

The nominal masses of each triplicate set of specimens were measured on the cone calorimeter load cell prior to conditioning. The conditioning of the specimens was carried out using a saturated solution of magnesium nitrate salt contained in a plastic

conditioning container, shown in Figure 4-1. The specimens were positioned on top of a metal rack mounted above the saturated salt solution which produced a relative humidity level of $53 \pm 5\%$ at 23°C . The whole assembly was maintained at air-tight conditions inside the container for 24 hours to ensure an equilibrium state was attained.



Figure 4-1. Foam specimens positioned atop a metal rack inside a conditioning container.

To control heat losses and prevent the spill of molten materials during the tests, a thin aluminum foil was cut and wrapped around each specimen to cover the sides and bottom before testing. The wrapping techniques used was consistent with the methods used by the fire research group at University of Waterloo in 2006 [61]. The technique involved wrapping the specimens and cutting off the excess foil from around the top surface of the specimen. The dimensions of the aluminum foil were cut as shown in Figure 4-2, to ensure that there was a complete seal of the specimen periphery except at the surface where heat irradiance was needed.

Different testing/mounting methods were used during the cone calorimeter tests. The first method used a steel edge frame, while the second used only a durarock board, as shown in Figures 4-3. The use of steel edge frame was in line with the ASTM E 1354 [75] test standard to restrain excessive flaming along the edges of the specimens during

tests. It was also intended to reduce the tendency for specimen deformation (delamination and intumescence) when irradiated with high heat flux.

The durarock block set-up was used to investigate the sensitivity of the specimens' heat release rates to changes in the testing procedure such as the use of butane igniter versus the cone heater. While the specimens tested with an edge frame were completely covered by the aluminum foil, for the durarock board set up, the specimens were wrapped to half their thickness with the thin foil and then placed on the board. The entire assembly was mounted on top of specimen holder platform within the combustion space. Effects of specimen mounting techniques will be discussed in section 4.6.



Figure 4-2. Thin aluminum foils for wrapping the conditioned specimens.



Figure 4-3. Specimen set-up using durarock board mounting.

During the steel edge frame/ specimen assembly, the bottom tray was positioned on top of two plywood boards for stability. MDF boards were inserted inside the bottom tray and a ceramic slab was placed on top of the boards. The wrapped specimen was positioned on top of the ceramic board and then the edge frame was used. Other pieces of plywood were also placed on top of the initial plywood slabs. These plywood pieces were placed close to the sides of the bottom tray to ensure that available height for the edge frame above the specimen did not cause compression as shown in Figure 4-4. It was ensured that the height of the frame above the bottom tray was constant throughout the coupling process. Note that an edge frame of depth 10 cm was constructed to accommodate the 7.5 and 10 cm thick specimens whereas for 2.5 cm thick specimens, a 5 cm thick holder inserted with MDF boards (to reduce the depth) was used.

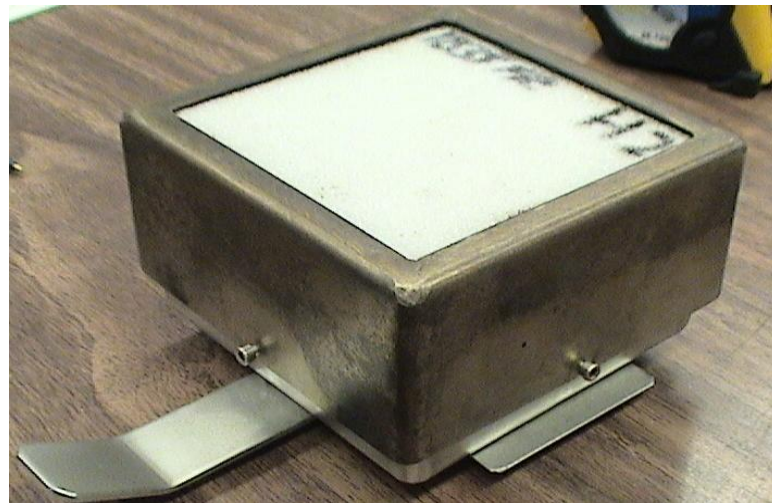


Figure 4-4. Specimen mounting using steel edge frame.

4.3 Calibration

To adequately investigate the fire behaviour of the foams in small-scale tests, the principle input variables included the air supply and incident heat flux. The apparatus was first calibrated using atmospheric oxygen to produce a voltage corresponding to 21% atmospheric oxygen. The oxygen, carbon dioxide and carbon monoxide were zeroed using Nitrogen gas. Thereafter, the carbon dioxide and carbon monoxide were

spanned to the correct percentages using a calibration gas mixture of carbon dioxide, carbon monoxide and nitrogen.

The heat release rate was calibrated using a 5 kW methane gas burner and at an air flow rate of 24 L/min. The calibration factor was $0.0402 \pm 10\%$ of the previously determined calibration factor. The cone heater heat flux for the tests was calibrated using a Schmidt-Boelter heat flux gauge (Medtherm, Huntsville, AL) that was irradiated with heat from conical heating element. A heat flux of 35 kW/m^2 was used for the entire test program based on CBUF work [24]. However, there was no means for calibrating the butane-igniter but it was ensured that the flame heat flux was high enough to ignite the foam specimens.

4.4 Experimental Procedure

Three different sets of tests were conducted. The first sets of tests were run on Nov. 6, 2008 using the standard steel edge frame with aluminum foil. The physical characteristics of the specimens are given in Table 4-1. The second tests using the durarock board were run on Nov. 10, 2008. The characteristics of these specimens are given in Table 4-2. The third tests were aimed to measure the vertical flame spread rates, and were carried out on Nov. 12, 2008.

For all the tests, the specimens were tested in a horizontal orientation at the irradiance level of 35 kW/m^2 . The butane-ignited specimens were tested in the same orientation except that ignition was localised to a fraction of the exposed surface. All specimens were positioned below the shutter plate which controls heat irradiance from the heating element. Prior to igniting each specimen, the distance between the top of the specimen and bottom of the shutter plate was adjusted to 25 mm. The shutter was then quickly opened by hand (for cone-ignited tests) to allow uniform heat irradiance on the specimen and simultaneously, the electric spark ignitor located above the surface of the specimen was positioned to provide pilot ignition. Once flaming ignition was established as shown in Figure 1-7, the spark ignitor was removed. To protect the

operator, the combustion hood was lowered in a horizontal position to cover the burning specimen. As the tests progressed, the data was collected every second using the data acquisition system supplied with the equipment. Each specimen was allowed to burn to completion as a reliable basis for comparing the total heat release of the specimens from run to run. The end of each test was marked as soon as no significant flame existed in the specimen holder.

Table 4-1. Summary of physical properties of specimens tested with the steel edge frame.

Specimen Description (cm)	Thickness (cm)	Conditioned Mass (g) without foil.	Conditioned Mass (g) with foil.
2.5 cm Test 1	2.21	5.00	5.80
2.5 cm Test 2	2.50	4.30	5.60
2.5 cm Test 3	2.50	4.40	5.60
5.0 cm Test 1	4.60	10.00	9.90
5.0 cm Test 2	4.53	8.00	9.80
5.0 cm Test 3	4.53	8.00	9.60
7.5 cm Test 1	7.40	13.00	15.40
7.5 cm Test 2	7.50	13.00	15.10
7.5 cm Test 3	7.40	13.00	15.90
10.0 cm Test 1	10.01	19.30	24.00
10.0 cm Test 2	9.85	17.30	22.00
10.0 cm Test 3	9.82	17.10	22.00

Table 4-2. Summary of physical properties of specimens tested using non-conventional technique (durarock board and butane ignition).

Specimen Name	Thickness (cm)	Initial Mass (g)
2.5 cm A Test 1	2.52	4.30
2.5 cm A Test 2	4.59	4.70
2.5 cm B Test 1	2.50	4.80
2.5 cm B Test 2	2.60	4.20
5.0 cm A Test 1	4.50	7.70
5.0 cm A Test 2	4.53	7.80
5.0 cm B Test 1	4.40	8.00
5.0 cm B Test 2	4.54	8.10
7.5 cm A Test 1	7.45	13.10
7.5 cm A Test 2	7.45	13.30
7.5 cm B Test 1	7.33	12.90
7.5 cm B Test 2	7.40	12.60
10.0 cm A Test 1	9.90	17.10
10.0 cm A Test 2	9.93	16.80
10.0 cm B Test 1	9.84	15.30
10.0 cm B Test 2	10.00	18.20

A = Cone heater-ignited specimen.

B = Butane-ignited specimen.

4.5 Vertical Flame Spread Tests

For the vertical flame spread tests, the specimens were cut and conditioned as discussed in section 4-2. Furthermore, the front side of each specimen was marked at 1 cm intervals to enable the measurement of the vertical flame propagation as shown in Figure 4-5. The specimen holder, however, was different from the ones described in section 4-2. The specimen holder used had a depth of approximately 20 cm so as to accommodate the depth of 5 and 10 cm composite specimens. The width of the holder

measured 12.5 cm in order to accommodate 1.25 cm thick insulating boards that lined the interior surfaces of the holder.

Prior to each test, a thick wooden block and several plywood slabs were placed on top of the bottom tray of the holder. This was to ensure that the top surface of each specimen was flush with the height of the specimen holder. Thin aluminum foil was also sandwiched between the specimen and the wooden block to reduce heat transfer from burning foams to the plywood. To facilitate the observation of the vertical flame spread, one side of the specimen holder was left open.

The tests were conducted at 35 kW/m² heat flux. Specimens tested include 2.5, 5.0, 7.5 and 10 cm single specimens, and 2.5 and 5.0, 5.0 and 5.0 and 5.0 and 10.0 cm composite specimens. The flame spread patterns were captured using a Sony MiniDV camcorder (Sony of Canada, Toronto, ON). Data obtained from the tests were based on the video records.



Figure 4-5. Vertical flame spread rate test of 10 cm specimen using the cone calorimeter.

4.6 Cone Calorimeter Results

The combustion histories for all the small-scale specimens are detailed in this section. All the HRR density-time curves presented here represent the average of three tests (edge frame-tested specimens) or two tests (durarock-mounted specimens). The results of the vertical flame spread rates are also presented. Prior to using the average HRR densities for these analyses, the repeatability of the results for specimens of the same size and test techniques was ascertained. As the specimens showed varying ignition times, the time correction technique discussed in section 3.5.1 was used to ensure there was a common starting point for the HRR plots. The fire responses (ignition times, peak HRRs, times to peak HRRs, THR_s, and average HRR after ignition) of the specimens are summarized in Tables 4-3, 4-4 and 4-5. The results of the vertical flame spread rates are given in Table 4-6.

Table 4-3. Summary of performance characteristics of specimens tested in steel edge frame.

Specimen Description	Time to Ignition (s)	Peak HRR (kW)	Time (s) to Peak HRR	THR (MJ/m²)
2.5 cm Test 1	3	396.90	23	12.33
2.5 cm Test 2	2	419.70	20	12.16
2.5 cm Test 3	5	392.49	19	11.93
5.0 cm Test 1	4	393.61	33	21.75
5.0 cm Test 2	2	404.69	31	21.08
5.0 cm Test 3	2	402.99	28	20.84
7.5 cm Test 1	4	333.74	28	36.17
7.5 cm Test 2	3	349.31	41	36.38
7.5 cm Test 3	4	325.79	79	36.55
10.0 cm Test 1	4	334.82	22	54.05
10.0 cm Test 2	4	330.79	26	50.75
10.0 cm Test 3	6	348.77	21	49.19

Table 4-4. Performance characteristics of specimens tested on durarock board.

Specimen Description	Ignition Time (s)	Peak HRR (kW/m²)	Time (s) To Peak HRR	THR (MJ/m²)
2.5 cm A Test 1	2	435.26	20	11.06
2.5 cm A Test 2	2	406.29	20	12.49
2.5 cm B Test 1	7	260.19	27	9.35
2.5 cm B Test 2	8	223.89	32	8.92
5.0 cm A Test 1	3	350.12	34	19.98
5.0 cm A Test 2	2	360.03	36	20.15
5.0 cm B Test 1	2	225.15	41	16.63
5.0 cm B Test 2	5	238.58	38	19.62
7.5 cm A Test 1	4	412.01	22	34.12
7.5 cm A Test 2	3	418.61	21	34.12
7.5 cm B Test 1	7	309.37	48	27.42
7.5 cm B Test 2	14	301.08	48	30.76
10.0 cm A Test 1	3	467.52	24	44.09
10.0 cm A Test 2	2	453.50	26	44.29
10.0 cm B Test 1	10	352.77	54	38.98
10.0 cm B Test 2	7	361.23	61	46.68

Table 4-5. Comparison of average HRR density at various times after ignition.

Specimen Description	Average HRR Density (kW/m²) After Ignition Time			
	60 s	120 s	180 s	240 s
2.5 cm Test (1, 2 & 3)	174.22	99.41	66.49	49.42
2.5 cm Test A (1 & 2)	191.65	94.20	N/A	N/A
2.5 cm Test B (1 & 2)	111.03	74.27	N/A	N/A
5.0 cm Test (1, 2 & 3)	241.35	163.08	118.06	88.59
5.0 cm Test A (1 & 2)	292.97	165.11	110.00	N/A
5.0 cm Test B (1 & 2)	125.31	110.15	62.45	74.63
7.5 cm Test (1, 2 & 3)	267.99	257.03	199.80	150.00
7.5 cm Test A (1 & 2)	336.59	281.68	187.28	241.61
7.5 cm Test B (1 & 2)	186.84	173.31	149.54	165.52
10.0 cm Test (1, 2 & 3)	254.77	208.02	189.50	178.00
10.0 cm Test A (1&2)	349.87	324.59	243.86	182.01
10.0 cm Test B (1&2)	200.11	211.29	194.35	168.05

N/A: Specimen was completely burned out (zero HRR value) at the reference time.

Table 4-6. Vertical flame spread rate measurements.

Foam Specimen (cm)	Ave. Flame Spread Rate (mm/s)
5 (cone)	3.0
7.5 (cone)	3.0
10 (cone)	2.8
2.5 and 5.0 (cone)	2.4
5.0 and 5.0 (cone)	2.4
5.0 and 10.0 (cone)	2.3

There were variations in the burning characteristics of the specimens related to different thicknesses of the specimens and heat fluxes used, and other factors such as the specimen setting and mounting techniques (heat sink and obstructed air passage effects due to edge frame).

The results for 10 cm (4 in) thick specimens tested using the three specimen preparation techniques are shown in Figure 4-6. Each of the profiles represents an average HRR density for a set of two or three specimens tested under similar condition. As visualised in the three profiles, the HRR-time histories show features such as the rapid growth phase, the plateau (point of peak HRR), fluctuating recession to a trough and extended gradual decay to steady state conditions. However, the rate at which the three curves attained these phases of burn varied with the testing procedure and ignition source.

The durarock-mounted, cone-ignited specimens showed the most active burning with a peak HRR density of 456 kW/m^2 attained at 24 s as opposed to 352 and 332 kW/m^2 attained at 56 and 21 s respectively for butane-ignited (durarock-mounted) and steel edge frame-tested specimens. The rapid flame growth for the cone-ignited, durarock-mounted specimens suggests that the surface of the specimens burned almost immediately after the heat flux irradiated the specimens. Also, it was likely that most of

the uncovered sides of the specimens received a fraction of the heat flux. So, it is expected that the variations in peak HRR densities were due to differences in intensity of the incident heat fluxes on the specimens.

As remarked by Rowen [76], materials with similar properties have the tendency to respond differently when subjected to different heat fluxes. At elevated heat fluxes, the resistance to thermal degeneration of materials are reduced and this results in an accelerated pyrolysis mechanism [8].

As illustrated in the curves (Figure 4-6), the 35 kW/m^2 heat flux from the cone heater uniformly irradiated the top surface (exposed area) of the specimens instantaneously with a significant generation of volatile gases. The rapid influx of the volatiles into the flame resulted to large HRR per unit area of the specimen. This is contrary for the butane-ignited, durarock-mounted-specimens where ignition was localised to a point on the exposed surface. With the localised ignition, an appreciable amount of time elapsed before the entire surface was set on fire. This accounted for the gap in the growth curves between the cone-ignited versus the butane-ignited curves.

However, the heat flux effects for edge frame-tested specimens did not support the findings by Rowen as the edge frame-tested specimens had a suppressed peak HRR of 328 kW/m^2 . This discrepancy was clarified by Babraskas et al [77] in their investigation of effects of steel edge frame on HRRs. Babraskas remarked that steel edge frame-tested specimens usually produce HRRs with reduced peak when compared with non-conventional tests (without steel edge frame) due to its heat-sink effects. Also, due to the use of the thin aluminum foil, the sink effect was enhanced but by a negligible amount [77].

Aside from the heat sink effect, restricted air entrainment to the sides of the burning specimens due to use of the edge frame resulted to restrained burning of the specimens. This also contributed to the reduced peak HRR. However, the use of the open durarock board provided a confinement to the molten specimen for continuous heat irradiance from the cone heater. As a result, the molten material had an extended flame area with

pool burning which caused a rapid burning and a high peak HRR measured by the system.

Another feature of significant interest is the recession from the peak HRRs. The cone-ignited, durarock-mounted specimens showed the most rapid recession to a trough at 295 kW/m^2 and steady state condition as opposed to fluctuating recessions to average trough of 150 kW/m^2 and extended burning duration for the edge frame and butane-ignited specimens. Part of the reason for the fluctuating recessions typical of the edge frame and butane-ignited specimens were due to flickering of the flame as the molten materials were confined within the edge frame with reduced air passage. Also, the butane-ignited specimens did not have enhanced radiative feedback from the cone heater to support rapid combustion/specimen burn out.

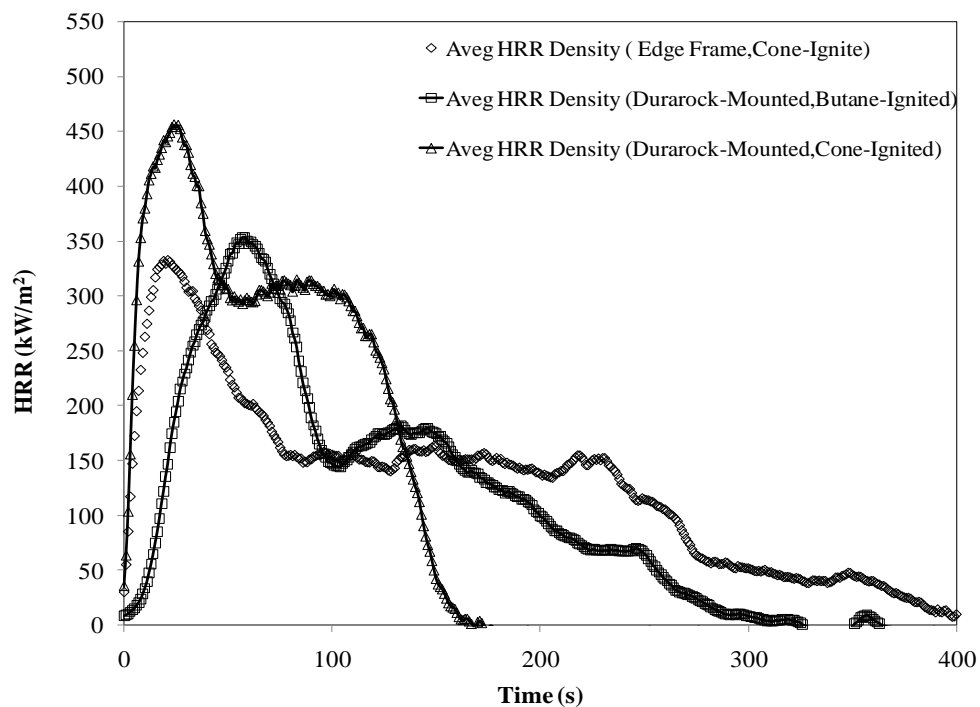


Figure 4-6. Average HRR densities for 10 cm thick specimens tested in edge frame, and on durarock board with cone and butane ignition.

These burning events are similar to responses by thermally thick materials where a considerable temperature gradient exists within the specimen due to delayed or restricted heat penetration in the thickness direction across the molten materials. This was observed during the vertical flame spread tests where a considerable amount of time was required for specimen burn through to occur. This delayed burning resulted in a vertical spread rate of 2.8 mm/s as shown in Table 4-6, measured from the open side of the specimen. However, for the cone-ignited durarock-mounted tests, the rapid specimen burn out was due to enhanced heating from the cone heater, sufficient air passage and the larger flame area of the molten specimen captured atop the insulating board.

Aside from the differences in the burning histories of the specimens, there were differences in the average total heat release rates of the specimens. For instance, the edge-frame tested 10 cm specimens have an average THR of 51 MJ/m² which is approximately 13 and 16% higher than those attained by cone and butane-ignited 10 cm specimens respectively. This is contrary to expectations since the specimens tested on the durarock board burned to completion as opposed to edge frame-tested specimens which had significant amount of residue after flame out.

Specimens with smaller thicknesses also showed the general trends observed for 10 cm thick specimens although there are distinguishing features peculiar to the thinner specimens. The HRR curves for the durarock-mounted, cone-ignited 7.5 and 5 cm thick specimens (Figures 4-7 and 4-8) have two peak HRRs: an initial peak which is followed by a rapid recession and a gradual recovery to a second peak.

As visualised in Figure 4-7, the 7.5 cm thick cone-ignited / durarock-mounted specimens attained the first peak of 410 kW /m² at 18 s while the second peak of 371 kW/m² was attained at 58 s. However, the edge frame and butane-ignited specimens displayed a single peak HRR. Other than that, the three curves followed the generalised characteristics observed for the 10 cm thick specimens.

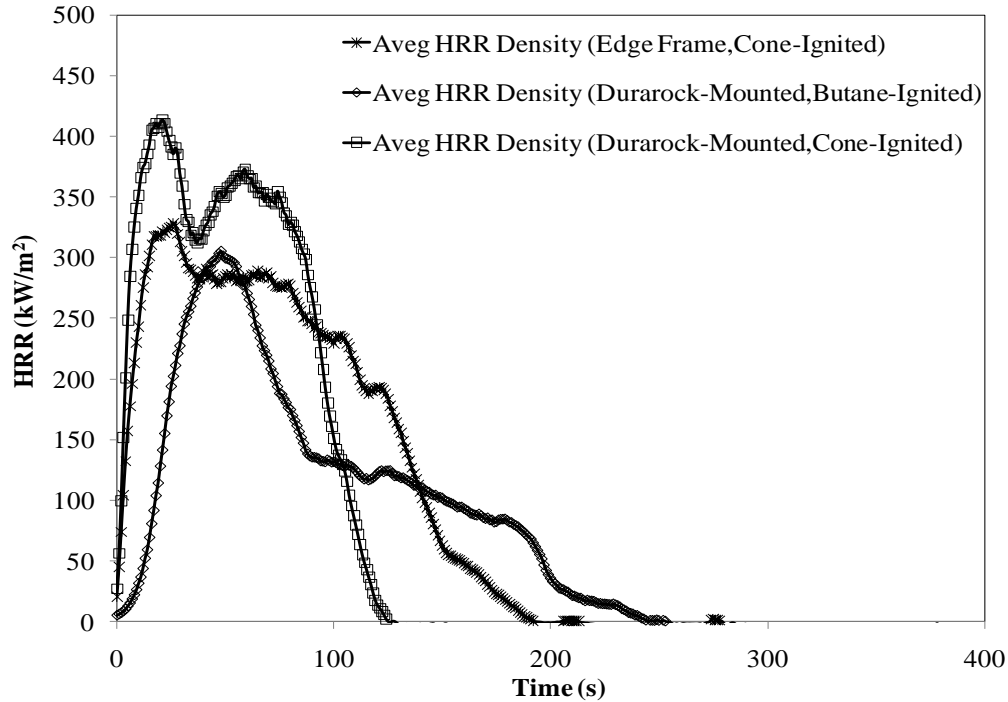


Figure 4-7. Average HRR densities for 7.5 cm thick specimens tested in edge frame, and on durarock board with cone and butane ignition.

For 5 cm thick specimens (Figure 4-8), there are unusual occurrences in the test results. The durarock-mounted, cone-ignited specimens, for instance, had a first peak HRR (329 kW/m^2) attained at 11s which is less than the second peak HRR by 7%. Also, the edge frame tested specimens attained the highest average peak HRR of 400 kW/m^2 relative to the butane-ignited and durarock-mounted specimens. This remarkably high peak HRR of the edge frame-tested specimens is contrary to observations for 10 and 7.5 cm specimens where the heat sink effect of the steel frame significantly suppressed the peak HRRs of specimens. More so, the decay curve for the edge frame-tested specimens showed the most significant decrease in HRR in comparison with the durarock-mounted/butane ignited and cone-ignited specimens. This occurrence also contradicts the fact that the edge frame has the effect of hindering specimens' rapid burn-out as flames are often attached to the interior edges/sides of the steel frame which sustains the flame on the specimen.

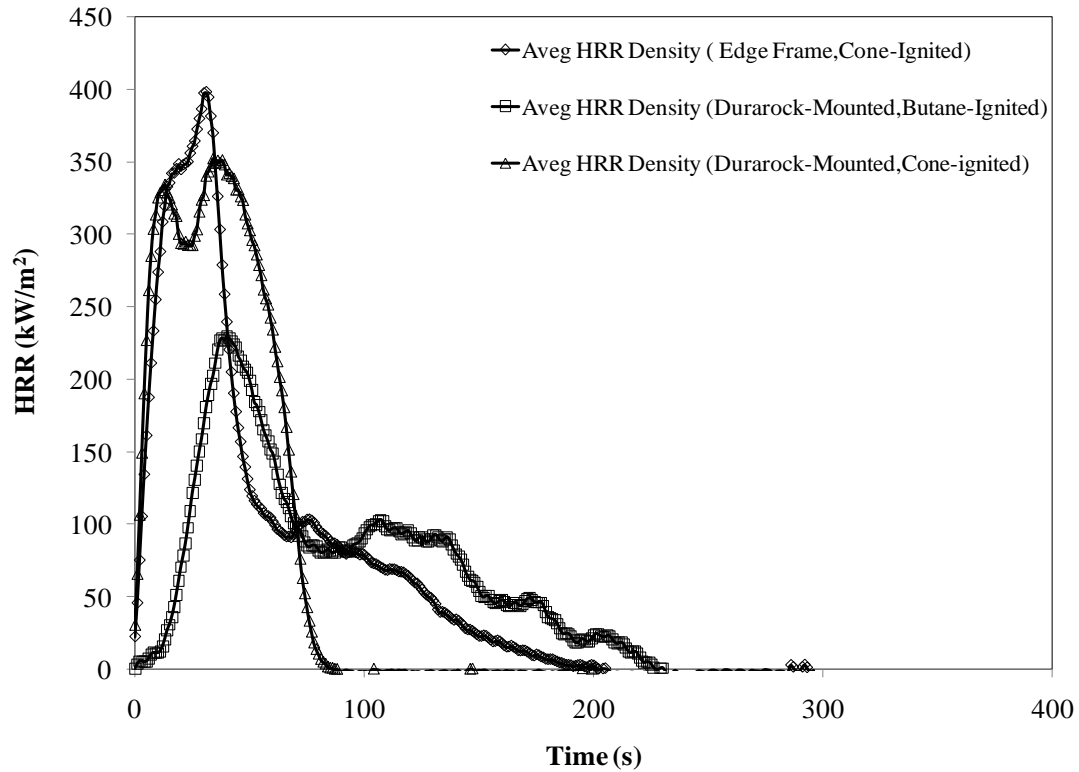


Figure 4-8. Average HRR densities for 5 cm thick specimens tested in edge frame, and on durarock board with cone and butane ignition.

For 2.5 cm thick specimens, the foams performed similar to the thicker specimens except that the specimens had shorter burning duration. Also, there is a single peak HRR for each set up since flame flickering was not intense. As the profiles (Figure 4-9) illustrate, the durarock-mounted, cone-tested specimens burned almost immediately to completion within 50 s while the edge frame and butane-ignited specimens showed a relatively extended burning duration. Most significantly, the peak HRRs and times to the peak HRR of durarock-mounted/cone-tested specimens and edge frame tested specimens are similar (410 kW/m^2). This is as expected since the 2.5 cm thick specimens behaved as thermally thin materials such that the temperature gradient is a function of time and independent of specimen thickness. For these specimens, thermal depth is very small which facilitated sufficiently rapid heat penetration in the thickness direction. However, this occurrence was not observed for the butane-ignited specimens

as the profile shows the lowest peak HRR of 233 kW/m². This is due to the localised flame impingement on the specimens which took an extended time for flame to engulf the entire specimen surface before intense burning commenced.

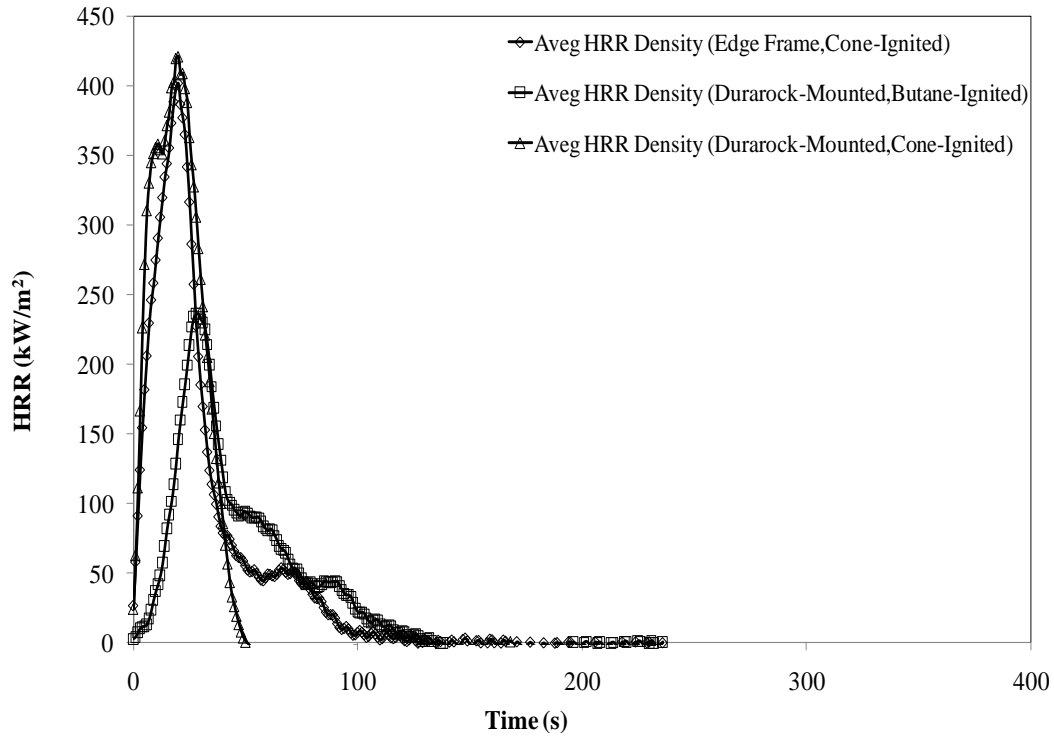


Figure 4-9. Average HRR densities for 2.5 cm thick specimens tested in edge frame and on durarock board with cone & butane ignition.

For effectiveness of the combustion process, the THR obtained from specimens tested in similar set-ups increases with the mass of the specimen as given in Tables 4-3 and 4-4. Also, the average THR of 51 MJ/m² for 10 cm specimens (edge frame-tested) is approximately 41, 143 and 325% higher than those for 7.5, 5.0 and 2.5 cm edge frame tested specimens. This trend occurs in similar fashion for the butane and cone-ignited specimens.

Figures 4-10, 4-11 and Table 4-5 compare the effects of specimen thickness (or mass) and test method on the average HRR. As given in Table 4-5, for each specimen

thickness, the highest heat energy release occurs within 60 s after ignition time. These are supplemented with information given in Tables 4-3 and 4-4 where the peak heat release rate occurs between 19 and 79 s. These indicate that for most of the specimens, the burning behaviour was vigorous which caused the production of greater heat energy early in the test. One important use of the average heat release rate density values is that they serve as important input data during full-scale fire prediction (Chapter Five). They are also used to rank the hazard level of specimens during fires since specimens which burn very rapid releases significant heat energy within the first 60 s of the fire.

As Figure 4-10 illustrates, the HRR curves for the specimens follow similar pattern, however the average peak HRRs attained by the different specimens vary considerably with thickness and mass. As the figure indicates, specimens with larger thickness (or mass), for instance the 7.5 and 10 cm specimens, showed the lowest average peak HRR of 325 kW/m^2 which is approximately 23% lower than that obtained by the 2.5 and 5 cm thick specimens. The thicker specimens (7.5 and 10 cm) have longer decomposition periods since fire duration increases with increasing mass of specimen. This is as expected since the total fire duration is dependent on the mass of the specimens which resulted in increased THR for such specimens as shown in Tables 4-3 and 4-4.

Also, the vertical flame spread rate for the specimens decreases as the thickness increases, as shown in Table 4-6. For 5.0 and 7.5 cm thick specimens tested as single components, the average vertical flame spread rate was approximately 7% higher than that for 10 cm thick specimen. The flame spread rate decreases further for the composite specimens since the thickness increased considerably. The average flame spread rate value of 2.4 mm/s for 2.5 and 5.0 cm, and 5.0 and 5.0 cm composites is roughly 4% higher than that for 5.0 and 10 cm composite.

As observed during the tests (e.g., Figure 4-5), the top surface of the specimens burned almost instantaneously and developed fire more rapidly at the early stage of the tests. The rate of vertical burn decreased as time elapsed until the entire depth of the specimen was burned out. This was similar to observation made during the full-scale tests. As the depth of heating increased, the spread rate decreased when the foams melted and formed

a liquid pool which prevented heat penetration. During this stage, the burning and spread rates were relatively constant until the specimen thickness was gradually consumed. The measurements were based on the flame propagation at the outer surface of the specimens. The flame spread rate, however, could not be determined at the inner region of the specimens.

A contrary fire history is illustrated in Figure 4-11 as the 10 cm thick specimens showed the highest average peak HRR (455 kW/m^2) which is 8% higher than those for 7.5 and 2.5 cm specimens, and 23% higher than those for 5 cm specimens. These can be attributed to the non-conventional test arrangement used as the specimens were simply wrapped in a thin foil without using the steel edge frame.

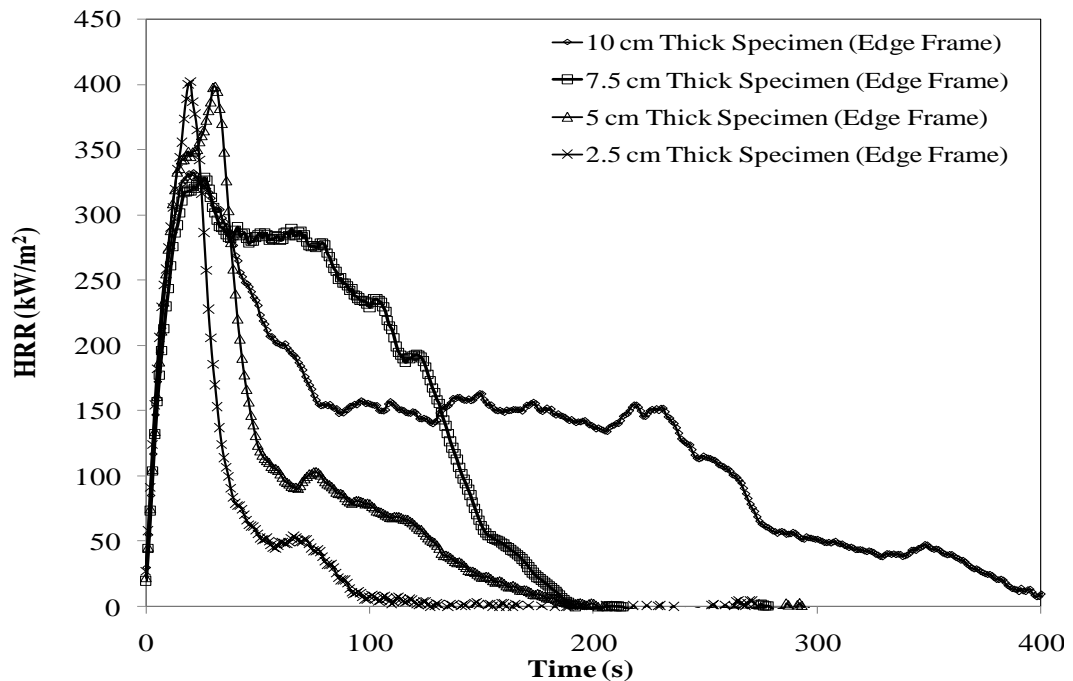


Figure 4-10. Comparing different thicknesses of specimens tested in steel edge frame with cone ignition.

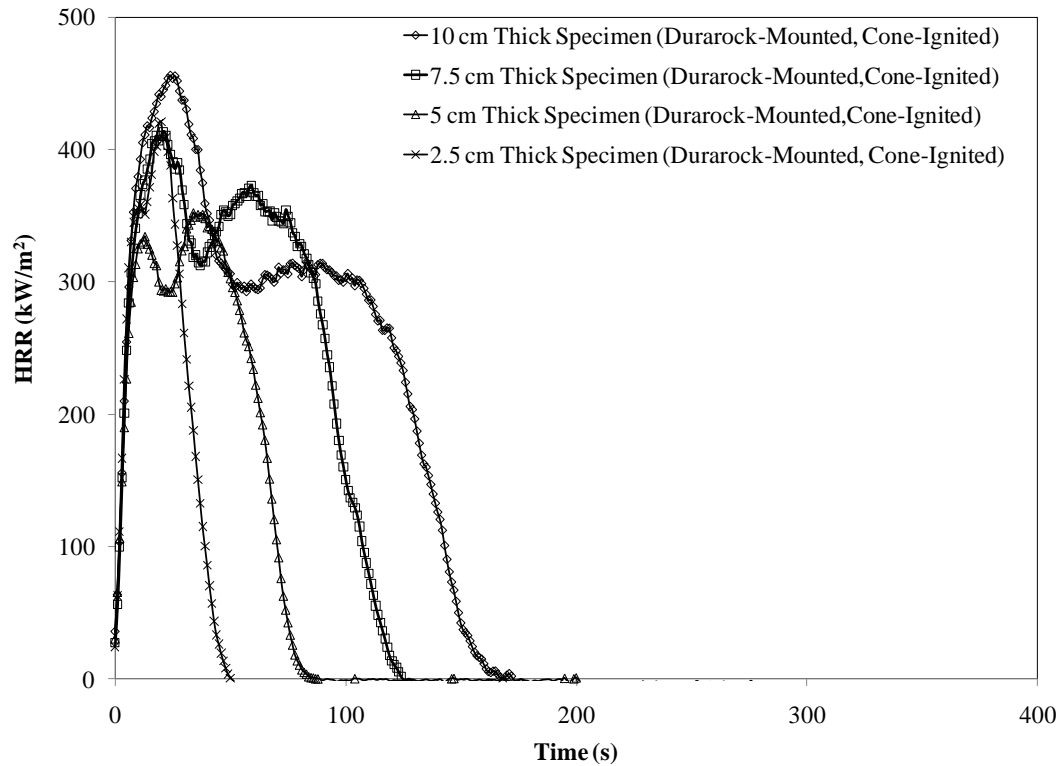


Figure 4-11. Comparing different thicknesses of specimens tested on durarock board with cone ignition.

4.7 Summary of Chapter

An examination of the small-scale burning behaviour of the polyurethane foams has been conducted. Test arrangements and the use of different heat sources had significant influence on the fire performance of the specimens. For specimens of the same size, tests conducted using the durarock board with cone ignition burned most vigorously with highest peak heat release rate densities. This was attributed to enhanced radiative heat flux from the cone heater and the extended burning surface area. Tests conducted with the steel edge frame had suppressed peak heat release rate densities with extended burning duration as a result of reduced air circulation and heat-sink effects of the edge frame. However, the PHRR values for the 5 cm specimens were higher in the steel edge

frame tests than in the other tests as shown in Tables 4-3 and 4-4. Durarock mounted, butane-ignited specimens produced the least severe fires due to the localized ignition.

For all the test arrangements, the heat release rate densities of the specimens varied considerably with thickness. Average peak heat release rate densities decreased as the specimen thickness increased with the thinnest specimens (2.5 cm) having the most active burn. However, thicker specimens (7.5 and 10 cm) burned longer since the fire duration increases with increasing mass of specimen. Also, vertical flame spread rates decreased as the specimen thickness increased with the composite specimens having the smallest vertical flame spread rates.

Examining the data for all the test arrangements and sizes of specimens shows that the average heat release rate density obtained from the 10 cm durarock-mounted, cone-ignited specimens is the most desirable for fire modeling of the full-scale behaviour of the specimens. The main reason for selecting the durarock-mounted specimens test data is because the durarock mounting and the burning behaviour of the foams are similar to the full-scale tests and fire behaviour of the specimens respectively, with the specimens having almost the same open surrounding in both tests. Another reason for the selection is due to the heat release rate density profile which had more consistent growth and decay patterns with characteristic higher peak heat release rate density and total heat release rate of the specimens compared to 10 cm edge-tested and butane-ignited specimens. The application of the 10 cm durarock-mounted, cone-ignited specimens' data for fire modeling purposes will be presented in Chapter Five.

CHAPTER FIVE: NUMERICAL RESULTS

This chapter discusses the numerical results of the models presented in Chapter Two. The objective of this chapter is to demonstrate the use of cone calorimeter data and the measured flame spread rates to simulate the full-scale fire behaviour of polyurethane foam specimens. The aim, further, is to build on earlier work [61] in the search for finer modeling techniques that use transient small-scale fire test data to predict full-scale fire behaviour.

The input data that are needed for the model include the time-dependent flame areas and the total and time-averaged cone calorimeter heat release rate densities. This information is used in the CBUF's integral model presented in section 2.3.1 and the flame spread model presented in section 2.2.2. Other input variables such as the incubation times determined during the full-scale tests and fire growth coefficients determined from fire protection engineering handbooks are used in the t-squared fire growth model presented in section 2.3.2.

5.1 Validation of The Integral Model

As mentioned in section 2.2.1, the Duhamel integral model (Equation 5-1) is used for the calculation of the heat release rate $\dot{Q}_f(t)$ for full-scale polyurethane foam fires using the transient heat release rate density $\dot{q}''(t)$ from cone calorimeter specimens and the time-dependent flame area $A_f(t)$ determined during the full-scale tests.

$$\dot{Q}_f(t) = \int_0^t \dot{q}''(t-\tau) \frac{dA_f(\tau)}{d\tau} d\tau \quad (5-1)$$

The choice for this model is because the time-dependent flame area and the transient heat release rate density can be represented with mathematical expressions. These two

functions are combined by convolution to synthesize the output ($\dot{Q}_f(t)$) [78]. For this model to work effectively, the flame area function $A_f(t)$ is divided into infinitesimal units ($\frac{dA_f(\tau)}{d\tau}$), with each elemental burning area assumed to produce the same transient heat release rate density. Put another way, it is assumed that each elemental burning area of the full-scale specimen has the same heat release rate density as if the specimen was tested in the cone calorimeter. The value of $\dot{Q}_f(t)$ is thus obtained by integrating the product of the two functions (elemental burning area and the heat release density) over the entire burning duration, as given in Equation 5-1. The choice of this model is due to its ability to calculate the total heat release rate ($\dot{Q}_f(t)$) at any arbitrary time (t).

The validation of this model is important to determine its effectiveness and also to ensure that the model is correctly implemented in the computer program. The validation process also demonstrates that the computer model does not contain errors.

Two techniques were used to validate the integral model. The first approach involved the use of a hypothetical expression for the transient heat release rate density $\dot{q}''(t)$ so that Equation 5-1 can have a closed-form solution. The hypothetical heat release rate density $\dot{q}''(t)$ is represented using a single Gaussian distribution function, given by:

$$\dot{q}''(t) = a \cdot \exp[-b(c-t)^2] \quad (5-2)$$

where:

$a = \dot{q}_{\max}''(t)$, the peak HRR density measured in cone calorimeter

(W/m²)

$b =$ an arbitrary variable that determines the width of the peak value (the larger the value of b , the sharper the peak)

$c =$ a parameter that represents the time of peak HRR density $\dot{q}_{\max}''(t)$.

The values of a , b and c were determined using 10 cm cone calorimeter specimens (durarock-mounted, cone-ignited specimen) tested during November 2008, assuming for case 1, $a = 455.93 \text{ kW/m}^2$, $c = 90 \text{ s}$ and $b = 0.001$ as given in Table 4-4. For these values, the idealised heat release rate density, which is characteristic to each elemental burning area of the full-scale specimens, is obtained as shown in Figure 5-1.

For the flame area function $A_f(t)$, Wickstrom and Goransson's [58, 59, 79] time dependent flame area (Equation 5-3) was used to fit the experimentally determined flame areas for specimens EE3 and EE4 as shown in Figure 5-2. Values for initial burning area ($A_o = 0.00321 \text{ m}^2$) in full-scale, fire growth coefficient ($a = 0.045 \text{ s}^{-1}$) and time to ignition ($t_{ig} = 3 \text{ s}$) gave a correlation coefficient, R^2 of 0.98. A value for $t_x = 0.2 \text{ s}$ was adopted from Wickstrom's work.

$$A(t) = A_o \left[1 + a \frac{(t - t_x)^2}{t_{ign}} \right] \quad (5-3)$$

The elemental burning area (Equation 5-4) needed in the integral model is obtained by differentiating Equation 5-3.

$$dA(t) = \left(\frac{2A_o \cdot a}{t_{ig}} \right) \cdot (t - t_x) dt \quad (5-4a)$$

But since t_x is negligible compared to t , Equation 5-4a becomes

$$dA(t) = \left(\frac{2A_o \cdot a}{t_{ig}} \right) \cdot t dt \quad (5-4b)$$

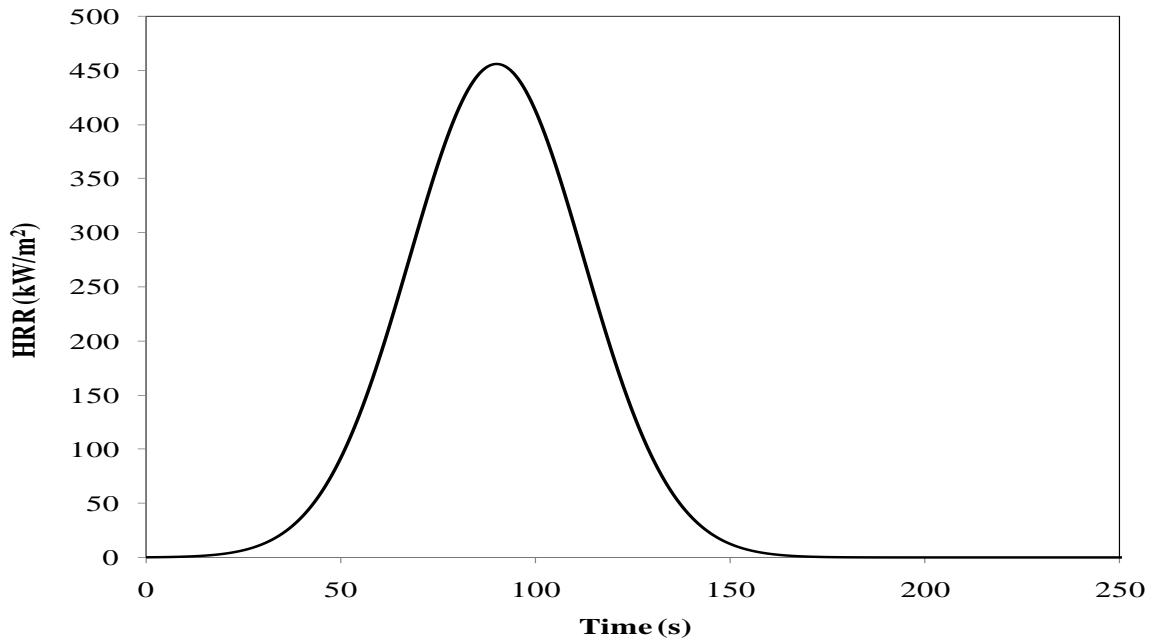


Figure 5-1. A hypothetical HRR density using a single Gaussian function.

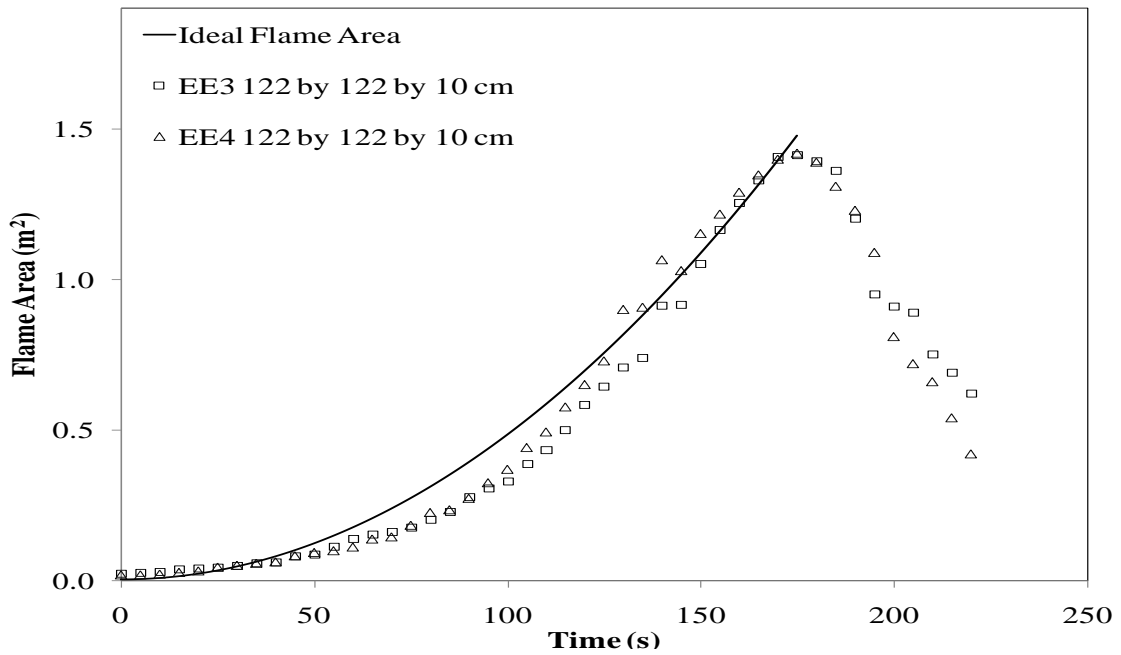


Figure 5-2. Idealized flame area compared with flame areas for specimens EE3 and EE4 measured during May 2008 full-scale tests.

Substituting Equations 5-4b and 5-2 into Equation 5-1, and changing the variable of integration ($t = \tau$) produced a simplified expression for the total heat release rate, as given in Equations 5-5 and 5-6.

$$\dot{Q}_f = \int_0^t \dot{q}_{\max}'' \exp(-b(c-t+\tau)^2) \cdot \frac{2A_o \cdot a \cdot \tau}{t_{ig}} d\tau \quad (5-5)$$

$$\dot{Q}_f = \frac{2\dot{q}_{\max}'' A_o \cdot a \cdot t}{t_{ig}} \int_0^t \exp(-b(c-t+\tau)^2) \cdot \tau d\tau \quad (5-6)$$

Using a time-step of 1 s, $t_{\max} = 178$ s (total burning duration for the full-scale specimen), and the values of a , b , c , \dot{q}_{\max}'' , t_{ig} and A_o given earlier, Equation 5-6 was solved numerically using the trapezoidal rule [80]. Equation 5-6 was further implemented in the computer program developed for the convolution model. The results obtained using the trapezoidal rule (also referred to as exact solution) and the computer program show an excellent agreement with a maximum variation of approximately 3%. The graphical results are as shown in Figure 5-3.

In case 2, the effects of varying the values of c and b in the heat release rate density $\dot{q}''(t)$ expression (Equation 5-2) was investigated and to illustrate the overall significance of this change in the heat release rate result. For the case 2, the value of b was changed to 0.000667 and the value of c was changed to 100 s; the resulting heat release rate density (Figure 5-4) and full-scale heat release rate $\dot{Q}_f(t)$ (Figure 5-5) are both 18% higher than the previous case (case 1). Reducing the value of b broadens the width of the heat release rate density while an increase in the value of c increases the time to the peak heat release rate density. The overall effect of these changes is an increase in the total heat release rate $\dot{Q}_f(t)$ of the system as shown in Figure 5-5.

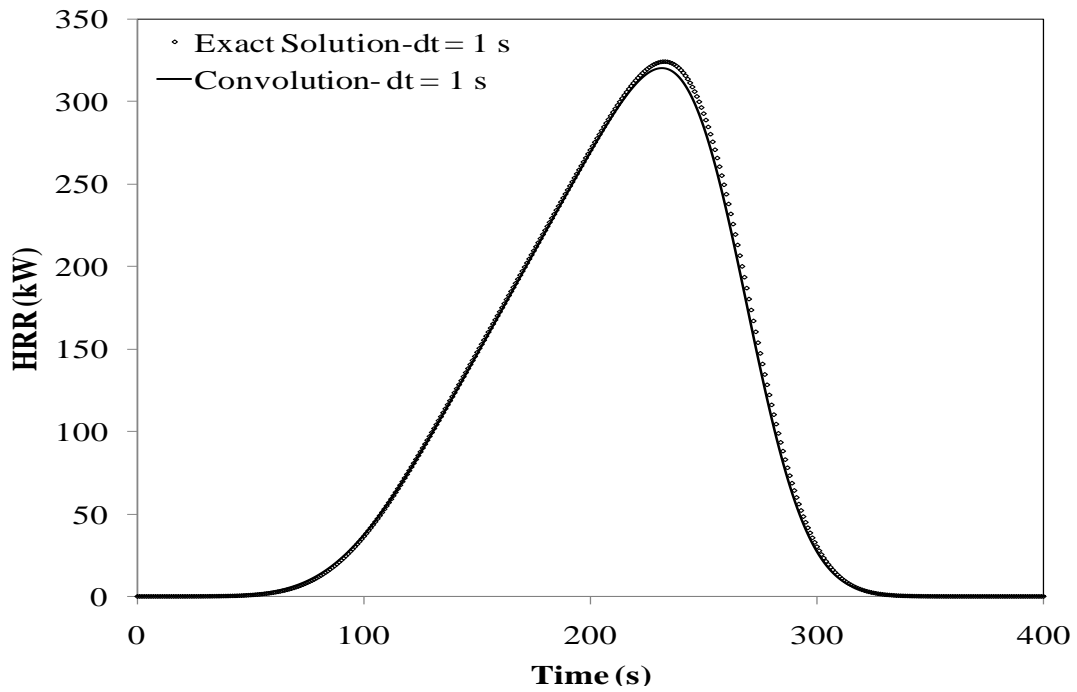


Figure 5-3. Comparison of numerical results obtained using the exact method and computer program.

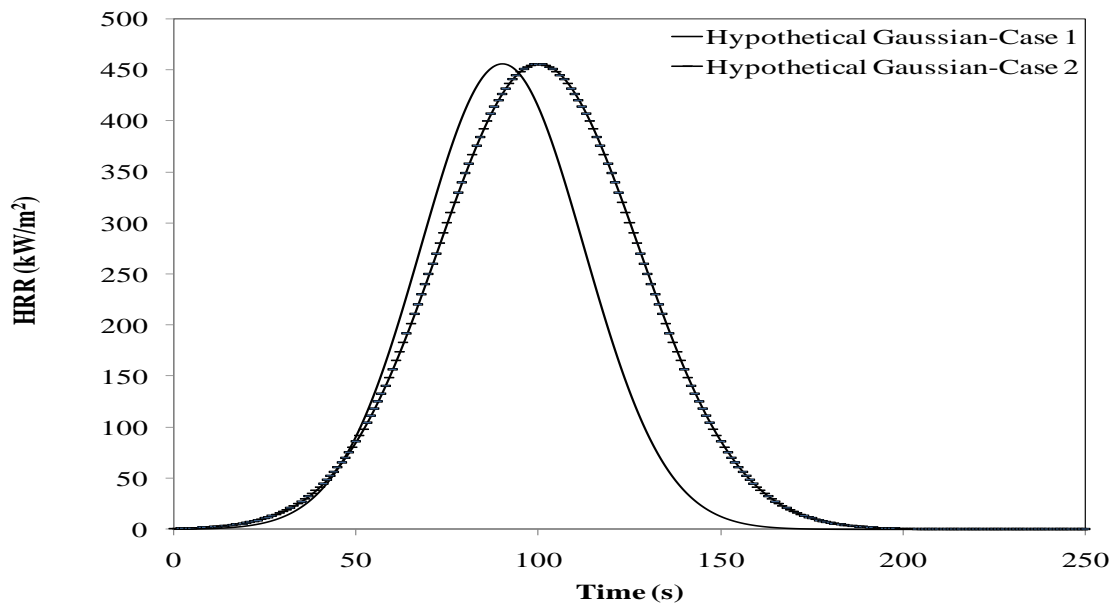


Figure 5-4. Comparing the effects of time to peak (c) and width of peak (b) on HRR density (Case 1: $a = 455.93 \text{ kW/m}^2$, $b = 0.001$, $c = 90 \text{ s}$. Case 2: $b = 0.000667$, $c = 100 \text{ s}$)

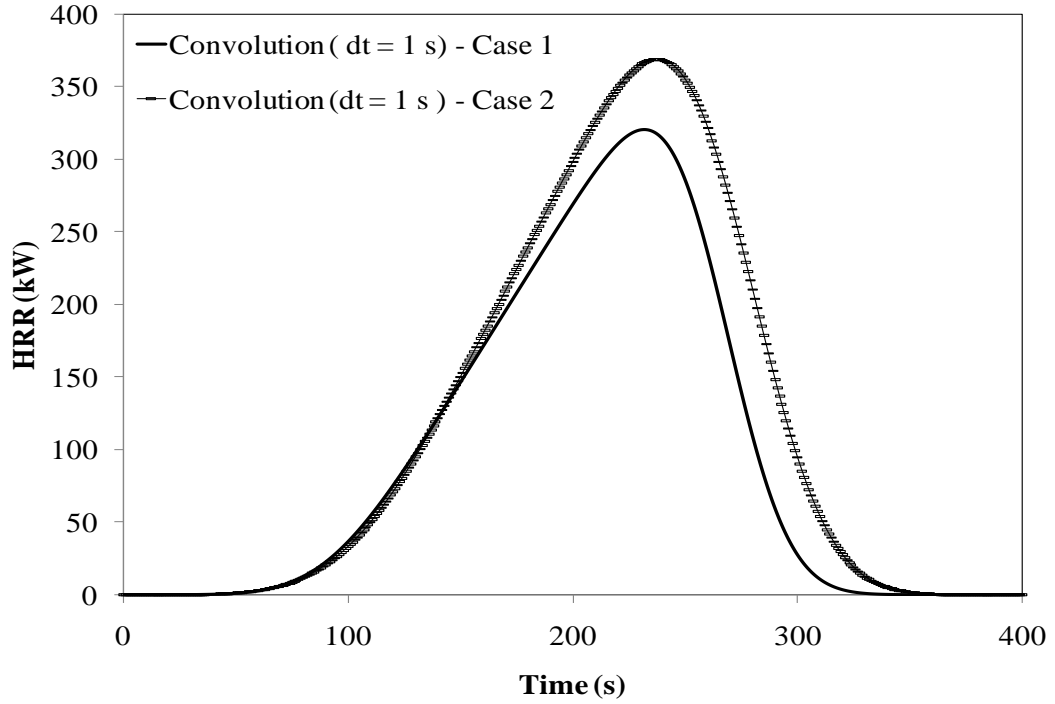


Figure 5-5. Effects of using different HRR densities on the predicted full-scale HRR.

The second validation was conducted using a 60 s average heat release rate density value ($\dot{q}''(avg, t = 60s) = 350 \text{ kW/m}^2$) from a 10 cm (durarock-mounted, cone-ignited) specimen tested in the cone calorimeter (Table 4-5). It was assumed that each cell ($dx = dy = 10 \text{ cm}$) in the full-scale specimen produces the same constant heat release rate per unit area, as shown in Figure 5-6. Replacing the transient heat release density $\dot{q}''(t)$ in Equation 5-1 with the average heat release rate density $\dot{q}''(avg, 60s)$ of 350 kW/m^2 , simplifies the expression to a discrete function given in Equation 5-7. The summation of the function over 270 s (assumed to be average burning duration of a full-scale specimen) produces the heat release rate $\dot{Q}_f(t)$.

$$\dot{Q}_f^N = \sum_{i=0}^{N=270} \dot{q}''(avg, 60s)^{N-i} \cdot \Delta A^i \quad (5-7)$$

where:

ΔA^i = the incremental burning area determined from Equation 5-4.

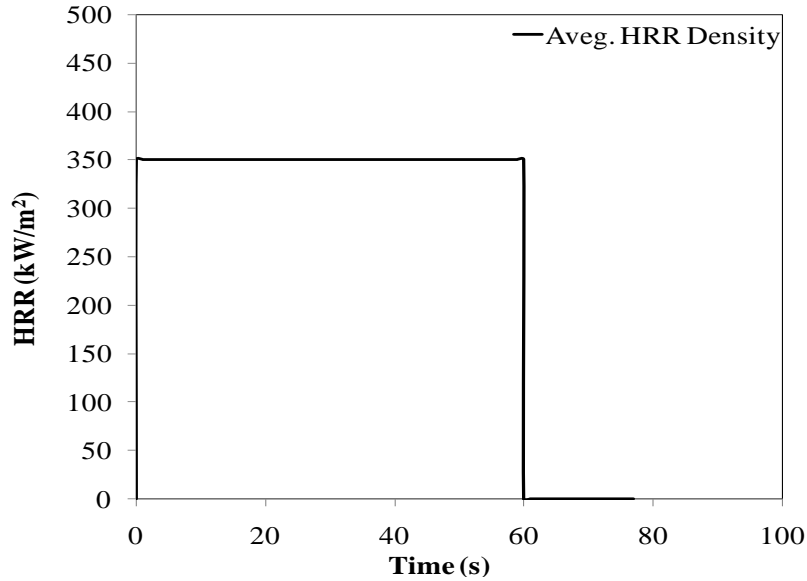


Figure 5-6. 60 s average HRR density (350 kW/m²).

Using different time steps ($dt = 1, 5$ and 10 s), Equation 5-7 was implemented in the computer program and the results are shown in Figure 5-7. The three profiles show an excellent agreement with variations in the total heat release ranging from 2.6 % for $dt = 1$ s and $dt = 5$ s to 3.65 % for $dt = 5$ s and $dt = 10$ s. Equation 5-7 was also solved by hand using the flame spread model (Equation 5-8) which calculates instantaneous heat release rate as a product of average heat release rate density and the total flame area used previously.

$$\dot{Q}_f = \dot{q}''(\text{avg}, 60s) \cdot A_f(t) \quad (5-8)$$

Equation 5-8 represents a special case of convolution model where the transient heat release rate density and the elemental burning area are replaced with a constant heat release rate density and an instantaneous total flame area respectively. A comparison of the results obtained from both techniques shows an excellent agreement with a difference of less than 1% at the growth part of the curve (Figure 5-8). However, since the transient heat release density was not used, the decay phase of the curve could not be estimated. As the various numerical solutions showed good agreement with the exact

solutions, it has been justified that the algorithm for solving the convolution model was well implemented in the computer program.

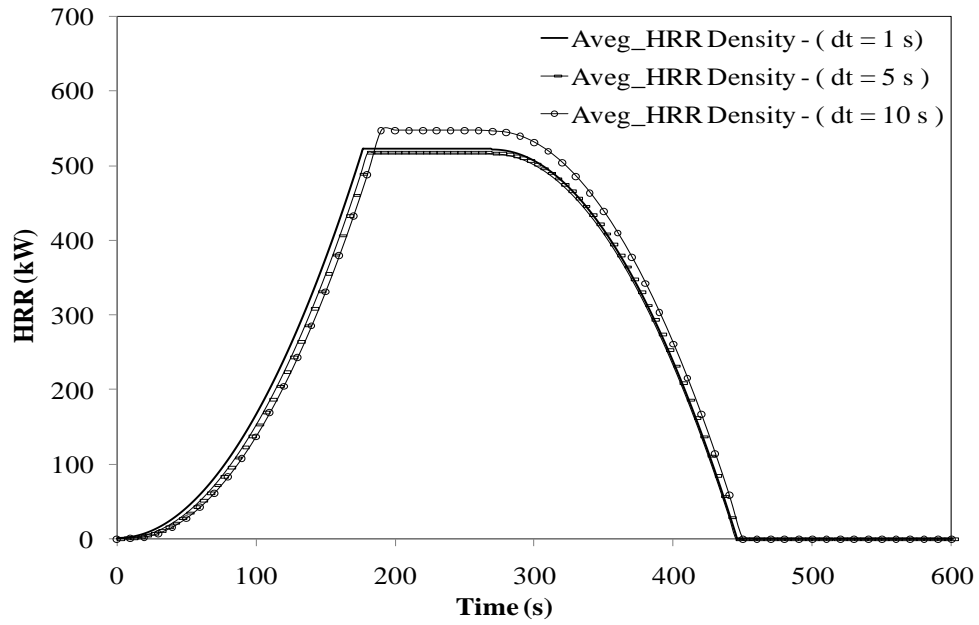


Figure 5-7. Comparison of convolution model results using different time steps.

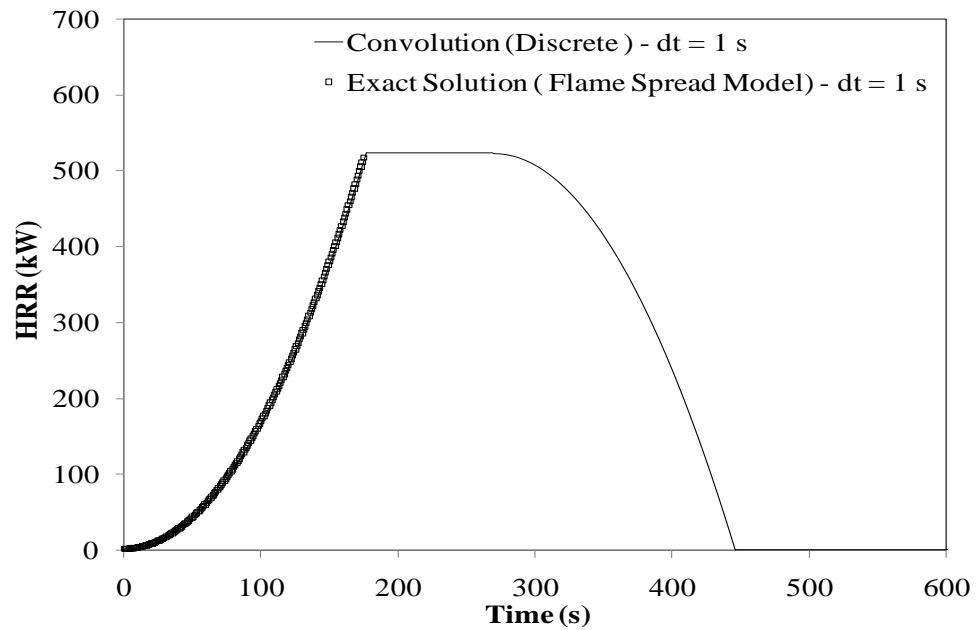


Figure 5-8. Comparison of exact solution (flame spread model) and the discrete model using $dt = 1$ s.

5.2 Input Data

As the analytical expression for the cone calorimeter heat flux $\dot{q}''(t)$ is difficult to establish due to the complexities of the profile, curve fitting the cone calorimeter data using the Gaussian function provides a dependable technique for generating a dataset which represents the $\dot{q}''(t)$ function used as input data in the computer program. This process, which involves the iterative operation of fitting the peak heat release rate density $\dot{q}_{\max}''(t)$ and the time to the peak c determined from the cone calorimeter data, is achieved using the generalised Gaussian function given as:

$$\dot{q}''(t) = \sum_{i=0}^N \dot{q}_{\max(i)}'' \cdot \exp\left[-b_i(c_i - t)^2\right] \quad (5-9)$$

where:

N = Number of terms in the series.

i = counter.

To generate the dataset given in Table 5-1 for the cone-ignited, durarock-mounted 10 cm cone calorimeter specimen, the initial ($i = 0$) peak HRR (455.93 kW/m^2) and the time to peak HRR (24 s) were obtained from the measured data (Table 4-4). A pre-determined time step ($dt = 1\text{s}$) and an arbitrary value for b were chosen. These variables were input into the Gaussian expression as the first term. The square of the difference between the measured and the Gaussian data was obtained, and then the value of b was adjusted repeatedly to minimize the value of the square of the difference. Once the lowest possible value for the square of the difference ($\leq 1.31\text{E}+06$) was attained (which is the stopping criteria for the first iteration), the value of b ($= 0.000111$) was recorded. The value of the difference between the measured cone data and the initial Gaussian dataset was plotted against time to determine the next peak HRR and time to peak HRR. The iteration was repeated for $i = 1$ to determine the next value of b (0.025000) using the stopping criteria value of $\leq 7.06\text{E}+05$. The entire exercise continued until the square of the difference could not be minimized further. The dataset determined from the iteration

are substituted into Equation 5-9 to produce the analytical expression (Equation 5-10) for the heat release rate density profile, as shown in Figure 5-9 and Table 5-1.

$$\dot{q}''(t) = 455.93 \cdot \exp[-0.000111(24-t)^2] - 397.02 \cdot \exp[0.025000(0-t)^2] \quad (5-10)$$

$$+ \dots + 12.21 \cdot \exp[-0.076923(89-t)^2]$$

This solution technique was used for all of the durarock-mounted, cone calorimeter datasets discussed in Chapter Four. The comparison between the measured and the calculated heat release rate functions for the entire cone calorimeter data gave a high correlation coefficient R^2 in the range of 0.96 and 0.99. The analytical expressions for the heat release rate density were used in the computer program as file-input.

Flame area dataset determined from the full-scale fire tests were also used in the model. The flame area dataset used in the model was specifically obtained from the growth phase of the flame area curve as shown in Figure 5-10. The decay phase of the flame area was not used in the model since the differential flame area dataset were negative values. The dataset obtained at 5 s intervals was interpolated to 1 s time-step and then used in the convolution model.

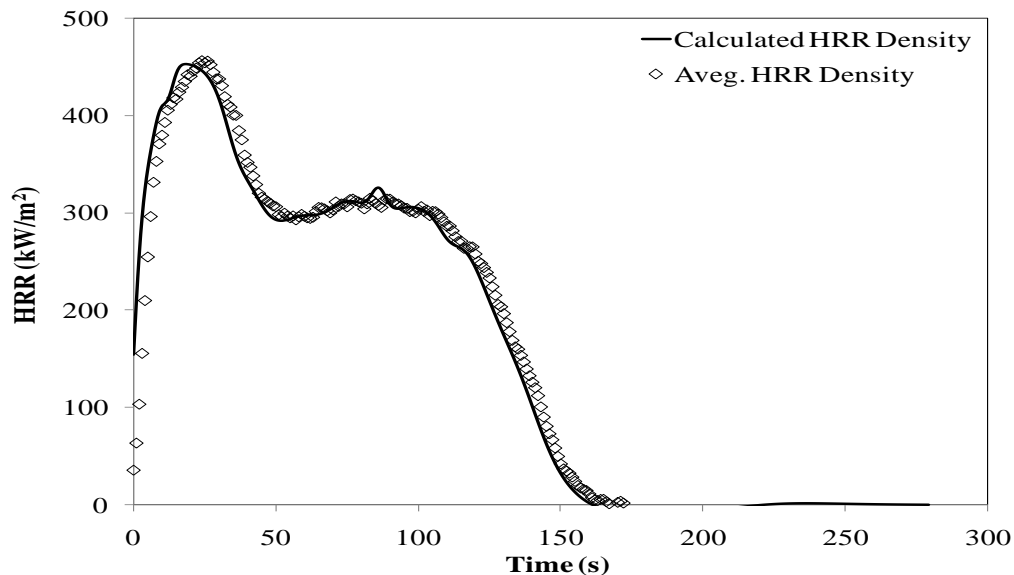


Figure 5-9. Comparison of measured and calculated HRR density for a durarock-mounted, cone-ignited 10 cm specimen.

Table 5-1. Dataset obtained from Gaussian curve fit of 10 cm foam tested at
35 kW/m².

Number of Series (N)	\dot{q}''_{\max} (kW/m ²)	Time to Peak (s)	Width of \dot{q}''_{\max}
0	455.93	24	0.000111
1	-397.02	0	0.025000
2	-122.57	51	0.004545
3	97.56	119	0.004000
4	-49.39	161	0.001754
5	-34.47	10	0.083333
6	38.14	4	0.111111
7	43.14	101	0.007692
8	29.13	139	0.010000
9	-36.37	69	0.011765
10	-29.32	15	0.125000
11	-21.93	39	0.033333
12	-17.15	197	0.001667
13	-14.24	114	0.040000
14	12.21	89	0.076923

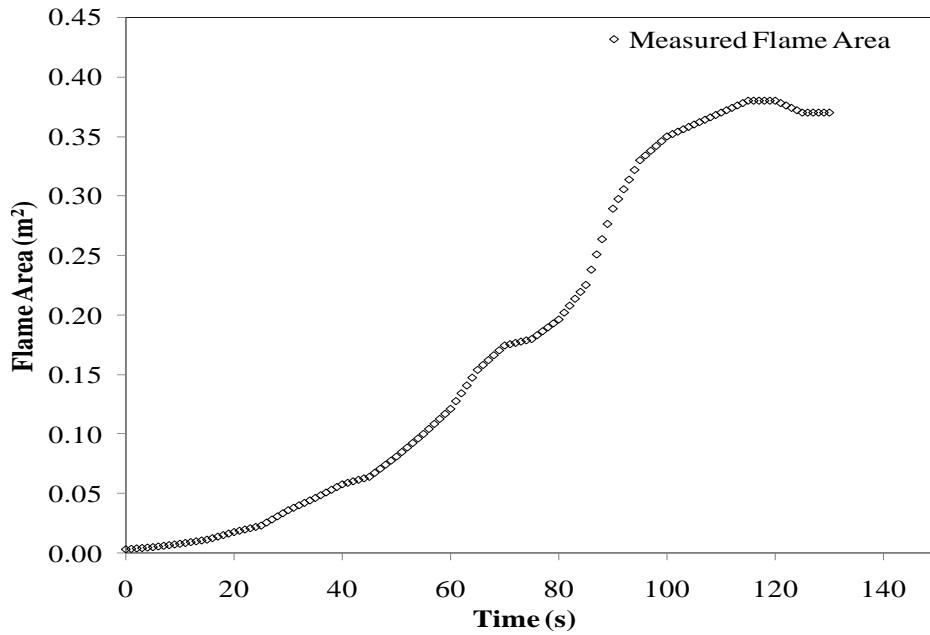


Figure 5-10. Measured flame area for specimen C1 (0.6 by 0.6 m by 10 cm).

5.3 Convolution Model Results

The predicted heat release rate for specimen C1 (0.6 by 0.6 m by 10 cm) obtained using the 10 cm heat release rate density (Equation 5-10) and the flame area dataset is shown in Figure 5-11. At any point on the curve, the heat release rate is the instantaneous value of the convolution product of the heat release rate density and the differential flame area lumped to the preceding total heat release rate. The integration of all the instantaneous heat release rate from each elemental burning area gives the total heat released from the specimen during fires.

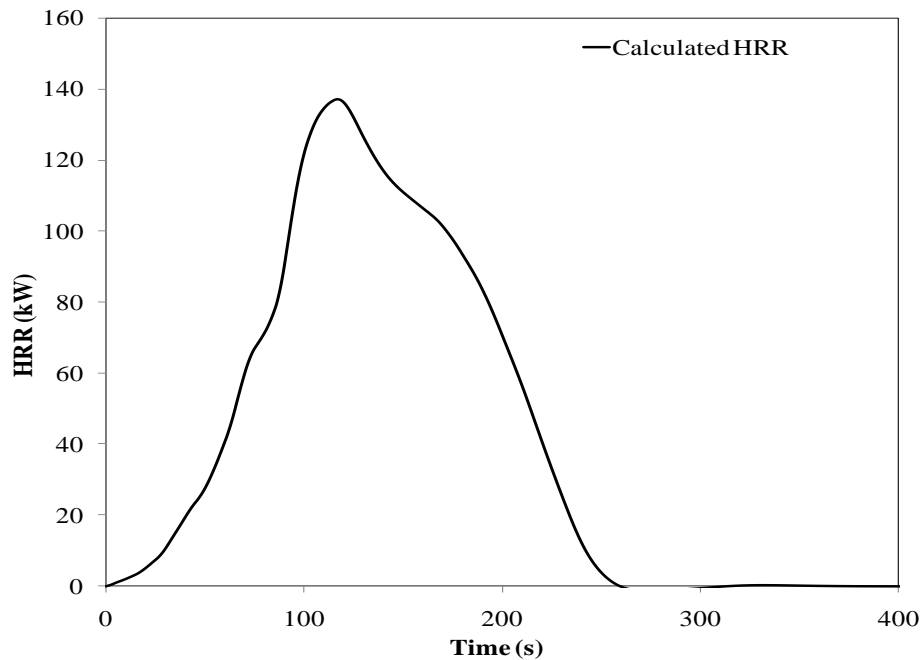


Figure 5-11. Calculated HRR result for specimen C1 and C2 using 10 cm (durarock-mounted, cone-ignited) HRR density expression.

Figure 5-12 shows the simulation result for specimen C3 using the full-scale measured time-dependent flame area and the transient heat release density for the 10 cm data, shown in Figure 5-9. The predicted heat release rate profile showed the four stages of fire growth development. These include the early stage of flame development when the flaming combustion is not well developed and during which initial burn through in the

thickness is occurring. This stage is followed by the exponential growth in the heat release rate and attainment of a peak heat release rate of 537 kW at 141 s which is due to rapid flame spread occurring as the fire plume becomes fully developed. After 141 s, the growth curve decayed until a steady state condition is reached at 300 s when flameout occurs.

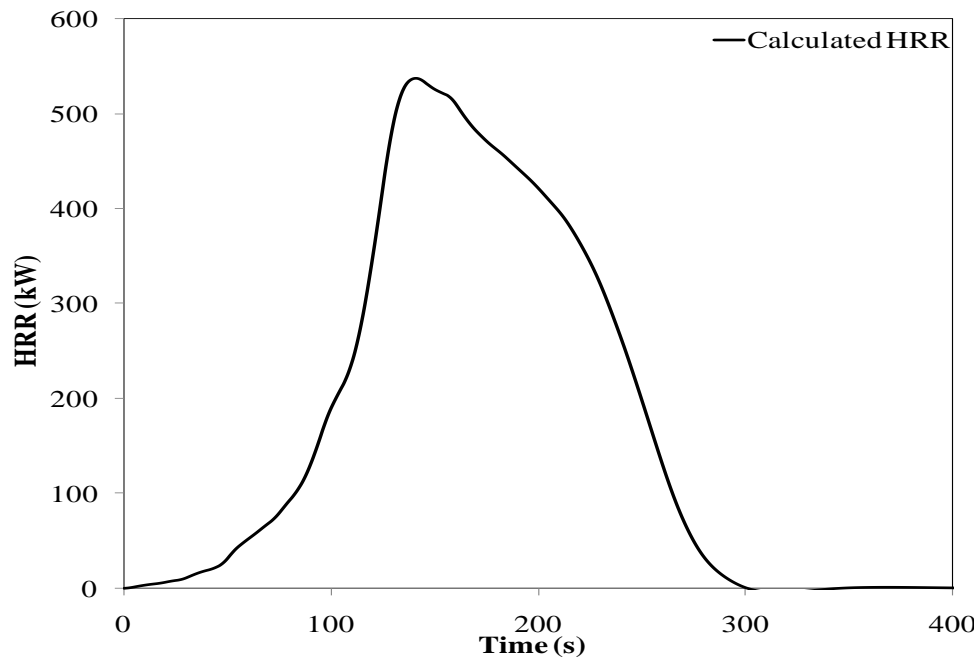


Figure 5-12. Calculated HRR result for specimen C3 using 10 cm (durarock-mounted, cone-ignited) HRR density expression.

For edge ignited specimens E5 and EE4 shown in Figure 5-13, the two predicted heat release rate profiles followed the same pattern within 100 s of the simulated fire and after this time, the heat release rate curve for specimen E5 deviated and attained a peak release rate of 268 kW at 181 s. The heat release rate for specimen EE3, however, developed consistently until the peak heat release rate of 475 kW was reached at 176 s. The discrepancy in the two growth curves is attributable to the pattern of flame area development for the two specimens discussed in section 3.4.2. Flame spread was similar for both sizes of specimens for the first 100 s of the tests, after which flames reached the

sides of the specimen E5 and then flame area increased at a slower rate. After the 100 s, flame areas increased at higher rates for specimen EE3. The predicted total heat release rate for specimen EE3 is 45% higher than that predicted for specimen E5.

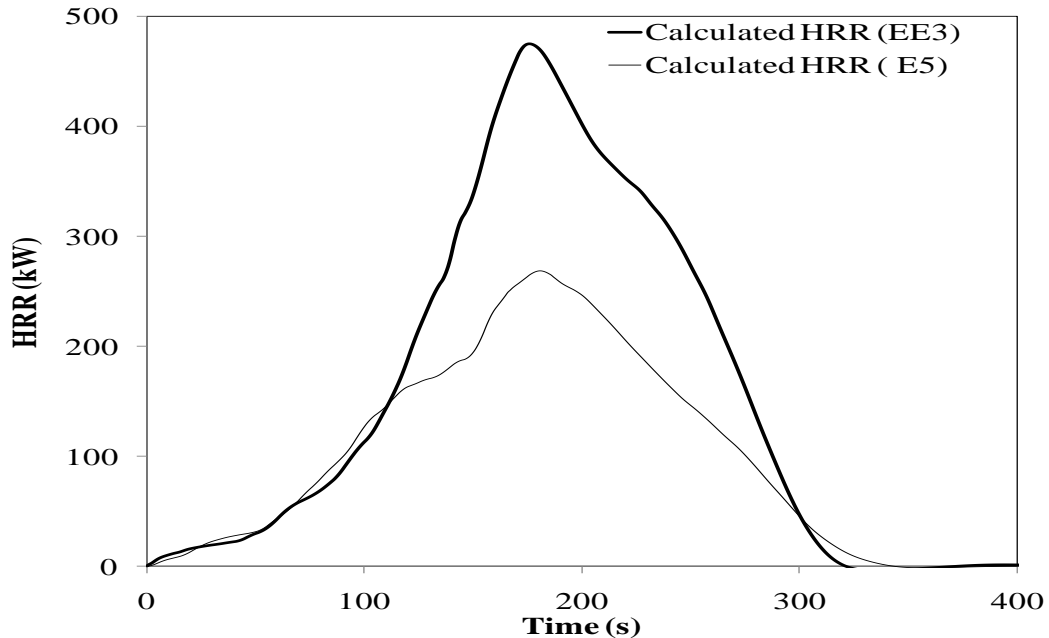


Figure 5-13. Calculated HRR results for specimens E5 and EE3 using 10 cm (durarock-mounted, cone-ignited) HRR density expression.

5.3.1 Sensitivity Analysis

As shown in the plots, e.g., Figure 5-11, the features of the heat release rate curve such as the accelerative growth of the curve, the peak heat release rate, time to the peak and the total time of the fire are significantly influenced by the cone calorimeter heat release rate density profile (Figure 5-9) and the flame area dataset plotted in Figure 5-10. As the model uses dataset from these two fire variables, the predicted result is expected to be sensitive to these input data.

Sensitivity studies, which were conducted using this model by varying input parameters, indicate that the distribution of the heat release rate density including the peak and total

heat released from the cone calorimeter data created a substantial difference in the peak and total heat release rate of the predicted results. These effects on the heat release rate results were investigated by varying the transient heat release rate density for the cone-ignited, durarock-mounted 10 cm data and flame area for specimen C1 by $\pm 10\%$.

As shown in Figure 5-14, a $\pm 10\%$ change in the heat release rate density produced a significant change in the heat release rate profile. For example, the 10% increase in the transient heat release rate density produced a 10% increase in the calculated peak heat release rate and the total heat release rate. This can be explained based on the fact that the 10% increase in the transient heat release rate density caused an increase in the total heat energy of the specimen by 10%. As each elemental burning areas now possesses this heat release rate profile, the cumulative effect of the total burning area will result in an increase in the predicted peak and total heat release rates.

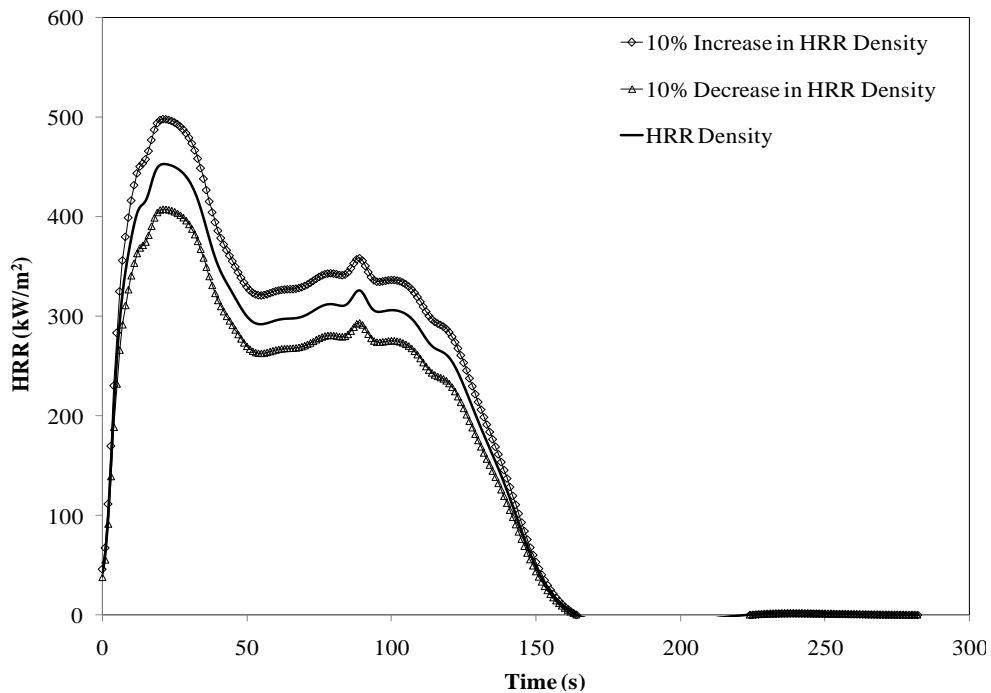


Figure 5-14. $\pm 10\%$ difference in the transient HRR density for a 10 cm durarock-mounted, cone-ignited specimen.

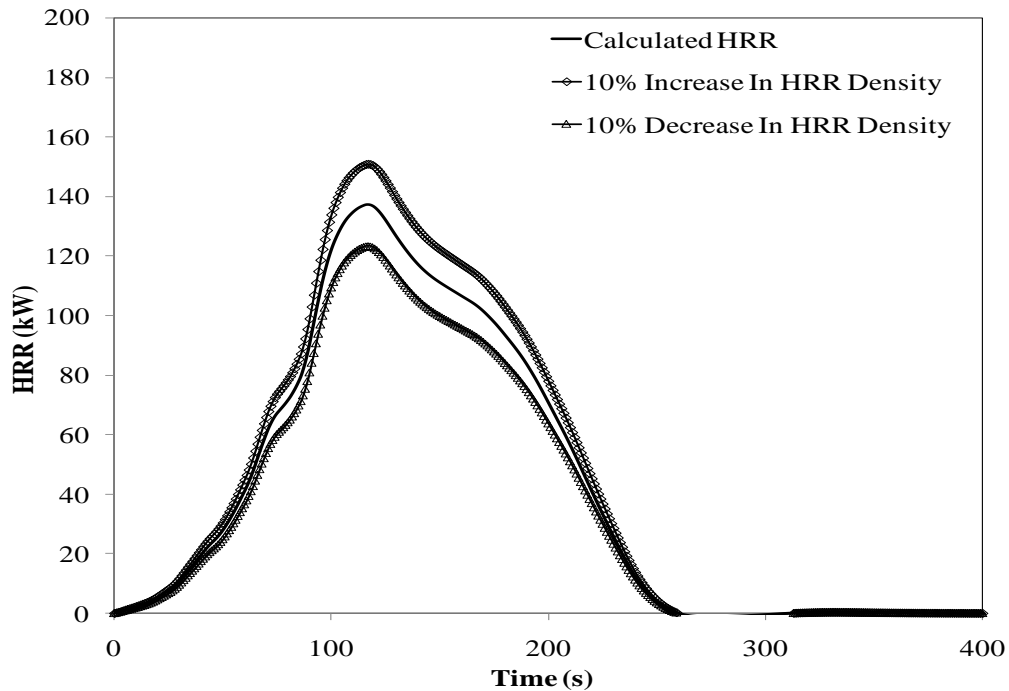


Figure 5-15. Effects of changing the HRR density on the predicted full-scale HRR for specimen C1.

Furthermore, the sensitivity study was carried out by investigating how changing the flame area by $\pm 10\%$ would affect the overall calculation of the heat release rate. The heat release rate density used in this calculation was as in Figure 5-9. The results obtained showed that by varying the flame area dataset by $\pm 10\%$ and using the original transient heat release rate caused a 10% increase in the calculated peak and total heat release rate. This follows from the established fact that increasing the burning area of a specimen causes an increase in the fire plume and radiative feedback effects which then results in higher heat release rate. This is illustrated in figures 5-16 and 5-17.

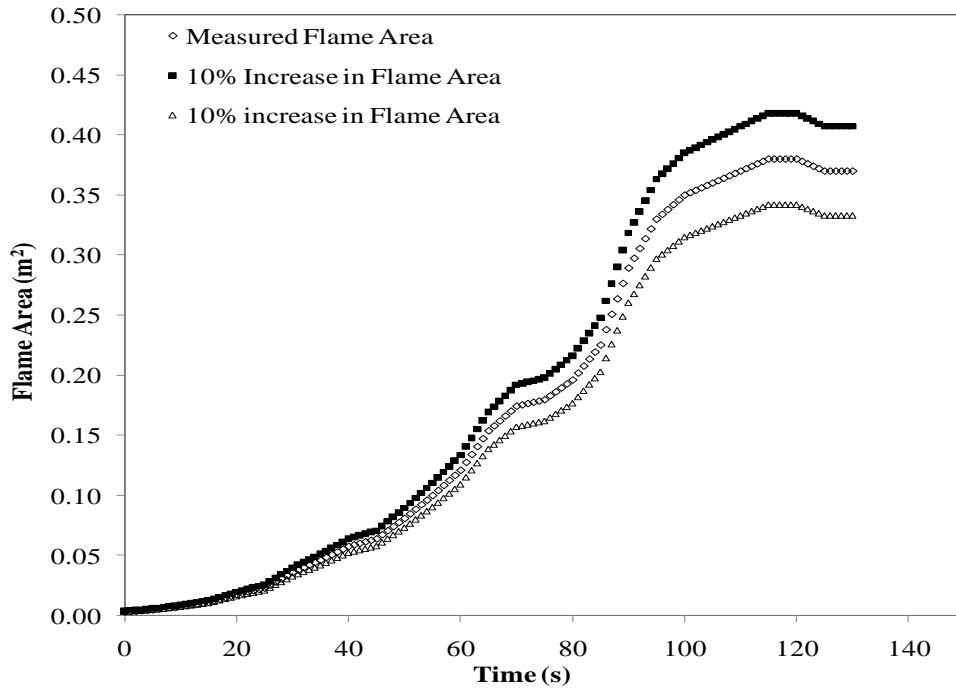


Figure 5-16. Measured flame area for specimen C1 and a $\pm 10\%$ change.

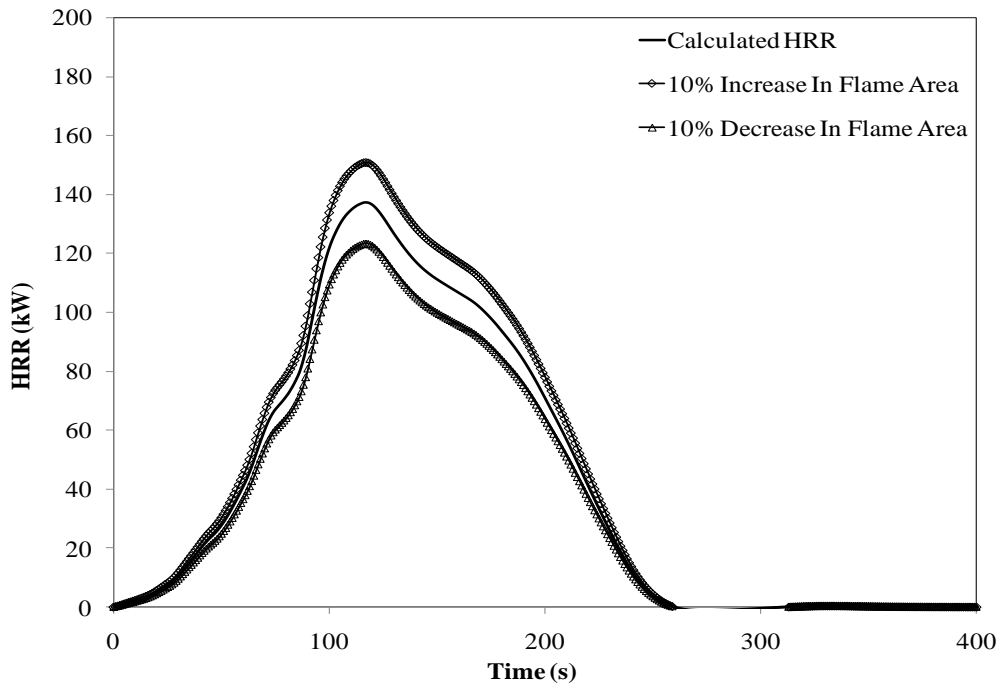


Figure 5-17. Effect of flame area on the predicted full-scale HRR for specimen C1.

One significant observation on the calculated results is that the variation in the input dataset for a particular specimen does not affect the HRR profile but has a significant effect on the total heat release as shown in Figures 5-15 and 5-17.

5.4 Flame Spread Model Results

The application of the flame spread model in predicting the full-scale fire behaviour of the foams is more straightforward than the integral model as the complications arising from using the transient heat release rate densities are eliminated. This is one possible simplification of the convolution model through the use of a constant heat release rate density. This work is intended to show whether or not the efforts of including the transient heat release rate density in the model was necessary. Thus, the model calculates the full-scale heat release rate as a product of an instantaneous total flame area $A_f(t)$ and the time-averaged heat release rate density measured in the cone calorimeter [24]. This model is expressed as:

$$\dot{Q}_f(t) = \dot{q}''(\text{aveg.}) \cdot A_f(t) \quad (5-9)$$

Similar to the integral model, the development of the flame spread is based on the assumption that the effective burning area in the full-scale specimen produces approximately the same heat release rate density as that produced in the cone calorimeter. The predictive ability of this model is dependent on the flame area profile measured during the full-scale tests, especially as the measured flame areas provide reasonable information relating to the specimen burn out. For a particular flame area $A_f(t)$, the sensitivity of the model is influenced by the magnitude of the time-averaged heat release rate density. The predicted heat release rate curves for C1 and C3 are shown in Figure 5-18.

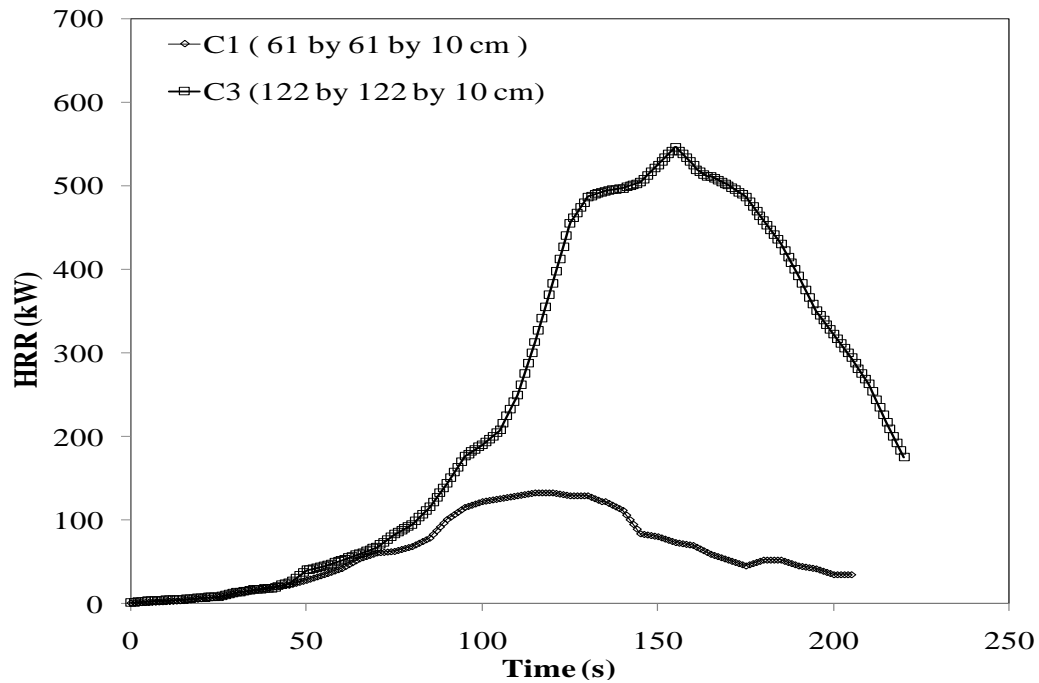


Figure 5-18. Predicted HRR for specimens C1 and C3 using 60 s average HRR density of 350 kW/m².

Predicted fire growth using a 60 s average heat release rate density of 350 kW/m² for specimens E5 and EE3 is shown in Figure 5-19. As evident in the graph, the model gave detailed information relating to different routes and stages followed by each specimen during the full-scale test. The initial flame spread for the three specimens developed in a uniform fashion within the first 100 s, thereafter the flame spread for specimen E5 assumed a different growth pattern. The flame spread continued in the same profile for specimen EE3 until the entire specimen surface was burning. For specimen E5, the flame growth reduced after 100 s and continued at a uniform rate until the peak heat release rate of 252 kW was attained. As expected, the predicted peak heat release rate for specimens EE3 was 97% higher than the predicted peak release rate for specimen E5.

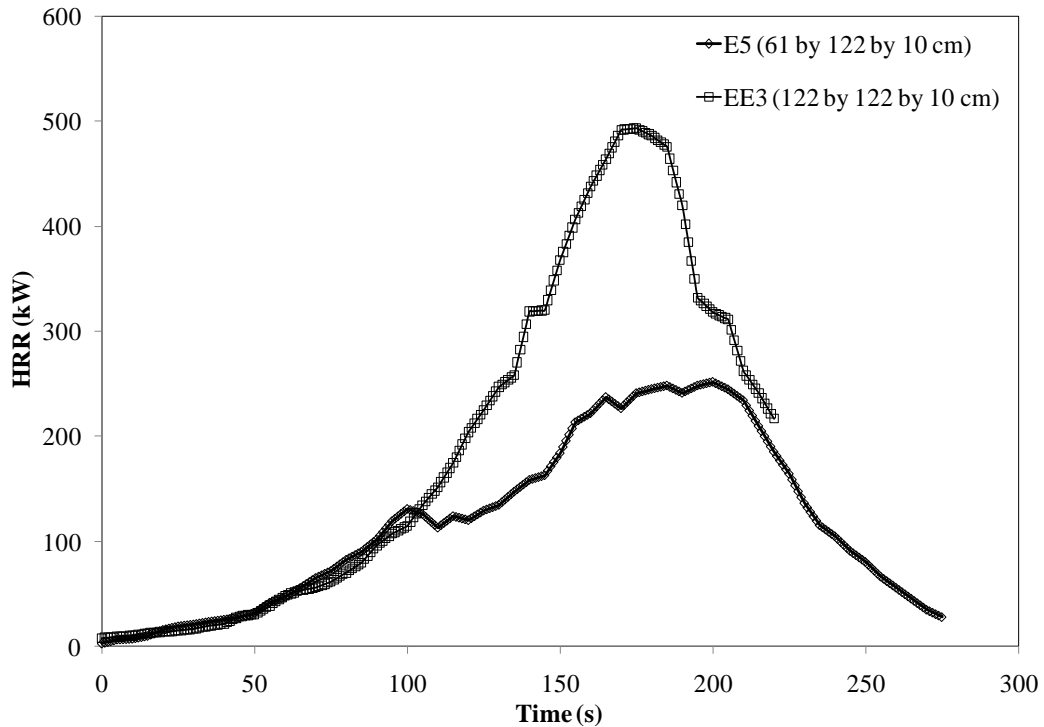


Figure 5-19. Predicted HRR for edge-ignited specimens E5 and EE3.

The 60 s average heat release rate densities were used for the flame spread model. One reason for this is that, for most fast developing fires, the peak heat release rate occurs during the early stage of the fire. However, since the heat release rate density is a constant, it does not affect the burning duration of the simulated fire.

The effects of using different average heat release rate densities calculated at 120 and 180 s are shown in Figure 5-20. As illustrated in the graph, although the three curves attained the peak heat release rate at 155 s due to using the same flame area, the prediction using the 60 s average heat release rate density produced a peak heat release rate approximately 7 and 30% higher than those calculated from 120 and 180 s average heat release densities. Also, despite having the same total burn duration of 220 s, the total heat release differs considerably.

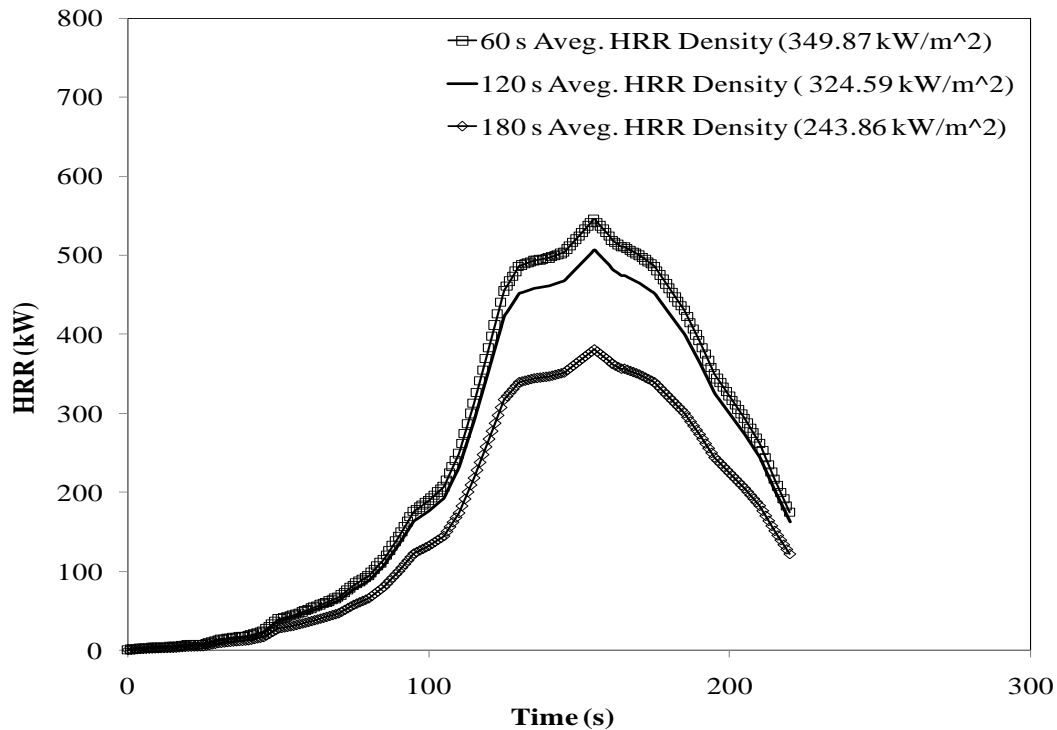


Figure 5-20. Effects of average HRR densities on predicted full-scale HRR for specimen C3.

5.5 Time-Squared Heat Release Rate Model

As discussed in section 2.3.3, the t-squared model is one of the most popular fire protection engineering models used to predict the accelerative growth of fire. This model enables the classification of fires from different materials such as ultra-fast, fast, medium and slow developing fires. Information from the literature, as given in Table 2.1, shows that polyurethane foams were thought to behave as fast developing fires while fires from upholstered furniture are classified as medium developing fires.

From the analyses of the full-scale results of the specimens discussed in Chapter Three, it was noted that the heat release rates from the specimens had a considerable exponential growth with time, with the center-ignition tests showing a more rapid fire growth and flame spread rate than the edge ignition tests. However, it was uncertain about the appropriate fire growth coefficient that could be used in the t-squared model.

Thus, a curve fitting approach was used whereby the fire growth coefficients given in Table 2.1 were used in the t-squared model and the results were plotted alongside the measured heat release rate data. Using this approach, the edge-ignited specimens EE3/EE4 and E5 were identified as fast and medium t-squared fires respectively while the center-ignited specimens C1/C2 and C3 followed the fast and approximately ultra-fast fire growth behaviours respectively. The prediction of the fire growth for the specimens will be discussed in Chapter Six.

5.6 NIST-CBHF Heat Release Rate Correlation

As discussed in section 2.3.4, NIST and CBHF developed a method to predict the full-scale peak HRR of the specimens from cone calorimeter data. The NIST/CBHF research work shows that materials producing a cone calorimeter three-minute average HRR less than approximately 100-150 kW/m² during tests at 35 kW/m², would produce a non-propagating full-scale fire. As evident in Table 4-5, the three minutes (180 s) average HRR densities for the 10 cm specimens exceeded the non-propagating fire criteria (100-150 kW/m²).

Specimens producing a cone calorimeter three-minute average HRR of approximately 200 kW/m² would produce a self-propagating full-scale fire. This criterion was met by the 10 cm cone calorimeter data for durarock-mounted specimens which produced the average HRR densities of 244 and 195 kW/m² (for cone and butane ignition respectively) as given in Table 4-5. This was verified by examining the video records of the full-scale specimens as the foams developed significant fires after ignition and then burned to completion. Also, based on edge frame tests, a fire protection engineer would be unsure if the fire would self-propagate. For intermediate region, where the three minutes-HRR density is between 100 and 200 kW/m², the edge frame-tested 10 cm cone calorimeter specimen with a three-minute HRR density of 190 kW/m² satisfied this criterion. However, the burning behaviour of the full-scale specimens indicated self-propagating fires.

Using the NIST/CBHF correlations given in Equations 5-10a and 5-10b, the predictions of the full-scale peak heat release rate can be obtained.

$$\dot{Q}_{FS} = 0.75 \cdot \dot{q}_{SC}^* \text{ \{Non-propagating\}} \quad (5-10a)$$

$$\dot{Q}_{FS} = 4 \cdot \dot{q}_{SC}^* + 800 \text{ \{Self- Propagating\}} \quad (5-10b)$$

where:

\dot{Q}_{FS} = Full-Scale Peak Heat Release Rate (kW)

\dot{q}_{SC}^* = Three-minute average cone calorimeter Heat Release Rate (kW/m²)

obtained at 35 kW/m² heat irradiance.

For propagating fire given in Table 5-2, it can be seen that the NIST/CBHF correlation predicted severe fires for the specimens with a high peak heat release rate, which is approximately 218% higher than the measured average values (558 kW) for specimens C3, EE3 and EE4 given in Table 3-3. The wide variation between the predicted and measured peak HRR indicates that the NIST/CBHF correlation is not an effective predictive tool for these particular specimens (although this correlation worked well in NIST/CBHF study). This is attributed to the fact that only one calorimeter data (durarock-mounted cone data which satisfied the criteria) was used for the prediction. Another reason for this over-prediction could be due to the differences in masses and sizes of specimens used in this project versus those used in the NIST/CBHF project. Also in the NIST/CBHF work, each component of the mattresses tested in full-scale (e.g., wool, leather) was predicted using its cone calorimeter data, whereas for this particular case, the prediction for the foam was based on results for cone calorimeter data for that foam.

As the correlation in Equation 5-10 is used to predict non-propagating and self-propagating full-scale fire behaviour based on cone calorimeter data, one major limitation with the model is that it does not give information about the time to peak heat release rate of the specimens. Another drawback of this method is that the model does not account for the heat release rate-time history of the specimens.

Table 5-2. NIST/CBHF peak HRR predictions.

NIST / CBHF Predicted Regime	Predicted Full-Scale Peak HRR (kW)
Self Propagating (Using 244 kW/m ²)	1776
Intermediate (Using 190 kW/m ²)	N/A
Non-Self Propagating (N/A)	1560

5.7 Summary of Chapter

The heat release rate models presented in Chapter Two were implemented in this Chapter. The validation of the convolution model was carried out using an idealized Gaussian expression representing the heat release rate density and flame area obtained from Wickstrom and Gorranson flame spread model.

Using the measured full-scale flame area and the 10 cm cone calorimeter transient heat release rate density obtained by curve fitting techniques, the convolution model gave results that are typical of fire growth. The effects of varying the input parameters were investigated. The results obtained indicated that a $\pm 10\%$ change in either the flame area

or the heat release rate density affected the predicted peak heat release rates and the total heat release rates by the same amount.

Using the flame spread model, results showed that the 60 s average cone calorimeter heat release rate density produced more energy compared to average heat release rate densities calculated at 120 and 180 s. The NIST/CBHF correlation was used to show that the specimens burned severely and produced self-propagating fires. However, the correlation over-predicted the peak heat release rate of the specimens due to differences in specimen sizes used in this project and the NIST/CBHF project. The correlation also does not account for the heat release rate-time history of specimens. In Chapter Six, the comparison of the predicted and experimental results will be made to show the effectiveness of each of the models.

CHAPTER SIX: COMPARISON OF PREDICTED AND MEASURED

RESULTS

In Chapter Three, the experimental methodologies and the results for the furniture calorimeter tests of seven polyurethane foam specimens were discussed. The relationships between the heat release rates and the flame areas for different sizes of the specimens were established. Results for foam specimens tested at 35 kW/m^2 in the cone calorimeter were analysed in Chapter Four. Small-scale results were used as the input data for the calculations discussed in Chapter Five. This chapter focuses on the comparison of the experimental and numerical results for the full-scale polyurethane foams. The comparison will establish the effectiveness of each of the fire models in tracking the progressive development of the fire growth and predicting the heat release rate for each specimen.

As will be illustrated in this chapter, the convolution model functions most effectively as a predictive tool for fire behaviour of thin specimens. It is assumed that in using the model, burn through did not occur and that the specimen did not melt during the fire. As the foams used in the full-scale experiments showed considerable burn-through with the formation of molten material, this chapter will also discuss this shortcoming of the convolution model. The model is also based on previous research for thin materials. Possible modifications of the model to help account for the heat transfer in these relatively thick pieces of foam will also be discussed. The t-squared fire growth model was also used to predict and classify the specimens based on the accelerative growth pattern of the measured results.

6.1 Comparison of Predicted and Measured Results

The summary of the results obtained using the convolution and flame spread model versus the experimental results is given in Table 6-1. The data given in Table 6-1 is the average value of the measured results.

Table 6-1. Summary of the measured and predicted full-scale combustion characteristics of polyurethane foams.

Specimen		C1/C2	C3	E4/E5	EE3/EE4
Peak Heat Release Rate (kW/m ²)	Measured	172.00	612.08	231.33	505.93
	Convolution Model	136.05	537.10	268.39	473.44
	Flame Spread Model	131.00	545.79	251.91	495.20
Time to Peak (s)	Measured	94.00	125.00	174.00	167.00
	Convolution Model	117.00	141.00	181.00	176.00
	Flame Spread Model	114.00	155.00	200.00	175.00
Total Heat Release (MJ)	Measured	14.48	57.34	30.63	60.12
	Convolution Model	15.75	68.47	40.49	58.73
	Flame Spread Model	11.83	53.24	32.76	43.58

Figure 6-1 illustrates the comparison between the measured and the predicted fire behaviour of specimen C1 using the convolution, flame spread and t-squared fire models. The predicted results were obtained using data from a 10 cm cone calorimeter specimen (durarock-mounted, cone-ignited specimen) as shown in Figure 5-10 for the convolution model, a 60 s average heat release rate density of 350 kW/m² for the flame spread model and the measured flame area interpolated to a 1 s time-step. The fire growth coefficient used in the t-squared fire model was the fast fire growth coefficient

based on the curve fitting result, information from the literature and as observed during the full-scale fire tests (Section 5-5).

As shown in the curves in Figure 6-1, the heat release rate profiles predicted from the convolution and flame spread models grew along the same path with the measured heat release rate until about 60 s. After this, the heat release rate curves for the convolution and flame models deviated from the measured profile and then grew at the same rate until both attained the peak heat release rates of 137 kW at 117 s and 132 kW at 114 s for convolution and flame spread models, respectively. The measured heat release rate, however, grew more consistently in an exponential fashion to a peak heat release rate of approximately 25% higher than those of the convolution and flame spread models. For the fast t-squared model, there was an excellent agreement between the measured and the ideal growth curve at the growth phase of the fire. The t-squared fire model did a good job of tracking the fire growth; however, it is unable to predict the peak heat release rate or the decay phase.

For this specimen, the striking differences between the predicted and measured heat release rates appear most significantly at the later stage of the curves. The convolution and flame spread models over-predicted the HRR during the decay phase of the curve. The difference between the measured result and the convolution model was larger than difference measured results and the flame spread model. The convolution model, thus, predicted a total heat release rate that was 14% higher than the experimental result while the flame spread model predicted a total heat release rate that was 11% less than the experimental results.

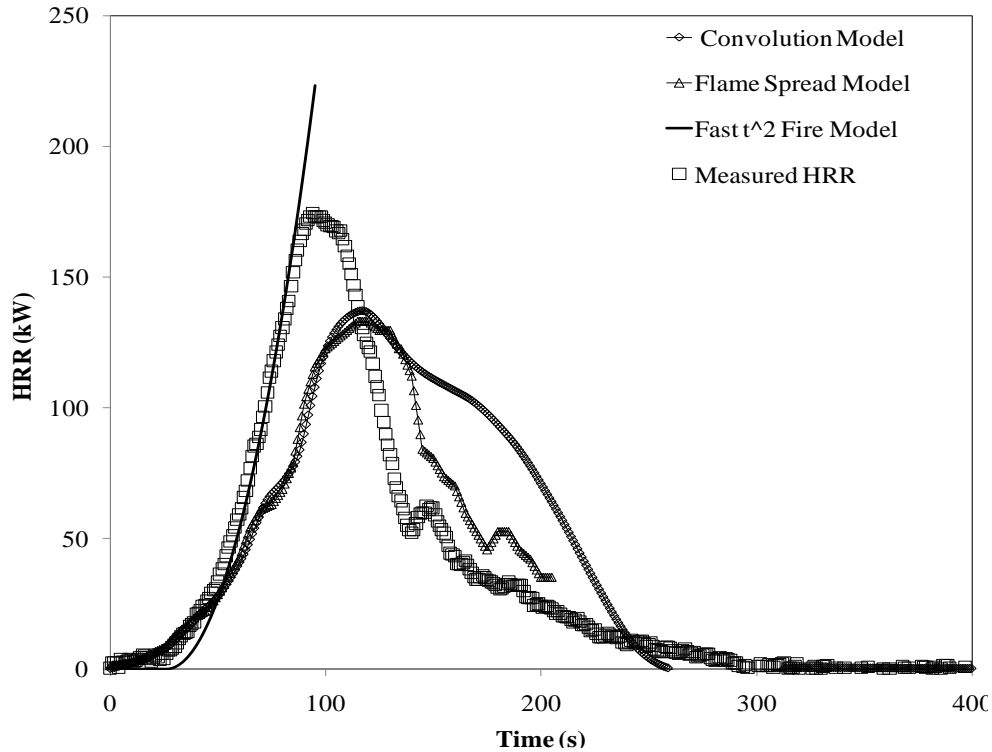


Figure 6-1. Comparison between measured and predicted HRR for specimen C1.

For specimen C3 shown in Figure 6-2, discrepancies between the measured and the predicted results were similar to those for specimen C1. The convolution, flame spread and t-squared fire models tracked the early stage of the measured heat release rate which grew exponentially with time to a reasonable degree until about 80 s. After this period, the model results deviated from the measured heat release rate curve until the peak heat release rates were reached. The average peak heat release rate predicted by the model is approximately 13% less than the measured peak heat release rate of 612 kW and the average time to peak of the predicted results which is approximately 16% higher than the experimental results.

During the decay part of the curves, the degree of disagreement between the measured and predicted profiles is most pronounced. The flame spread model produced a smaller deviation than the convolution model which produced a considerable bulge and then decayed rapidly until 300 s whereas for the flame spread model, the curve dropped until

about 180 kW and then the profile followed the measured heat release rate curve. The protrusion resulting from the convolution model caused an over-prediction of 16% for the measured total heat release while the flame spread model predicted a total heat release that was approximately 8% smaller than the measured value.

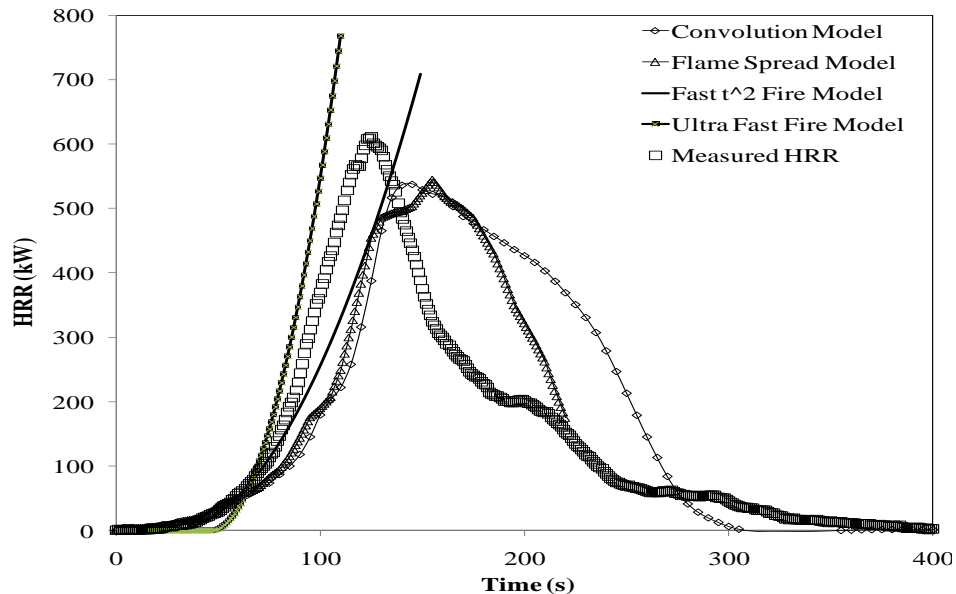


Figure 6-2. Comparison between measured and predicted HRR for specimen C3.

The predicted results for the edge-ignited specimens E5 and EE3 shown in Figures 6-3 and 6-4 illustrate the case where the three models gave more dependable results when compared with the measured heat release rates. As shown in Figure 6-3, the predicted heat release rates for specimen E5 from the three models tracked the measured heat release rate more closely than for center-ignited specimens. The medium t-squared fire model predicted the exponential growth phase of the fire until the peak heat release rate was attained. The average predicted peak heat release rates from the convolution and flame spread model were approximately 7% higher than the measured peak heat release rate.

During the decay phase of the curves, the flame spread model was able to track the fire extinction profile for the measured specimen which resulted in a difference of 2% in

total heat release rate. The convolution model, however, showed a typical protrusion during the decay phase similar to observation for the center-ignited specimen and this caused an over-prediction of the total heat release rate by 17%.

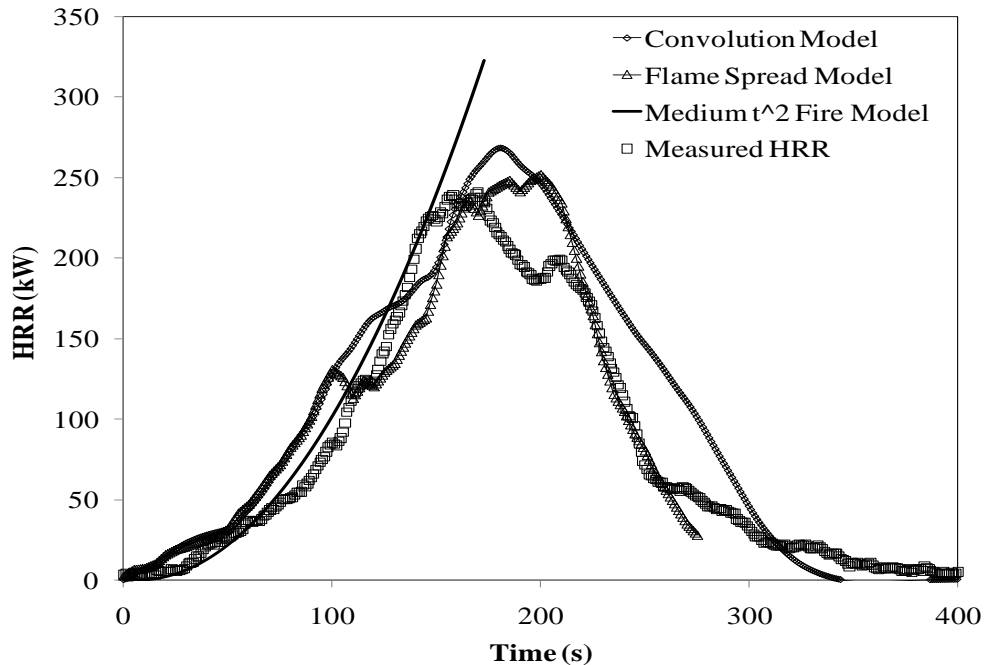


Figure 6-3. Comparison between measured and predicted HRR for specimen E5.

For specimen EE3, very good agreement between the measured and predicted results was obtained as shown in Figure 6-4. The three models predicted the fire growth of the specimen well within the first 110 s of the tests and after this period the convolution and flame spread model showed a slight deviation from the measured growth curve until the peak heat release rate was attained. The average predicted heat release rate using the convolution and flame spread model is roughly 4% lower than the measured peak heat release rate.

For the fast t-squared fire model, the predicted and measured heat release rate growth followed the same path. The models also showed a varying level of agreement with the measured heat release rate during the decay phase of the curves. The flame spread model showed a good tendency to track the decay curve but the curve did not track the

later part of the profile which resulted in under-prediction of the total heat release rate by 41%. Although there was a protrusion at the decay stage, the convolution model predicted the total heat release with only 2% variation.

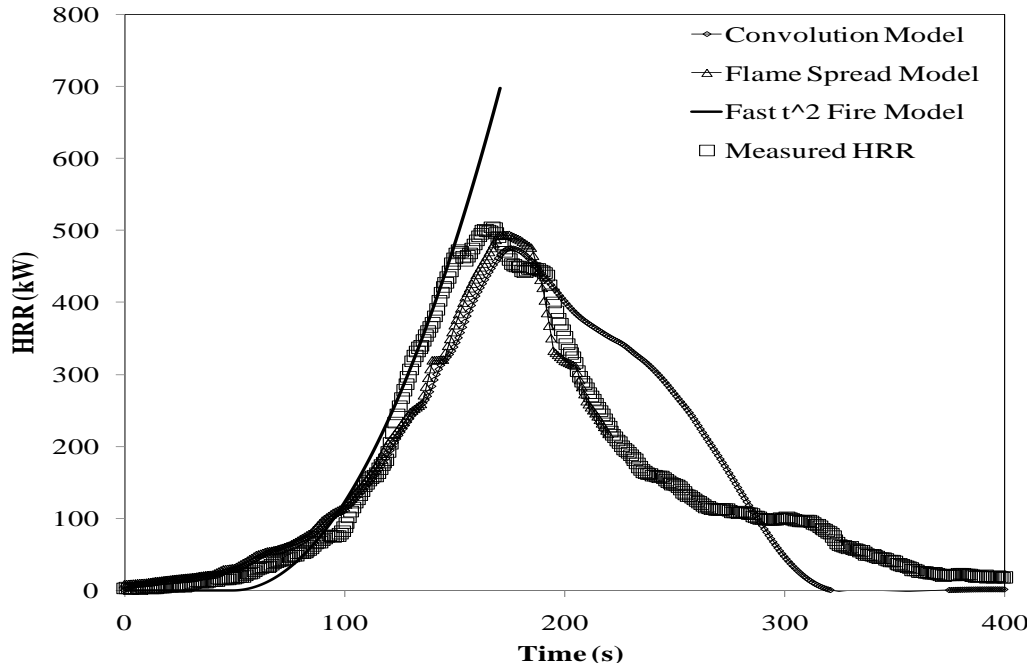


Figure 6-4. Comparison between measure and predicted HRR for specimen EE3.

6.2 Discussion of Results

The agreement between the measured and predicted heat release rates has been illustrated in Table 6.1 and Figures 6-1, 6-2, 6-3 and 6-4 in section 6-1. Of all models used, the t-squared fire growth model did the best job of predicting the fire growth of the measured heat release rate especially for the edge-ignited specimens. The appropriate choice of the t-square fire growth for each specimen was achieved by investigating which t-squared fire curve resulted in a best fit with the measured heat release rate data.

As shown in Figure 6-2, the fire growth for specimen C3 developed in the same fashion as the fast t-squared curve at the initial stage of the fire. At approximately 80 s of the test, the fire growth for specimen C3 assumed a steeper growth pattern slightly close to

ultra-fast fire behaviour. As observed during the full-scale test of specimen C in section 3.5.2, at about 80 s of the test, the flame started to flicker with the formation pool fire. The pool burning coupled with the minimal heat losses, produced a considerable amount of heat energy which accounts for the approximately ultra fast fire behaviour of the specimen at this point in time.

For specimen C1 (and for C2) there is an excellent fit between a measured and the fast t-squared fire. Although the three center-ignited specimens had similar flame spread pattern, C1 and C2 could not attain the ultra fast behaviour as the flame diameter was approximately 35% of the flame area for specimen C3. This is because larger fuel areas have the tendency to produce rapid fire growth and flame size. As shown in Figures 6-3 and 6-4, the medium and fast t-squared fire models showed good agreement with the measured results for specimens E5 and EE3. These are as expected as observed during the flame spread, the width (diameter of flame front) for specimen E5 (similar for specimen E4) was one half those of specimen EE3 and EE4. As a result, the semi-circular flame growth was more rapid with an enhanced heat release rate in specimens EE3 (or EE4) compared with specimens E4 and E5. Also, the predictions for specimens C3 and EE3/EE4 using ultra fast and fast t-squared fires models further supports the heat losses that are typical of the two ignition locations as discussed in Chapter Three.

One major reason both sizes of specimens (C3 and EE3) could not be predicted with the same t-squared fire model is that for specimens C3, pool fire was more pronounced with more intense flickering flame behaviour than in the edge-ignited specimen EE3. As shown in Table 3-3, the heat intensity produced by specimen C3 is approximately 22% higher than that produced from specimen EE3 (which supports the observation) as the ratio of the peak heat release rate to peak flame area is larger compared to that produced by specimen EE3. This higher heat release rate density for specimen C3 is attributable to its approximate ultra fast fire behaviour.

These differences in heat transfer between the edge and center tests also account for the difficulty in using the fast t-squared fire model to predict the accelerative growth of the fire from specimen C3 as the fire plume during the center burn was less open to air

circulation than in the edge ignition. The heat release rate was more rapid and resulted in the formation of a pool fire during the center test within 80 s of the tests and a significant radiative feedback which caused the fire to behave as an approximately ultra fast developing fire.

One drawback of these t-squared fire models is their inability to predict the flame area of the specimens. With the varying fire behaviour of these specimens, arbitrary selection of fire growth coefficients as provided in Table 2-1 for fire design analysis might lead to misleading results. One reason for this is that the fire response of most combustible items varies with the test and environmental conditions. Also, the materials used in this project go through different burning regimes.

For the flame spread model, the predicted results were obtained using a 60 s average heat release rate density obtained from cone tests. As shown in Figures 6-1 and 6-2, the shape of the predicted heat release rate curves for both center-ignited specimens are in good agreement with the measured results within 70 s of the tests; after this time flame spread model curves deviated from the experimental curves. For specimen C3, the deviation from the measured heat release rate curve had a uniform gap until the predicted peak heat release rate was reached and then continued at this gap until about 220 s at the decay stage.

One possible reason for the differences between the measured and predicted results for specimens C1 and C3 could be that the magnitude of the average heat release rate density used was insufficient to account for the rapid fire growth of the specimens. As discussed in Chapter Three, specimens C1/C2 and C3 had the least energy losses and extensive flame spread during the fire growth, thus it is supposed that the inability of the model to account for these losses resulted in the gaps between the two sets of curves. Another reason for the variations could be due to change in the state of the specimens to molten material (pool fire) which the model does not account for. More so, the behaviour of the specimen in small-scale was not the same as the fire behaviour of the specimen in full-scale. For instance, the cone calorimeter specimen used for this prediction was tested in a durarock board which was more open to air circulation,

whereas the flame from the center ignition tests had more flame and with less air entrainment.

For specimens E5 and EE3, the model did a better job of tracking the measured heat release rate curve for edge-ignited specimens as shown in Figures 6-3 and 6-4. One possible reason for this is that the test arrangement and the condition of the cone calorimeter specimen were relatively similar with the specimens tested in the full-scale. As discussed in Chapter Three, the specimens used for this prediction were tested in an open durarock board which allowed air circulation during the test. This is similar to the edge-ignition tests where the ignited section of the specimen caused a considerable air entrainment and more air circulation which resulted to higher heat losses than in the center-ignition tests.

Another factor which might have resulted to the erroneous prediction for the flame spread model is that the heat release rate density of the cone calorimeter specimen was obtained at a heat flux of 35 kW/m^2 . The use of the 10 cm data resulted in more diverging results especially with the center-ignited specimens. The deviation between the predicted and measured heat release rate is attributed to the combustion dynamics of the thicker specimen in the cone calorimeter. This is certainly because the 35 kW/m^2 heat flux used during the test was too weak to cause a more rigorous combustion needed to enhance the decomposition process and generate a higher peak release rate [76].

For the convolution model, the discrepancies between the measured and the predicted results are more pronounced in the center tests than in the edge tests especially during the decay part of the curves. One major contributing factor to the divergence between the measured and predicted results is that the model was developed for thin materials assuming that there is no temperature gradient in the bulk of the specimen. The differences in the early growth of the curves result from the fact that the model assumes a lateral flame spread without consideration of the vertical burn [24, 81].

As observed during the vertical flame propagation tests, the cone calorimeter specimen vertical flame spread rates (ranging between 2.3 and 3.0 mm/s) varied within 23 to 41%

with the measured vertical flame spread rate of 1.76 mm/s for full-scale tests. These differences in the spread rates between the two types of tests are expected to produce a level of diverging results between the measured and predicted heat release rates. As the specimens used in this research were 10 cm thick, a considerable amount of heat was conducted in the vertical direction during the lateral flame spread and this occurred at different rates in the thickness direction as discussed in section 3.4.3. However, this vertical burn and the heat penetration are not accounted for in the integral model, which is why there were difficulties tracking the growth phase more accurately. Most importantly, it should be remarked that a considerable amount of energy is lost in the thickness direction which is not accounted for by the model.

The error associated with under-estimating the peak and the total heat release using 10 cm cone calorimeter data is expected considering that the model was developed for thin materials with no internal temperature gradient. For instance, consider a 0.6 by 1.2 m by 5 cm full-scale specimen tested during July 2006 [61]. The convolution model was used to predict the full-scale result of the specimen as shown in Figure 6-5 using flame areas determined from video of this test and the heat release rate density of a 5 cm specimen tested in the cone calorimeter in 2006.

The model did a good job of tracking the progressive development of the heat release rate profile especially after 100 s of the test, as shown in Figure 6-5. The better agreement between the predicted and the measured results is attributable to the smaller thickness (5 cm) of the specimen. Although, there was divergence between the two curves at the early stage of the profiles due to vertical burn and heat loss in the thickness direction, it is expected that the model will perform better as the specimen thickness decreases.

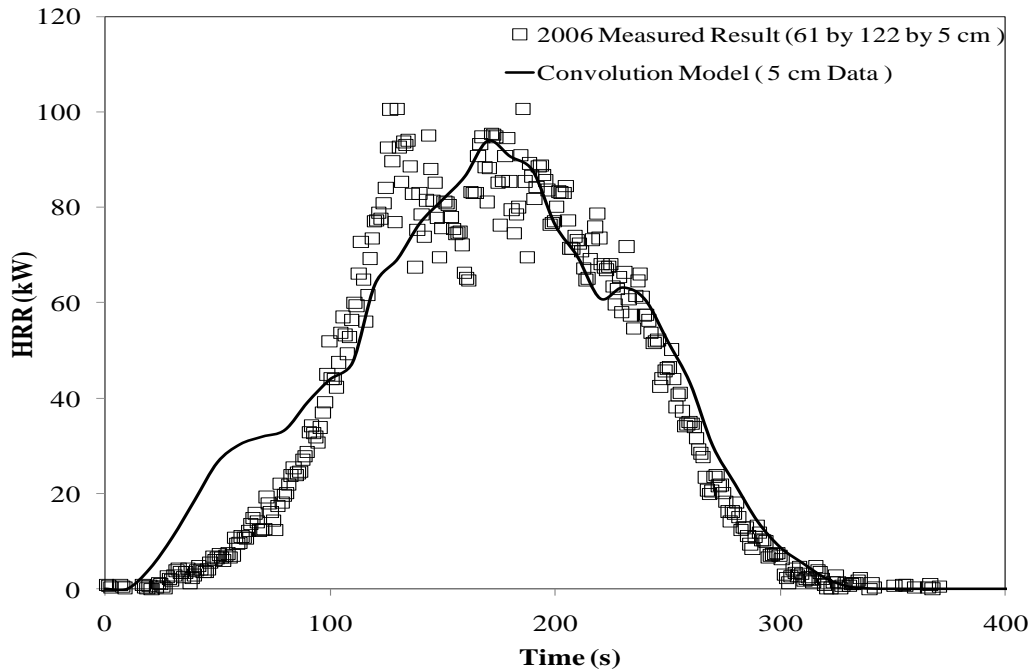


Figure 6-5. Comparison between the measured and predicted HRR for 61 by 122 by 5 cm specimen tested during July 2006.

Aside from the growth phase, other striking differences between the predicted and measured heat release rates appear most significantly at the later stage of the curves. One reason for these discrepancies (over-prediction of the total heat release in virtually all the full-scale tests) is that the total heat release per unit area was larger in the cone tests (approximately 44 MJ/m²) than in the full-scale tests (40-42 MJ/m²).

Another reason for these differences can be attributed to the mechanism of the integral model. The model calculates the heat release rate by the summation of each instantaneous heat release rate from the burning element assuming that each elemental flame area burns at the same heat release rate density as the cone calorimeter specimen. So, as the model assumes that the burned out specimen continued to burn after the peak flame area was reached, the cumulative effect of the calculated heat release rate after the peak flame area resulted to the over-prediction of the decay phase of the HRR curve.

The reason the model assumes that the burn out area was burning after the peak flame area was reached was to be able to maintain the total energy of the system. To verify this, the decay part of the flame area curve (as shown in Figure 5-2) was used during the simulation and the result obtained is as shown in Figure 6-6. Incorporating the decay flame area dataset in the model, the specimen appeared to burn out more completely and then dissipated energy almost instantly after the peak heat release rate was reached as opposed to gradual energy dissipation observed in real life fires. This resulted in under-prediction of the total heat release rate by 55% as opposed to 2% over-prediction when the peak flame area was used as the cut-off value without considering the decay flame area data. This deviation is shown by the large gap between the two predicted curves, shown in Figure 6-6.

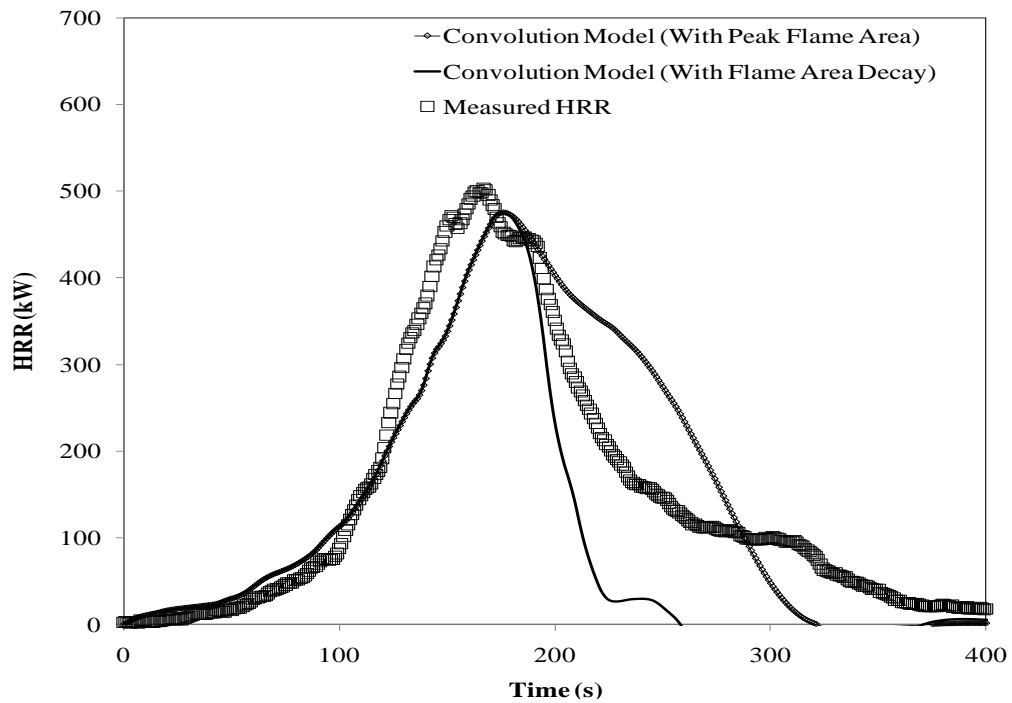


Figure 6-6. Effects of using flame area decay in the convolution model.

To further explain the reason for the over-prediction of the decay part of the heat release rate, it was thought that the shape of the 10 cm cone calorimeter heat release rate density profile shown in Figure 5-10 (especially the later part of the curve) played a significant

role in the over-prediction. To investigate this, the heat release rate density profile was truncated at 120 s to reduce its total heat release rate, assuming that the specimen burned to completion instantly at this time as shown in Figure 6-7.

Using the truncated heat release rate density in the convolution model for edge-ignited specimens, the results were obtained as shown in Figures 6-8 and 6-9. For both graphs, the effects of using the truncated heat release rate density can be clearly seen in the decay phase of the graphs. The growth phase of the curves was unaffected. The new predicted results using the truncated heat release rate density more closely tracked the later part of the curve better than the results obtained with the non-truncated heat release rate density which produced protruded curves.

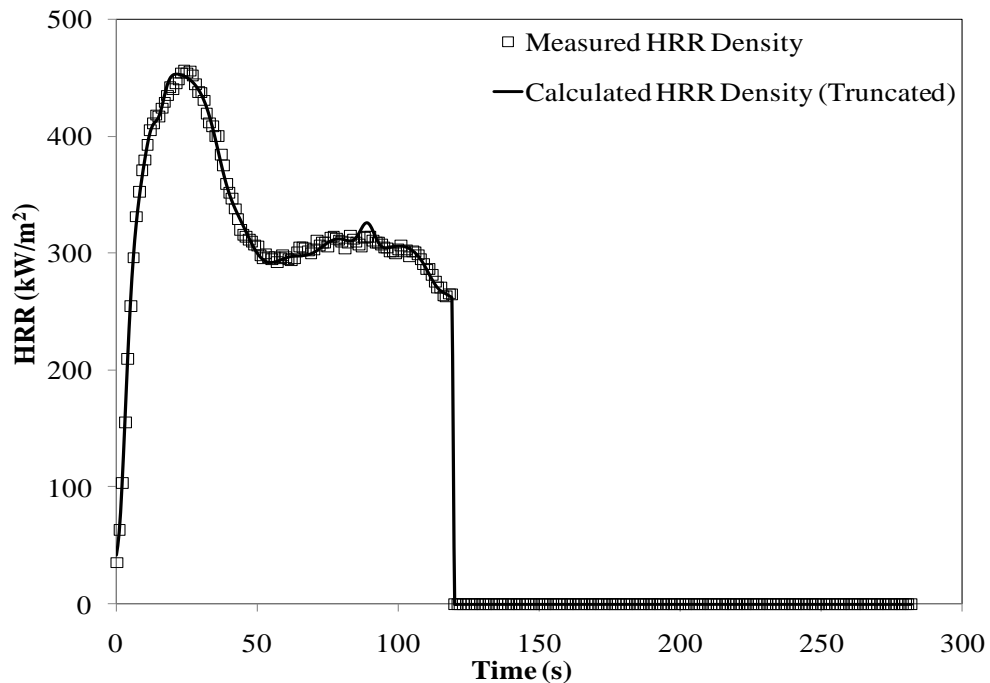


Figure 6-7. Truncated HRR density for 10 cm specimen.

From these results, it is evident that the shape and total heat release rate of the cone calorimeter specimen were partly responsible for the over-predicted decay phase of the curves. As the graphs show, the growth phases of the curves and the peak heat release

rates were unaffected by the new cone calorimeter data which implied that the majority of the discrepancies between the measured and predicted results were due to the extended burn duration and total heat release rate of the cone calorimeter input data. For specimen E5, the model over-predicted the measured total heat release rate by 8% while it under-predicted that for EE3 by 9%, when the truncated heat release rate density curve was used.

As reported by Sundstrom [24], the integral model was developed to produce valid results for specimens in which there is no burn through during the fire. As observed during the full-scale tests, the foams started to form a liquid pool with flickering flame behaviour which began after burn through had occurred. Thus, the burning behaviour of the specimen during the pool fire stage complicates the ability of the model to track the heat release rate development more realistically.

The use of the cone calorimeter specimen tested at 35 kW/m^2 is another factor that is thought to contribute to the breakdown of the model as the irradiance may not be high enough to cause a more vigorous combustion of the small-scale specimens as in the full-scale tests. During the cone calorimeter tests, the intensity of burn and the level of radiative heat flux produced from the specimen was not the same as the fire plume and heat release intensity produced during the full-scale tests. These differences in the heat transfer behaviour of the specimens in the small and full-scale tests make it more difficult to predict the heat release rate accurately.

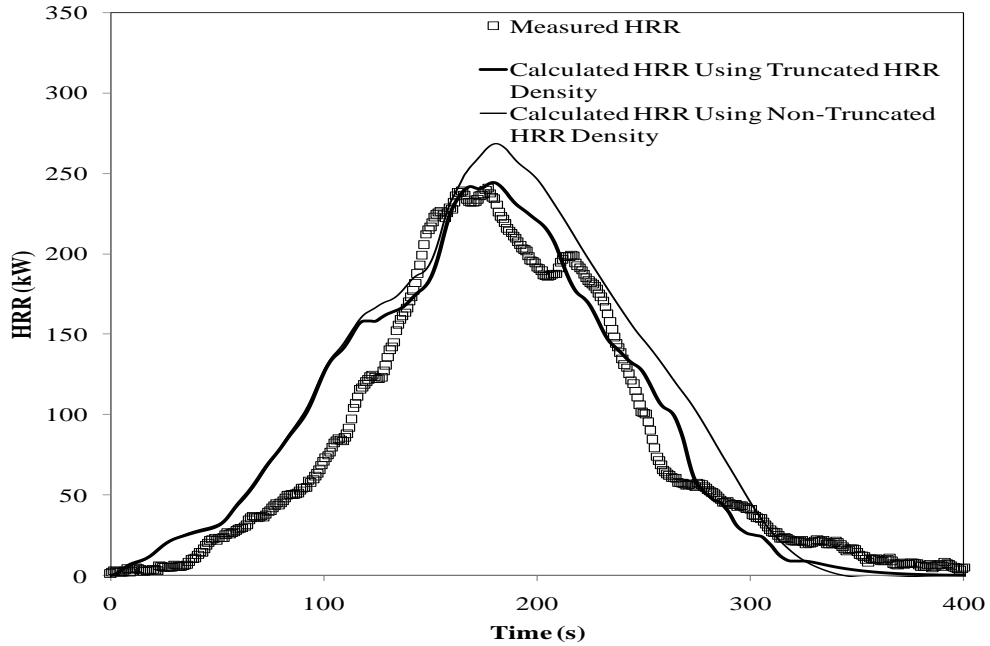


Figure 6-8. Comparison of measured and predicted HRR using truncated and non- HRR density for specimen E5.

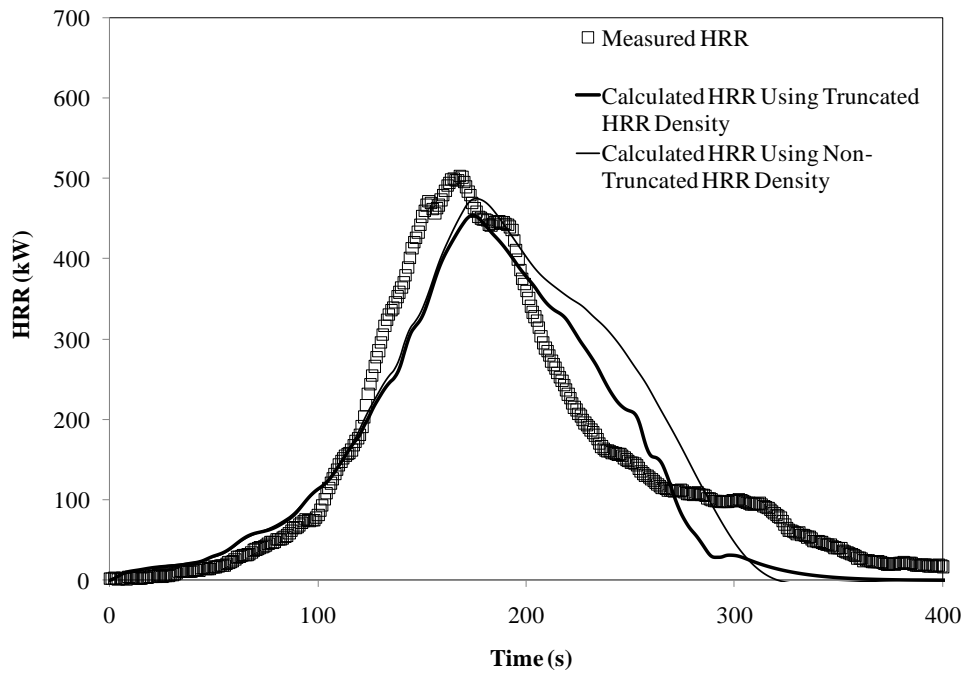


Figure 6-9. Comparison of measured and predicted HRR using truncated and non-truncated HRR density for specimen EE3.

6.3 Possible Modifications of The Convolution Model

Due to the challenges of predicting the heat release rate of the specimens using the 10 cm cone calorimeter data, one alternative approach is to assume that the 10 cm full-scale specimens are made of two layers of 5 cm thick specimens with each specimen releasing the same heat release rate.

To achieve this, two segments of the 5 cm thick polyurethane foams tested at 35 kW/m^2 heat flux in the cone calorimeter (Figure 6-10 shows a single 5 cm cone data) were used as a single data set (in superposed form) to simulate the 10 cm specimen data. The heat release rate data from the two 5 cm specimens were superposed with a time lag of 17 s to simulate a 10 cm data. The time lag was determined ($t = \frac{50 \text{ mm}}{3 \text{ mm/s}}$) using the vertical spread rate of 3.0 mm/s measured during the vertical burn test of the 5 cm thick cone specimen. The 17 s time-lag is expected to be the time when the second layer of 5 cm cone calorimeter specimen will ignite assuming both layers were tested together.

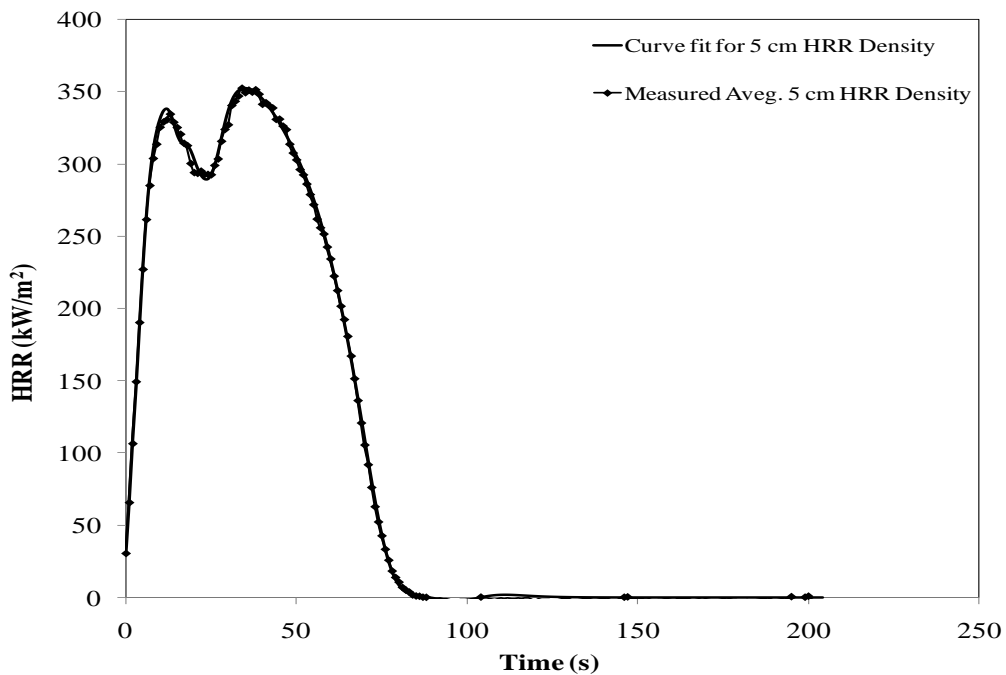


Figure 6-10. Curve fit of HRR density for 5 cm cone specimen tested at 35 kW/m^2 .

The predicted results are plotted side by side with measured results to facilitate comparison and to illustrate agreement in using the composite specimens. As given in Table 6-2, the predictions made using the 10 cm composite data over-predicted the total heat release for the center-ignited specimens and over-predicted the peak heat release rate for all the specimens. For the single 10 cm cone calorimeter specimen, the model under-predicted the peak heat release rate but performed reasonably well at accounting for the total heat release of the specimens.

Table 6-2. Summary of predicted full-scale results using the integral model.

Specimen	Peak HRR (kW)			Time to peak (s)			Total Heat Release (MJ)		
	2 x 5 (cm)	10 (cm)	Exp.	2 x 5 (cm)	10 (cm)	Exp.	2 x 5 (cm)	10 (cm)	Exp.
C1,2	186.07	137.86	174.35	119	113	94	15.25	16.95	14.32
C3	748.49	510.00	612.08	154	163	125	62.62	68.79	57.34
E4, 5	269.52	249.36	241.07	183	156	156	37.05	32.44	33.47
EE3, 4	585.83	474.45	503.35	179	179	165	56.63	65.99	60.45

As Figure 6-11 shows for specimen C1 (61 by 61 by 10 cm), the three plots illustrate the techniques of using predictions obtained from a single 5 cm cone calorimeter data which are superposed to 10 cm data to predict the results obtained by a single 10 cm cone calorimeter data. As the plots show, using a single 5 cm cone calorimeter specimen to generate the heat release rate was limited to a peak heat release of 95 kW which is approximately 83% lower than the measure peak heat release for specimen C1. Thus, by using superposition technique, as shown in Figure 6-11, the heat release rate from each of the 5 cm specimens were added using the time lag of 17 s, assuming that each foam layer has the same heat release rate density. The results obtained from the 5 and 5cm composite data produced a peak heat release rate roughly 6% higher than that obtained from measurement. Burning duration for the 10 cm composite (5 and 5 cm) was almost

75% of that obtained from experiment. The total heat release rate, however, showed a fair degree of agreement with only 7% variation.

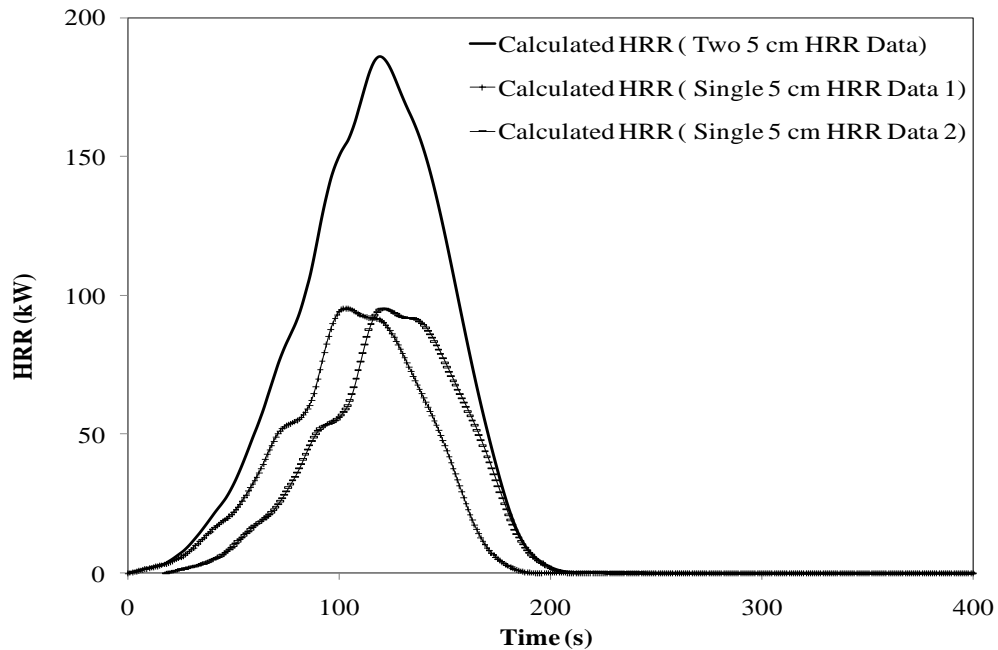


Figure 6-11. Predicted HRR using two 5 cm HRR densities incorporating 17 s time delay.

As illustrated in Figure 6-12, the predictions made using the composite data did a good job of growing at the same heat release rate as the measure data until about 70 s. From the plot, it is evident that the prediction using the composite data helped to release heat earlier in the simulated fire since the heat release rate growth curve grow faster than the prediction using the 10 cm data. However, after 70 s, the two curves deviated and then maintained a steady gap until the peak heat release rates were attained. For the 10 cm data, the divergence of the prediction from the measured heat release rate was more pronounced. The decay part of the two curves also showed a high degree of disagreement with the measured result; however, the composite data produced a comparatively better decay curve than the single 10 cm data.

One possible reason for the variation between the predicted (using the composite data) and measured results could be that the vertical flame spread rate during the small-scale tests was over-estimated which resulted in time lags longer than it actually took the

specimen to ignite the next layer. Using this time lag thus might have resulted in an unsatisfactory gap at both the growth and decay parts of the curves.

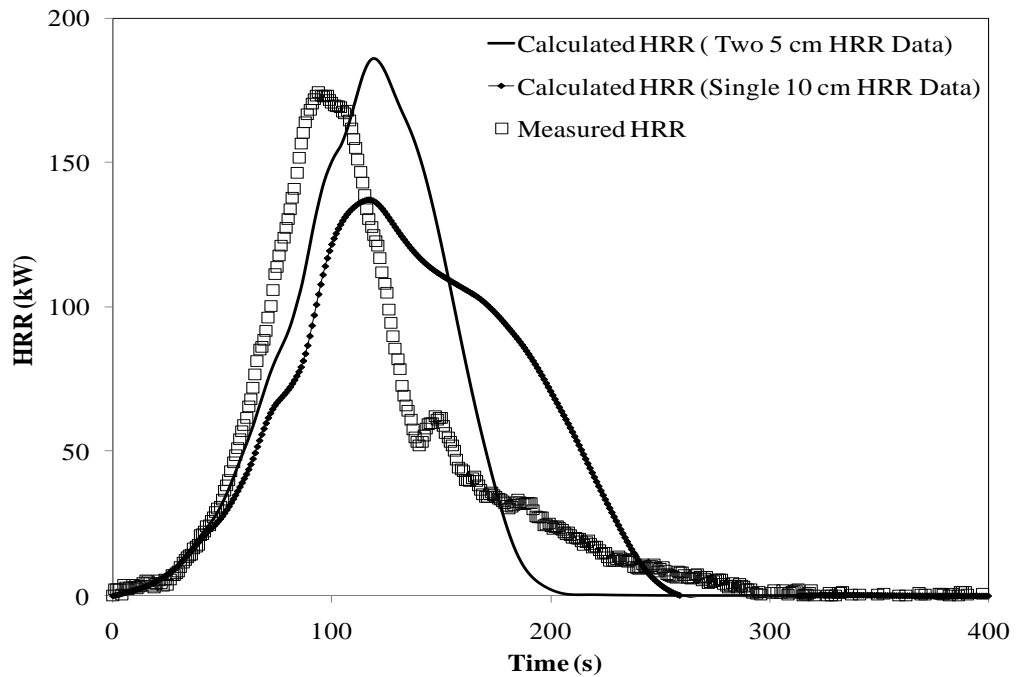


Figure 6-12. Comparison of the measured and predicted results for specimen C1 using 5 cm HRR density.

As shown in Figure 6-13, the superposition technique performed better than the 10 cm data in tracking the measured heat release rate growth. The growth phase is, however, characterised by a deviation in the three curves at 70 s and this gap persisted until the peak heat release rates were reached. The predictions (peak and total heat release rates) using the composite data are 18 and 8% higher than the measured values. For the 10 cm data, the predicted peak heat release rate was 17% lower than the measured result while the total heat release rate was over-predicted by 20%.

One reason for this discrepancy, especially at the growth stage, is attributed to the burning behaviour of the specimen in full-scale, which was different from the cone calorimeter tests as the test arrangement during the small-scale tests were more open to air flow and heat losses than in the center burn test where flame spread was more uniform due to reduced air entrainment. Another reason is that, as mentioned in section

6-2, the burning of the specimen C3 is characterised by a flickering flame and a larger liquid pool which resulted in rapid heat release rate.

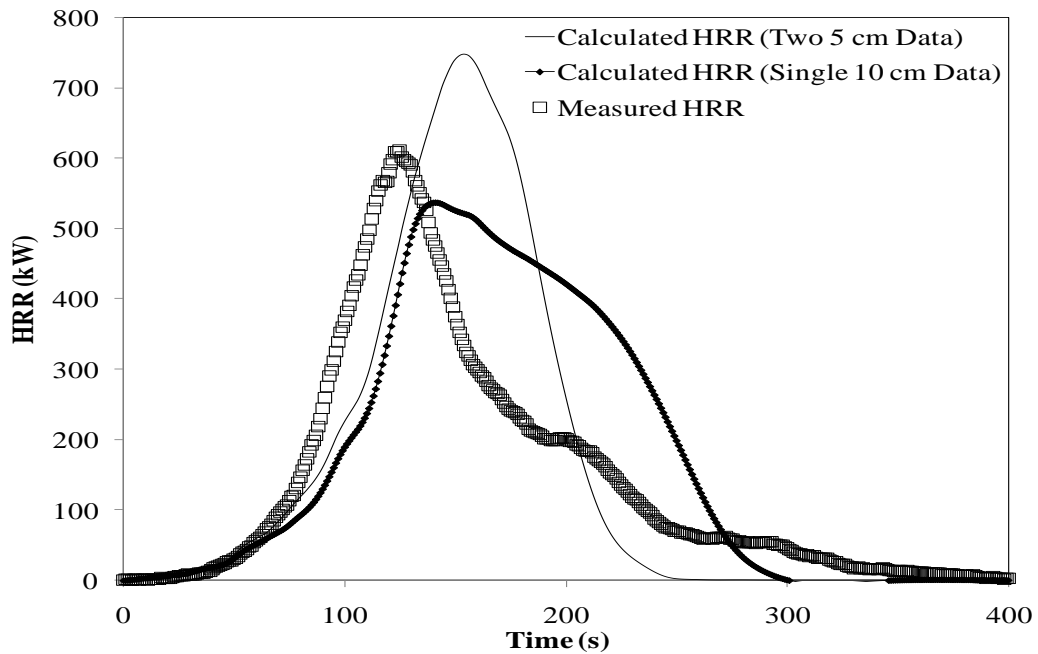


Figure 6-13. Comparison of the measured and predicted HRR for specimen C3 using 5 cm composite HRR density.

For the edge-ignited specimen EE3 shown in Figure 6-14, there was a better agreement between the predicted and measured results especially during the growth phase of the curves. The three growth curves showed approximately the same growth pattern. This can be attributed to the similar burning behaviour of the specimens during the full-scale and small-scale tests where both specimens had a small level of exposure to air circulation. It is also expected that the 35 kW/m^2 heat exposure was adequate to cause vigorous combustion of the specimen in the cone calorimeter and then produce the heat release rate density sufficient to account for the full-scale specimen fire behaviour. However, the 5 and 5 cm composite data over-predicted the peak heat release rate by 13% while the single 10 cm data under-predicted the peak heat release rate by 6%. As the predicted result from the 5 and 5 cm data dissipated energy very rapidly after the

peak heat release, this affected the total heat release rate from the model which is 7% lower than the measured value. On the other hand, the 10 cm data over-predicted the total heat release rate by 9%.

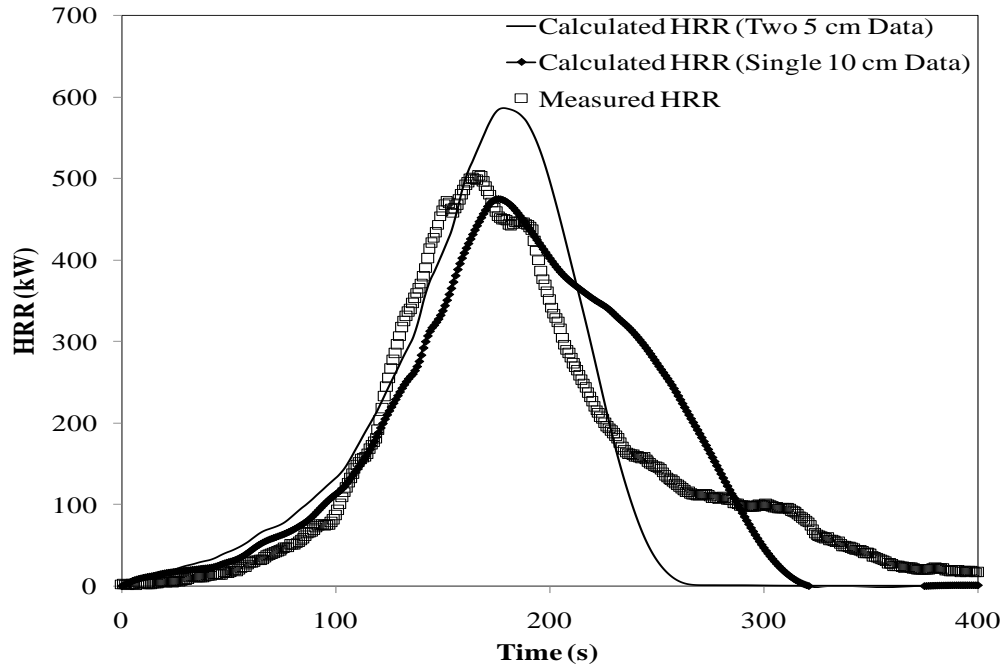


Figure 6-14. Comparison of the measured and predicted HRR for specimen EE3 using 5 cm composite HRR density.

6.4 Summary of Chapter

Predicted and measured full-scale heat release rate histories of the polyurethane specimens were compared with a reasonable degree of agreement. The t-squared fire model was most successful in accounting for the growth phase of the full-scale heat release rate curves. The convolution and flame spread models were effective in tracking the progressive fire development and predicting the total heat release rates of the specimens. The flame spread model also worked well due to use of constant heat release rate density and measured flame area which made it easier to use than the convolution model. However, the choice for the convolution model was to demonstrate the use of a transient approach to predict the heat release rate curves. Reasons for discrepancies

between the predicted and measured results and the modification of the convolution model have been given.

CHAPTER SEVEN: CONCLUSIONS AND RECOMMENDATIONS

The main objective of the research was to model the full-scale fire test behaviour of polyurethane foams using cone calorimeter data and full-scale flame spread data. The full-scale tests of the polyurethane foams were conducted using a furniture calorimeter to investigate the fire response of these items when ignited at both the center and edge ignition locations. Heat release rates resulting from these tests were analysed and the flame area growth and spread rates were estimated based on regular and infra-red video records to investigate the effects of the different ignition locations on the flame spread pattern. Several cone calorimeter tests of the representative foam specimens were conducted using different testing procedures.

A computer program based on the convolution model was developed for calculating the heat release rate of the full-scale foam specimens. Data obtained from the cone calorimeter tests and the measured flame areas from the full-scale tests were used as input variables during the modeling section of the research. The conclusions and recommendations which form the basis for future work are discussed below.

7.1 CONCLUSIONS

- The results from the full-scale fire tests of the polyurethane foams indicate that there are considerable differences in the fire behaviour of the forms tested at the center and edge ignition locations. For specimens of the same size, the peak heat release rate obtained during the center-ignition tests was approximately 17% higher than those obtained during edge-ignition tests, while the peak flame area was approximately 10% larger in center-ignition tests than in edge-ignition tests. For each specimen, flame area and HRR were similar for the first 80 s and 50 s and thereafter, there were deviations in the curve.
- Flame spread measurements using the video and the infra-red cameras gave repeatable results for all specimens with a small variation of 2 to 4%. The more accurate results were obtained using the infra-red camera due to the high

precision outlines obtained from its images. For the same size of specimens, the flame spread rate and flame growth constant developed more rapidly for center-ignited specimen than for edge-ignited specimens with a variation of 17 and 31% respectively. The average flame spread rate of 3.4 mm/s determined during the horizontal flame propagation measurements was in excellent agreement with the literature. Flame spread rates in the vertical downward direction were much slower with an average value of 1.76 mm/s and standard deviation of 0.3 which has a fair agreement with literature.

- The cone calorimeter results vary considerably with the testing procedure. For specimens of the same thickness, the edge frame test arrangement produced peak heat release rates which are significantly lower compared to those obtained by placing the specimens on a durarock board. Also, specimens burned more rigorously when ignited with the cone heater compared with butane-ignition. Overall, the durarock-mounted, cone ignited specimens were thought to produce more dependable results than the edge frame method since the later method allowed air circulation during tests of the specimens and also eliminated the challenges of suppressed burning observed for edge-frame test procedure.
- When expressed as a Gaussian function, the transient cone calorimeter data obtained at 35 kW/m^2 heat exposure and the measured flame areas can be used in the integral model to calculate the heat release rate of the specimens. The variations between the predicted and measured results were due to thickness effects and differences in the combustion dynamics of the specimens in both small and full-scale tests. A related reason for the divergence between the predicted and measured results is that the model calculates the heat release rate by the summation of each instantaneous heat release rate from the burning element assuming that each elemental flame area burns at the same total time as the cone calorimeter specimen. Overall, the convolution model was more successful in predicting the heat release rate for edge-ignited specimens than for

center-ignited specimens since the fire behaviour of the cone calorimeter specimens was similar to edge-ignited specimens.

- The use of the cone calorimeter 5 and 5 cm composite data was one possible modification in modeling the full-scale specimens as a layered material. Using this technique, the predicted and measured results (peak heat release rate and total heat release) varied between 1 and 11%. The main reason for this modeling approach was that the specimens were observed to burn in layers in the vertical direction during the furniture calorimeter tests.
- Using the cone calorimeter 60 s average heat release rate density and measured flame area, the flame spread model produced results that are similar to the measured data. This is because more heat intensity was produced within 60 s of the tests. The model predicted the edge-ignited specimens better than the center-ignited specimens. This was attributed to more pool fires and rapid burning behaviour associated with the center tests than for edge tests.
- The t-squared fire growth model did a good job of predicting the heat release rate of the specimens. The fire growth for center ignition tests were modeled as approximately ultra fast and fast developing fires while edge ignition tests were best modeled by using fast and medium t-squared fire heat release rate models. One drawback with the use of the t-square fire model is its inability to predict the flame area of the specimens.
- The NIST/CBHF correlation did a good job of predicting the self propagating fire behaviour of the specimens.

7.2 RECOMMENDATIONS

The challenges encountered while analysing the experimental and numerical results form the basis for these recommendations for future work.

- The position of the camera instrumentation relative to the test specimens during the full-scale tests affected the visual observations of the flame propagation and thus the accuracy of the measurements. As the camera was positioned at one side of the furniture calorimeter, only a section of the burning specimens was captured without information relating to other sides/corners of the specimens. Thus, in subsequent full-scale tests, the camera instrumentation should be located at least two different positions and at appropriate angles in order to capture full view (i.e. top and side views) of the specimen including the ignition and non-ignition sides of the specimen, area of flame impingement at the time of ignition, and the test floor so that the liquid pool could be captured, especially for the large surface area specimens. Also, the digital photos should be acquired at small time intervals (e.g., capturing burning events once every second).
- Improved measurement techniques should be used to estimate the flame spread rates on the specimens. The techniques used in this investigation were subjective and are prone to systematic errors. Techniques such as the use of temperature distributions on the burning specimens obtained from infra-red data can be used to determine the flame propagation rates.
- Develop an idealized flame spread model based on the flame propagation pattern observed during full-scale tests. The idealised flame spread model will eliminate the need to perform full-scale tests, and would be used in the convolution model.
- Further cone calorimeter tests should be conducted at higher heat flux (e.g., 50 kW/m^2) to help determine which heat release rate density is most appropriate for the model. This is because the cone calorimeter data obtained at 35 kW/m^2 for 10 cm specimen under-predicted the peak heat release rate for specimens C1 and C2.
- Conduct further modeling work using the pool fire and heat transfer models discussed in Chapter Two. One approach is to use the net heat flux used in

Tewarson expression [8], given as: $\frac{Q_c}{A_f} = \dot{Q}_{net} X \left(\frac{\Delta H_c}{L_v} \right)$ to determine the heat

release rate. The appropriate value of the combustibility ratio $\left(\frac{\Delta H_c}{L_v} \right)$ for

polyurethane foams can be found in the literature [8]. Another approach is to investigate the use of more sophisticated models, e.g., CFD and three dimensional heat transfer models, to estimate the amount of heat flow in the thickness direction of the specimens. The results obtained from this investigation will help in explaining the reasons for discrepancies between the measured and predicted results from the convolution integral model. It is worth mentioning that using a more detailed and sophisticated model, such as the CFD model may not give more accurate results than those obtained by using the convolution model (presented in this project). For instance, Prasad et al [82] conducted simulations of flame spread and HRR of 10 cm thick polyurethane foams using the NIST Fire Dynamic Simulator (FDS). The simulated flame spread and HRR profiles were similar to those discussed in this project. However, analyses of their results show that the predicted flame spread rate was twice as fast of the experimentally determined values while the peak HRR values showed a reasonable agreement.

- Perform full-scale tests of thinner foam specimens. This will help in evaluating how well the convolution model works for thinner specimens.

REFERENCES

- [1] Polyurethane Foam Association, 1997. "Flexible Polyurethane Foam: A Primer," INTOUCH: Information on Flexible Polyurethane Foam, 3(1).
- [2] Polyurethane Foam Association, 1997, "Flexible Polyurethane Foam in the Transportation Industry," INTOUCH: Information on Flexible Polyurethane Foam, 6(1).
- [3] Polyurethane Foam Association, 1992, "Polyurethane Foam in Furniture Design," INTOUCH: Information on Flexible Polyurethane Foam, 2(3).
- [4] Polyurethane Foam Association, 1991, "Flexible Polyurethane Foam Carpet Cushion," INTOUCH: Information on Flexible Polyurethane Foam, 4(1).
- [5] Fried, J.R., 2003, *Polymer Science and Technology*, Prentice Hall Professional Technical Reference, Upper Saddle River, NJ.
- [6] Sorathia, U., Lyon, R., and Gann, R. G., 1997, "Materials and Fire Threat," *Fire Technology*, 33(3), pp. 260-275.
- [7] Lyon, R.E., and Janssens, M.L., 2005, "Polymer flammability," DOT/FAA/AR-05/14, Office of Aviation Research, Washington, D.C.
- [8] Drysdale, D., 2000, *An Introduction to Fire Dynamics*, Second Edition. John Wiley and Sons.
- [9] Apte, V.B., 2006, *Flammability Testing of Materials Used in Construction, Transport and Mining*, Woodhead Publishing Limited, Cambridge, UK.
- [10] Polyurethane Foam Association, 2005, "The Combustion Modification of Flexible Polyurethane Foam," INTOUCH: Information on Flexible Polyurethane Foam, 12 (1).

- [11] Thomas, T. A., and Brundage, P. M., 2006, "Quantitative Assessment of Potential Health Effects from the use of Fire Retardant (FR) Chemicals in Mattresses", pp. 189-264, U.S. Consumer Product Safety Commission, Bethesda, MD.
- [12] Marotta, E., 2002, "Fire Losses in Canada", Council of Canadian Fire Marshals and Fire Commissioners, Ottawa, ON.
- [13] Roegner, R., Nov. 2005, "Upholstered Furniture Addressable Fire Loss Estimates for 1999-2002." U.S. Consumer Products Safety Commission, Memorandum to Directorate for Economic Analysis, Bethesda, MD.
- [14] Gann, R. G., Steckler, K. D., Ruithberg, S., 2001, "Relative Ignition Propensity of Test Market Cigarettes." National Institute of Standards and Technology (NIST) Technical Note 1436, Gaithersburg, MD.
- [15] Code of Federal Regulations (CFR) 1633, 2006, "Standard for the Flammability (Open Flame) of Mattress Sets," U.S. Consumer Product Safety Commission, Bethesda, Maryland.
- [16] Polyurethane Foam Association, 1999, "Flammability Update: Flexible Polyurethane Foam Industry Strives to further Reduce Fire Deaths and Injuries," INTOUCH: Information on Flexible Polyurethane Foam, 7(1).
- [17] Hilado, C. J., 1968, "Flame Retardant Urethane Foams," *Journal of Cellular Plastics*, 4(339-344).
- [18] Peacock, A.J., 2006, *Polymer Chemistry: Properties and Applications*, Hanser Gardner Publications, Munich.
- [19] Quintiere, J.G., 2006, *Fundamentals of Fire Phenomena*, John Wiley and Sons, New York.

- [20] Janssens, M. L., Kimble, J., and Murphy, D., 2003, "Computer Tools to Determine Material Properties for Fire Growth Modelling from Cone Calorimeter Data," *Fire and Materials*, 8th International Conference. San Francisco, CA, pp. 377-387
- [21] Paul, K. T., 1986, "Fire and Upholstered Furniture." *Fire and Materials*, 10, pp. 29-39.
- [22] Quintiere, J. G., 2006, "A Theoretical Basis for Flammability Properties." *Fire and Materials*, 30(3), pp. 175-214.
- [23] Incropera, F.P., and Dewitt, D.P., 2002, *Introduction to Heat Transfer*, Fourth Edition, John Wiley and Sons, New York.
- [24] Sundstrom, B., 1995, *Fire Safety of Upholstered Furniture: The Final Report on The CBUF Research Program*. Director-General Science, Research and Development. EUR 16477 EN, London, UK.
- [25] Ohlemiller, T. J., 1978, "Survey of Several Factors Influencing Smouldering Combustion in Flexible and Rigid Polymer Foams," *The Journal of Fire and Flammability*, 9, pp. 489-509.
- [26] Ohlemiller, T. J., 2002, "Smouldering Combustion", *SFPE Handbook of Fire Protection Engineering*, 3rd Edition, Chapter 9, Section 2, pp 200-210, National Fire Protection Association, Quincy, MA.
- [27] Krasny, J.F., Parker, J.W., and Babrauskas, V., 2001, *Fire Behaviour of Upholstered Furniture and Mattresses*, William Andrew Publishing, New York.
- [28] United States Nuclear Regulatory Commission, 2008, "Estimating Burning Characteristics of Liquid Pool Fire, Heat Release Rate, Burning Duration, and Flame Height." <http://www.nrc.gov/reading-rm/doc-collections/nuregs/staff/sr1805/final-report/ch3-6.pdf>. Last accessed March 10, 2009. Washington, DC.

- [29] Clark, F. R. S., 1981, "Fire Spread Tests-A Critique," *Fire Technology*, 17(2), pp. 131-138.
- [30] Walton, D. W., and Thomas, H. P., 1995, "Estimating Temperatures in Compartment Fires." *The SFPE Handbook of Fire Protection Engineering*, Section 3, Chapter 6, 2nd Edition, National Fire Protection Association, Quincy, MA.
- [31] Novozhilov, V., and Koseki, H., 2004, "Computational Fluid Dynamics Prediction of Self-Sustained Pool Fire Combustion," *Journal of the Institution of Engineers*, Singapore, 1(5), pp. 69-82.
- [32] Rew, P.J., and Hulbert, W.G., 1996, "Development of Pool Fire Thermal Radiation Model," HSE Contract Research Report No.96/1996, Epsom, Surrey, U.K.
- [33] Babrauskas, V., 1983, "Estimating Large Pool Fire Burning Rates," *Fire Technology*, 19(4), pp. 251-261.
- [34] Cowley, L. T., 1992, "Behaviour of Oil and Gas Fires in the Presence of Confinement and Obstacles," *Offshore Technology Information* 92 597, Shell Research Limited, Berkshire.
- [35] Cowley, L.T., and Johnson, A.D., 1992, "Oil and Gas Fires: Characteristics and Impact," *Offshore Technology Information* 92 596, The Steel Construction Institute, Berkshire.
- [36] Qian, C., Tashtoush, G. and Ito, A., 1995, "Structure of Large Scale Pool Fires," *International Conference on Fire Research and Engineering*, Orlando, FL, pp 147-152.
- [37] Babrauskas, V., and Peacock, R. D., 1992, "Heat Release Rate: The Single Most Important Variable in Fire Hazard." *Fire Safety Journal*, 18, pp. 255-272.
- [38] Babrauskas, V., and Grayson, J.S., 1996, *Heat Release Rate in Fires*, E and FN SPON, New York.

- [39] Babrauskas, V., 1986, "Cone Calorimeter - A Versatile Bench-Scale Tool For The Evaluation of Fire Properties," *New Technology to Reduce Fire Losses and Costs*, Elsevier Applied Science Publication, London, pp. 78-87.
- [40] Babrauskas, V., 1986, "Comparative Rates of Heat Release From Five Different Types of Test Apparatuses," *Journal of Fire Sciences*, 4(2), pp. 148-159.
- [41] Huggett, C., 1980, "Estimation of Rate of Heat Release by Means of Oxygen Consumption Measurements." *Fire and Materials*, 4(2), pp. 61-65.
- [42] ASTM E 1590, 2007, "Standard Test Method for Fire Testing of Mattresses," American Society for Testing and Materials, West Conshohocken, PA.
- [43] ASTM E 2067, 2003, "Standard Practice for Full-Scale Oxygen Consumption Calorimetry Fire Tests," American Society for Testing and Materials, West Conshohocken, PA.
- [44] ISO 9705, 1990, "Large Scale Room Fire Test-Room Corner Test," International Organization for Standardization, Geneva, Switzerland.
- [45] Babrauskas, V., 1986, "Simplified Characterization of Upholstered Furniture Heat Release Rates," *Fire Safety Journal*, 11(3), pp. 181-192.
- [46] Cleary, T. G., Ohlemiller, T. J., and Villa, K. M., 1992, "The Influence of Ignition Source on the Flaming Hazard of Upholstered Furniture," *Fire Safety Journal*, 23, pp. 79-102.
- [47] ASTM E 1537, 2007, "Standard Test Method for Fire Testing of Upholstered Furniture," American Society for Testing and Materials, West Conshohocken, PA.
- [48] ASTM E 1822, 2007, "Standard Test Method for Fire Testing of Stacked Chairs," American Society for Testing and Materials, West Conshohocken, PA.

- [49] ASTM E 1623, 2004, "Standard Test Method for Determination of Fire and Thermal Parameters of Materials, Products and Systems Using An Intermediate Scale Calorimeter," American Society for Testing and Materials, West Conshohocken, PA.
- [50] Babrauskas, V., 1997, "Cone Calorimeter Used for Predictions of the Full-Scale Burning Behaviour of Upholstered Furniture," *Fire and Materials*, 21(2), pp. 95-105.
- [51] O'Connor, D. J., Morris, B., and Silcock, G. W. H., 1997, "A Methodology for the Fire Resistance Testing of Structural Components at Reduced Scale," *Journal of Testing and Evaluation*, 25(3), pp. 273-282.
- [52] ASTM E 1354, 2007, "Standard Test Method for Heat and Visible Smoke Release Rate for Materials and Products Using an Oxygen Consumption Calorimeter," American Society for Testing and Materials, West Conshohocken, PA.
- [53] CAN/CGSB 4.2 NO.27.7-M89, 2002, "Textile Test Methods-Combustion Resistance of Mattresses-Cigarette Test", Canadian General Standards Board, Ottawa, ON.
- [54] Technical Bulletin 117, 2000, "Requirements, Test Procedure and Apparatus for Testing the Flame Retardance of Resilient Filling Materials Used in Upholstered Furniture", State of California Department of Consumer Affairs Bureau of Home Furnishings and Thermal Insulation, North Highlands, CA.
- [55] ASTM E 1474, 2004, "Standard Test Method for Determining the Heat Release Rate of Upholstered Furniture and Mattress Components Or Composites using a Bench Scale Oxygen Consumption Calorimeter", American Society for Testing and Materials, West Conshohocken, PA.
- [56] Technical Bulletin 106 (16 CFR 1632), 1986, "Requirements, Test Procedures and Apparatus for Testing the Resistance of a Mattress or Mattress Pad to Combustion which may Result from A Smouldering Cigarette," U.S Consumer Product Safety Commission, Bethesda, MD.

- [57] Jacqueline, J. S., and Harwood, B., 1993, "Overview of Practicality of Developing a Performance Standard to Reduce Cigarette Ignition Propensity," U.S Consumer Product Safety Commission, Bethesda, MD.
- [58] Wickstrom, U., and Goransson, U., 1992, "Full-Scale/Bench-Scale Correlations of Wall and Ceiling Linings," *Fire and Materials*, 16(1), pp. 15-22.
- [59] Wickstrom, U., and Goransson, U., 1990, "Flame Spread Predictions in the room/corner Test Based on Cone Calorimeter, Proceedings of the Interflam 1990 Conference, University of Kent, Canterbury, UK.
- [60] Threlfall, T. G., and Torvi, D. A., 2005, "Temperature Measurements in Full-Scale Fire Tests of Mattresses," Combustion Institute Canadian Section, Spring Technical Meeting, Halifax, NS, pp. 66-71.
- [61] Hurd, M., Torvi, D., Weckman, E., 2007, "Effects of Polyurethane Mattress Foam Properties and Geometry on Small and Large-Scale Fire Test Results," 10th International Fire and Materials Conference, San Francisco, CA.
- [62] Threlfall, T. G., 2005, "Investigation of Methods Used to Predict the Heat Release Rate and Enclosure Temperature during Mattress Fires," MSc Thesis, University of Saskatchewan, Saskatoon, SK.
- [63] Quintiere, J. G., 1989, "Scaling Applications in Fire Research," *Fire Safety Journal*, 15, pp. 3-29.
- [64] Leung, C. W., Yuen, W. W., and Chow, W. K., 2003, "A Practical Model on Flame Spreading Over Materials," The 6th ASME-JSME Thermal Engineering Joint Conference, pp. 1-9.
- [65] Dietenberger, M., 1999, "Analytical Model of Flame Spread in Full-Scale Room/Corner Tests (ISO 9705)," *Fire and Materials*, 6th International Conference, San Antonio, TX, pp. 211-222.

- [66] Gregory, S., 2000, "The Use of Cone Calorimeter and Associated Techniques in the Determination of Fire Hazards," PhD Thesis, South Bank University, London, UK.
- [67] Hansen, A. S., 2002, "Prediction of Heat Release in the Single Burning Item Test," *Fire and Materials*, 26 (2), pp. 87-97.
- [68] Baroudi, D., and Myllymaki, J., 1999, "Prediction of Smoke Production and Heat Release Rate by Convolution model," NORDTEST Technical Report 1297-96, VTT Technical Research Center of Finland, Espoo, Finland.
- [69] Janssens, M.L., 2000, *Introduction to Mathematical Fire Modeling*, Second Edition, Technomic Publishing Company, Lancaster, PA.
- [70] Grimwood, P., "Fire Growth and Flow-Rate," (www.firetactics.com), Last assessed March 10, 2009.
- [71] Hirschler, M. M., 1999, "Use of Heat Release Rate to Predict Whether Individual Furnishings Would Cause Self Propagating Fires," *Fire Safety Journal*, 32(3), pp. 273-296.
- [72] Babrauskas, V., 1986, "Free-Burning Fires," *Fire Safety Journal*, 11(2), pp. 33-51.
- [73] Atsushi, N., February 1994, "Heat Transfer in Small-Scale Pool Fires," *Combustion and Flame*, 96(3), pp. 311-324.
- [74] Martini, R. E., Finney, M. A., Moina, D. M., "Dimensional Analysis of Flame Angles Versus Wind Speed," A Paper Presented at the 11th Conference on Fire and Forest Meteorology, Missoula, MT, pp.212-217.
- [75] ASTM E 1354, "Standard Test Method for Heat and Visible Smoke Release Rates for Materials and Products using an Oxygen Consumption Calorimeter," American Society for Testing and Materials, West Conshohocken, PA.

- [76] Rowen, J. W., 1978, "Importance of Externally Imposed Heat Flux on the Burning Behaviour of Materials," *Journal of Cellular Plastics*, 14(1), pp. 25-32.
- [77] Babrauskas, V., Twilley, H. W., and Parker, J. W., 1993, "The Effects of Specimen Edge Conditions on Heat Release Rate," *Fire and Materials*, 17(2), pp. 51-63.
- [78] Proakis, J.G., and Manolakis, D.G., 1996, *Digital Signal Processing: Principles, Algorithms and Applications*, Prentice-Hall, Inc., Upper Saddle River, New Jersey.
- [79] Wickstrom, U., and Goransson, U., 1987, "Prediction of Heat Release Rates of Surface Materials in Large-Scale Fire Tests Based on Cone Calorimeter Results," *Journal of Testing and Evaluation*, 15(6), pp. 364-370.
- [80] Bradie, B., 2006, *Numerical Analysis*, Pearson Prentice Hall, Upper Saddle River, New Jersey.
- [81] Hakkarainen, T., 2001, "Application of One-Dimensional Thermal Flame Spread Model on Predicting the Rate of Heat Release in the SBI Test," *Fire and Materials*, 25(2), pp. 61-70.
- [82] Prasad, K., Kramer, R., Marsh, N., and Nyden, M., 2009, "Numerical Simulation of Fires Spread on Polyurethane Foam Slabs," 11th International Fire and Materials Conference, San Francisco, CA, pp. 697-708.

Appendix A: C++ Source Code

```
#define _USE_MATH_DEFINES//In the context of <cmath>,allows the use of
constants such as pi
#include <cmath>//Defines sin,cos,exponential and all maths functions defined in c++
#include<iostream>//Allows output on the screen and input in the keyboard
#include "Read_read.h"//Defines file for the program
#include <fstream>//Gives the ability to read and write from a file
#include <string>//Creates strings and adds one string to another
using namespace std;//Contains all the standard c++ type,e.g. double,int,char

int main()
{
    burn full_scale_mattress;
    full_scale_mattress.calc_spread();//bracket means that a function
        is being called
    full_scale_mattress.output();
    return 0;//means a msg to the operating system to indicate no
        error
}
burn::burn()//The function that initializes class "burn" data members
{
    int tmp=0;// Counter variable which is an integer
    char dummy;//Character variable that is used to capture comma
    ifstream fin;// Entry that allows one to read from a file
    fin.open("gaussian4inCone.csv");//Opens the gaussian data file
    T_o.resize(6);//Resizes the vector "T_o" or array to 6
    mag.resize(6);// Resizes the vector "mag" or array to 6
    spread.resize(6);Resizes the vector "width" or array to 6
```

```

if (! fin.is_open()) // Checks if the file is successfully
    opened:Return time if open;!= Not, then
    display "file not found"
{
    cout <<"gaussian4inCone.csv not found\n";
    exit(1);
}
while (! fin.eof())// Means to do what is in the curly bracket if
    the end of file have not been reached.
{
    fin>>T_o[tmp]>>dummy>>mag[tmp]>>dummy>>spread[tmp];//Reads
    T_o from the file,reads in comma into dummy;reads
    mag,reads in comma into dummy,reads width,then goes
    to new line
    if(fin.eof()) continue;//if upon trying to read
        T_o,mag,spread,we find end of
        file,then skip to the end of while
        loope
    tmp++;//References the next point
    if((tmp%6)==0)
    {
        int tmp2=T_o.size();
        tmp2+=6;
        T_o.resize(tmp2);
        mag.resize(tmp2);
        spread.resize(tmp2);
    }
}

```

```

    }
    fin.close();
    T_o.resize(tmp);
    mag.resize(tmp);
    spread.resize(tmp);
}

```

`void burn::calc_spread()`//Void means the function does not return

anything;`burn::` means `calc_spread` is a member function of class “`burn`”

```

{
    ifstream fin;//Allows one to read from a file
    fin.open("d_area_Wickstrom_2_4_1s_edge.csv");//Opens the file

        "differential burning area"
    if (! fin.is_open())//Checks if the file is successfully
        opened;return time if open;!=Not,the display
        "file not found"
    {
        cout<<"file not found\n";//displays file not found
        exit(1);// quits program with error;exit(0)= quit without
        error
    }
    double time=0,dt,tmax,dA;//Defining all the variables,initializing time
    cout<<"please enter tmax:";//Displays tmax on the screen
    cin>>tmax;//Reads the value of tmax from the keyboard
    times.resize(ms);//Allocating ms(minimum size) for the vector or
        array of times
    Qs.resize(ms);//The same as above for Qs
}

```

```

areas.resize(ms);//The same as above for areas
int ctr=0;//Defines integer variable “counter” and initializes to
    zero
char dummy;//Defines the character type variable “dummy”

while(! fin.eof())//means while the end of file has not been
    reached,do what is in the curly bracket
{
    fin>>time>>dummy>>dA;//Reads in the time from the file,read
        in comma into dummy and read in
        differential burning area dA.If new
        line is found after dA,ignore

    if (fin.eof()) continue;//If after reading time,dummy and
        dA,then we find the end of
        file,then skip to
        the end of the while loope
    times[ctr]=time;//Storing the instantenous time just read
    areas[ctr]=dA;// Storing the instantenous diff. Area just
        read
    ctr++;//Referencing the next point/increasing the counter
variable by 1
    if(ctr%ms==0)
    {
        areas.resize(ctr+ms);
        times.resize(ctr+ms);
        Qs.resize(ctr+ms);
    }
}

```

```

count=0;//Initializes another counter variable to zero
dt=times[1]-times[0];// Time step assuming all the time steps are
    equal
int maxsize(tmax/dt+2);    //Maximum size to which the fire will
    grow based on tmax or max number of
    timesteps needed
tmax+= dt;//Increases the tmax by time step

areas.resize(maxsize);//Allocating ms (minimum size) for the
    vector or array of areas
times.resize(maxsize);//The same as above for time
Qs.resize(maxsize);//The same as above for Qs
if(ctr>maxsize) ctr=maxsize;//Means a continuation condition
Qs[count]=0;//Defining the real variable Q(HRR) and initializing
    to zero
count++;//increasing the counter by 1

for (;count<ctr;count++)//Performs a continuation check
    without further initialization
    Qs[count]=calcQ();//Stores the convolution into the array
    of vector Qs at position count

time=times[count-1];//Stores the new time at the new position
    based on the previous time in array of
    vector times
for (;count*dt<=tmax;count++)// Performs a continuation check
{
    areas[count]=0;//diff. Area at this position is zero
    time+=dt;//increases time by time step
    times[count]=time;//Stores the new time at the new position

```

```

        in array of vector times
        Qs[count]=calcQ();//Performs the convolution calculation as
        previous
    }
    fin.close();//Closes the datafile
}
double burn::calcQ()//Double indicates that it returns a real number or floating
number;burn:: indicates calcQ()is a member function of burn
{
    double Q=0;//Defines the real variable Q and initializes it to
    zero
    for (int i=0;i<count;i++)
        Q+=areas[i]*q(times[count-i]);// Adding the convolution
        result(Q)
    return Q;// Returns the calculated result(Q)
}

double burn::q(double time)// Doble indicates that it returns a real
variable; burn:: indicates q(double time)
is a member function of the burn class
“double”,time indicates that one must
supply a real variable argument
{
    double sum=0;//Defines the real variable sum and initialize it to
    zero
    for (unsigned int tmp=0;tmp< T_o.size();tmp++)
        sum+=mag[tmp]*exp(-(time-T_o[tmp])*(time-
T_o[tmp])/spread[tmp]);//Adding the contribution of each gaussian function
    return sum;//Returns the calculated q”
}

```

```

/*double burn::q(double time)//As above but uses constant q”
{
    if (time<270)// performs continuation check for burning duration of q”
        return q_prime;
    else return 0;
}*/

```

void burn::output()//Void returns nothing;empty bracket suggests that
the function burn does take/require an argument
being supplied

```

{
    int time=0;
    string fname;
    ofstream myfile;//The object that lets one write to a file
    cout <<"please enter filename: ";//Display filename on the screen
    cin >> fname;// Read file from the keyboard
    myfile.open(fname.c_str());//Specify the filename to which to
        write and prevent other program
        from writing on it
    if (! myfile.is_open()) exit(1);//If the file is not
        open,exit,else
        print data

    printf("times\tareas\tQ\n");//Displays times<tab> Areas<tab>Q<n>
        i.e new line
    myfile << "times,areas,Q\n";//write to my file: times,Areas,Q
        then new line
    double totalArea=0;//Defines the real variable “totalArea” and
        initialize it to zero

```

```
for (int i=0;i<count;i++)
{
    totalArea+=areas[i];//Calculates the diff. Area and adding
    to the previous total area to obtain
    the new area
    printf("%3.3lf\t%3.3lf\t%3.3le\n",times[i],totalArea,Qs[i]);
    myfile<<times[i]<<','<<totalArea<<','<<Qs[i]<<endl;
}
}
```

APPENDIX B: C++ Header file

```
#include<vector>// Gives the opportunity to use vector class template
using namespace std;//Gives automatic use of standard C type
#define ms 1024//arbitrarily chosen growth step size
#define c1 0
/*#define q_prime 350*// defines the constant heat release rate density

class burn {
private:// creates a new type of variable which contains elements that are variables and
elements that are functions//
    vector<double> times,Qs,areas,T_o,mag,spread;
    double sdt,calcQ(),q(double);
    int count;

public:
    void output();
    void calc_spread();
    burn();
};
```